AD-A017 590

MULTIPLE SEISMIC EVENTS

Robert W. Taylor, et al

Wisconsin University

Prepared for:

Air Force Office of Scientific Research
Advanced Research Projects Agency

1 July 1975

Form Approved
Budget Bureau No. 22-R0293

Fourth Semiannual Technical Report

ARPA Order Number:	1827
Program Code:	3F10
Name of Contractor:	University of Wisconsin-Milwaukee
Effective Date of Grant:	1 June 1973
Grant Expiration Date:	30 November 1975
Amount of Grant Dollars:	$119,470
Grant Number:	AFOSR 73-2543C
Co-Principal Investigators:	Assistant Professor Robert W. Taylor Professor David E. Willis
Telephone:	Area Code 414, 963-4561
Program Manager:	Mr. William J. Best
Telephone:	Area Code 202, 694-5454
Short Title of Work:	Multiple Seismic Events
Report Number:	144-E123-12-T
Date:	1 July 1975

Sponsored by

Advanced Research Projects Agency
ARPA Order Number 1827

Approved for Public Release; Distribution Unlimited

16

Unclassified

SECURITY CLASSIFICATION OF THIS PAGE (When Data Entered)

REPORT DOCUMENTATION PAGE		READ INSTRUCTIONS BEFORE COMPLETING FORM
1. REPORT NUMBER AFOSR - TR - 75 - 1523	2. GOVT ACCESSION NO.	3. RECIPIENT'S CATALOG NUMBER AD-A017 590
4. TITLE (and Subtitle) Multiple Seismic Events		5. TYPE OF REPORT & PERIOD COVERED Scientific Interim 6. PERFORMING ORG. REPORT NUMBER
7. AUTHOR(s) Robert W. Taylor David E. Willis		8. CONTRACT OR GRANT NUMBER(s) AFOSR-73-2543
9. PERFORMING ORGANIZATION NAME AND ADDRESS University of Wisconsin-Milwaukee Department of Geological Sciences Milwaukee, Wisconsin 53201		10. PROGRAM ELEMENT, PROJECT, TASK AREA & WORK UNIT NUMBERS AO 1827-8 62701E
11. CONTROLLING OFFICE NAME AND ADDRESS Advanced Research Projects Agency/NMR 1400 Wilson Boulevard Arlington, Virginia 22209		12. REPORT DATE 1 July 1975 13. NUMBER OF PAGES ~~143~~ 140
14. MONITORING AGENCY NAME & ADDRESS(if different from Controlling Office) Air Force Office of Scientific Research/NP 1400 Wilson Boulevard Arlington, Virginia 22209		15. SECURITY CLASS. (of this report) Unclassified 15a. DECLASSIFICATION/DOWNGRADING SCHEDULE

16. DISTRIBUTION STATEMENT (of this Report)

Approved for public release; distribution unlimited

17. DISTRIBUTION STATEMENT (of the abstract entered in Block 20, if different from Report)

18. SUPPLEMENTARY NOTES

Fourth Semiannual Technical Report

19. KEY WORDS (Continue on reverse side if necessary and identify by block number)

Earthquakes, multiple nuclear shots, detection, identification, magnitudes, unmanned observatories, radiation pattern, amplitude spectra and cross-correlation studies

20. ABSTRACT (Continue on reverse side if necessary and identify by block number)

Spectral and correlation analyses were conducted with an earthquake and eight selected nuclear explosions, one known to be a double detonation, another known to be a single shot, and the rest of possible multiple sources. All these seismic events were fired or occurred at the Nevada Test Site.

In this study, it was found that the elastic source dimension of the natural event was significantly larger than those corresponding to the nuclear explosions. Clear differences were also found to exist in the slope of the

DD FORM 1 JAN 73 1473 EDITION OF 1 NOV 65 IS OBSOLETE

Unclassified

SECURITY CLASSIFICATION OF THIS PAGE (When Data Entered)

displacement spectra of the nuclear explosions and earthquake in the range of frequencies from .20 Hz to the corresponding peak frequency. This last result suggests a potential tool for the discrimination of seismic events. In an attempt to investigate the possibility of a multiple explosive nature for the remaining events, comparisons of theoretical modulation functions with the actual amplitude spectra of each event and with the amplitude spectrum ratios of the double event with the unknown events were conducted. The results indicate that complex modulation factors which are difficult to evaluate are contained in the spectra.

Correlation analyses were applied to the four following cases; cross-correlation of natural event with nuclear events, known single explosion with known double explosion, shots of unknown multiplicity with single detonation, and known double explosion with detonations of unknown multiplicity. The results indicate that higher correlation at zero lag exists when nuclear events were correlated with other nuclear events than when nuclear explosions and the natural event are compared. Although the data used in this study are limited, correlation techniques appear to be a potential tool for the discrimination of seismic events.

ACKNOWLEDGEMENTS

The authors would like to acknowledge the assistance of the following organizations who provided copies of the seismic recordings used in preparing this report:

University of California - Lawrence Livermore Laboratory

SANDIA Laboratory

U. S. Geological Survey - S.R.A.B.

Technical Report Summary

This is the fourth semiannual report dealing with an investigation of multiple seismic events and first zone discriminants. Reported here are the results obtained from studying the ratio of amplitude spectra and cross-correlation studies in the time domain.

Based on first zone measurements and the application of the appropriate equations, calculated source radii were found to be clearly different for the different type sources. On the basis of this radius study, the source dimension of an earthquake is significantly larger than the source dimension of a nuclear explosion, for the same order of magnitude m_b. It should be noted, however, that the difference in source radii results from application of the correct equations and does not result from a difference in peak frequency. Hence, equivalent source radii does not appear an unambiguous method of differentiation. In addition, this kind of test suffers from the failure of not being able to be performed by automated devices.

The slope of the displacement spectra in the range of frequencies from .20 Hz to the corresponding peak frequency are clearly different for natural events and nuclear explosions. The slope for this range of frequencies is near zero for the Massachusetts Mountain earthquake and clearly positive for all unknown nuclear events and the double detonation BLENTON/THISTLE. The fact that the

slope of the displacement spectra is positive is very significant when compared with the results obtained by Wyss and others (1971) for the single detonation MILROW, suggesting that the multiplicity of BLENTON/THISTLE appears to have no influence on the general behavior of the considered part of the displacement spectra. The advantage of this potential discriminating method, under the concept of an unmanned observatory, is that of being amenable to analogue methods.

While the slope of the displacement spectra for the long periods appears to be a good method of identification, it suffers in that broad band seismic data is required. This limits the utility of uncorrected data from the relatively narrow band-pass short period Benioff system. Attempts to correct the Benioff data used in this study were unsuccessful for frequencies less than 0.2 Hz.

The spectra of the seismic background noise in the area of study appear to have a strong peak around .16 Hz, as has been established by Brune and Oliver (1959) and Brune (1971).

The modulations present in the amplitude spectra appear to be very complex. The use of the theoretical modulation functions were successful only for events BLENTON/THISTLE for KNB and LAC stations, A for MNV station, B for ELK, LAC, and MNV stations, C for ELK and KNB stations, D for LAC stations, and E for LAC station. For the remaining

stations, no reasonable results were obtained. The modulation functions appear to be highly sensitive to the variation of the delay times. The use of more involved theoretical modulation functions will increase this sensitivity and therefore be of doubtful value as a sole approach to determine the multiplicity of a source, but nevertheless, can complement other methods. The attempts made to determine the theoretical envelopes of the amplitude spectra ratios were unsuccessful due, in part, to the number of parameters involved and the strong dependency on frequency of these theoretical modulation functions. In addition, for the purpose of this study, events A through E were assumed to have an unknown character (single or multiple event). If they were multiple events it was not known what the source geometry or delay times were.

Higher values of the correlation at zero lag were obtained when nuclear events were correlated with nuclear events than when a natural event was correlated with nuclear explosions. Although the value of .08 for the correlation of the single explosion DIDO QUEEN with the double event BLENTON/THISTLE is anomalously low, conclusions should not be derived from the results of only one station. Although an exhaustive study was not attempted, it appears that the correlation at zero lag is useful as the actual correlation waveform.

The consistent high values obtained for the correlation of Event B with the double detonation BLENTON/THISTLE suggest, on the basis of the theoretical frame considered in this investigation, the possibility of a multiple source for Event B. On the same theoretical basis, the consistently low values obtained for the correlation of Events A and C with the known double explosion BLENTON/THISTLE indicate the possibility of a single detonation for both events. The significant differences in the values of the correlation at zero lag of Events D and E with BLENTON/THISTLE ban any suggestion about the nature of the source.

Although the results obtained with the correlation analysis suggest the method as a potential tool for the discrimination of nuclear events on the basis of the multiplicity of their source, it suffers from the difficulty of not being adaptable to analogue methods due to the large number of reference signals required.

THE UNIVERSITY OF WISCONSIN-MILWAUKEE / MILWAUKEE, WISCONSIN 53201

DEPARTMENT OF GEOLOGICAL SCIENCES
SABIN HALL
GREENE MUSEUM
TELEPHONE: (414) 963 4561

July 1, 1975

AFOSR Grant No. 73-2543
Investigation of Multiple Seismic Events and First Zone Discriminants
ARPA Order No. 1827
Program Code 3F10
The University of Wisconsin-Milwaukee

Report No. 144-E123-12-T
Effective Date of Grant 1 June 1973
Grant Expiration 30 Nov 1975
$119,470
Project Scientists: R. W. Taylor and D. E. Willis

Air Force Office of Scientific Research
ATTN: NPG
1400 Wilson Boulevard
Arlington, Virginia 22204

Subject: Fourth Semiannual Technical Report for Period Covering 1 December 1974 through 31 May 1975

Dear Sir:

This report is a summary of research dealing with multiple seismic events and first zone discriminants. The research is divided into the following categories and will be discussed individually.

Introduction

An underground nuclear explosion will generate seismic waves that can be detected and recorded providing the yield is large enough and the distance between source and seismograph is not too large. During the past approximately 18 years considerable effort has been directed toward the development of seismological methods to detect underground nuclear events and to discriminate between earthquakes and nuclear explosions.

For seismic events at teleseismic distances, Willis and others (1963) approached the problem in terms of amplitude characteristics. The same authors (1963) carried out a study of the spectral differences of earthquakes and nuclear explosions. Brune and others (1963), Press and others (1963), Liebermann and others (1966), Evernden (1969) and Liebermann and Pomeroy (1969) have investigated various criteria which are mainly related to the detection of depth and excitation of surface waves recorded on long-period seismographs. On the basis of these and other studies, it is generally accepted that given an earthquake and a nuclear explosion releasing equivalent amounts of energy, the earthquake will generate more long-period surface waves than the nuclear detonation. For teleseismic events of magnitude above 4.75 and possibly ≤ 4 (Evernden and others, 1971), the most reliable method appears to be the difference in the average ratio of surface-wave

magnitude (M_s) to body-wave magnitude (m_b), which in general is smaller for nuclear explosions than for earthquakes. When this identification method fails, there are other criteria that could be applied, which are based on an accurate depth determination, the different complexity of the recorded seismic waves and the ratio of P-waves energy to S-waves energy. Therefore, at the present time, the identification at teleseismic distances of single seismic events with magnitudes $m_b \geq 4.75$ appears to be feasible with a high degree of reliability.

When the energy released by a seismic event is less than that resulting from a magnitude 4.75 event, the reliability of the mentioned methods decreases. In addition, the situation becomes more complex when multiple sources are considered. Furthermore, it has been recognized that the degree of differentiation that can be obtained by seismological methods is strongly dependent upon spatial distribution and density of detectors and upon the distance of the receiving stations from the unknown event. The net result is that at the present time, identification cannot be achieved with the required degree of confidence. In full awareness of this, nations interested in a comprehensive treaty continue research on the subject.

The majority of the effort to date has involved the identification of seismic events at teleseismic distances.

For smaller yield events, especially small multiple source events, it is necessary to resort to seismic data recorded at first zone distances. First zone distances as used in this report are distances less than 1000 km between the source and the receiver.

Notable differences in the amplitude spectra of earthquakes and nuclear detonations in the frequency range from .02 Hz to 0.5 Hz have been reported to exist by Pasechnik in the International Institute for Peace and Conflict Research Report of August, 1968. Wyss and others (1971) conducted an investigation of the P-waves spectral differences in the frequency range from .03 Hz to 2.0 Hz for natural events and underground nuclear explosions, recorded at teleseismic distances with magnitudes (m_b) from 5.6 to 6.5 and from 5.9 to 6.6, respectively. The results of this investigation, as reported by the authors, indicated a marked difference in the behavior of the displacement spectra of natural and explosive sources and this suggests a potential discriminant for both types of events. It does not appear, however, that these spectral differences have been investigated at first zone distances.

Based on the results obtained by Wyss and others (1971), a similar study will be conducted using eight nuclear explosions, one of them known to be multiple, and one earthquake from the Nevada Test Site. The recording stations utilized will all lie within the first zone.

Since, in the amplitude spectra of a seismic signal the phase information is lost and, furthermore, the spectra is dependent upon the propagation path of the seismic energy, cross-correlation studies in the time domain will also be conducted in conjunction with the ratio of the amplitude spectra.

In summary, the purpose of the research effort reported here is to investigate the potential of spectral analysis and correlation techniques as first zone discriminants between nuclear explosions and earthquakes. This report is based on the thesis prepared by Tarazona (1975) which was sponsored by this project.

Theory

Amplitude Spectra

The mechanisms of earthquakes and explosions have been studied and modeled theoretically by several investigators (Sharpe, 1942; Kasahara, 1957; Archambeau, 1964; Savage, 1966; Berchkemer and Jacob, 1968; Aki, 1968; Haskell, 1964, 1969; Brune, 1970, 1971). In all models with a faulting mechanism, there exists a frequency, f_o, known as the corner frequency, which is related to the source dimension through:

$$f_o = c\frac{v}{d} \qquad (1)$$

where c is a constant whose value is near 1 and depends upon the specific type of model used; v is the velocity of the body waves (P-waves or S-waves velocity, depending on the phase used in the far-field spectrum calculation); and d is the source dimension. The corner frequency, f_o, is defined at the intersection of the two linear segments which represent the spectrum and is shown in Figure 1.

Following Savage (1966), whether using P-waves or S-waves, the displacement signal has an unidirectional pulse character and, consequently, the displacement spectrum for any of the body phases should have a maximum at zero frequency and, therefore, the displacement spectrum in the frequency range between $o < f < f_o$ should have zero slope. This behavior of the spectrum of the body phases in the

range of frequencies less than the peak frequency is then conditioned by the long-time displacement conduct of the source and is very probably due to the offset on both sides of the faulting surface. The expected spectrum is illustrated in Figure 1. In the case of an explosion, it is not probable that permanent differential movement takes place beyond the equivalent elastic cavity, or, in other words, there is no offset as in the case of an earthquake with a faulting mechanism and, therefore, the slope of the displacement spectrum of the P or S phases will be positive for frequencies smaller than the f_o. This is illustrated in Figure 2.

For frequencies greater than f_o, the spectral displacement will reflect the rise time of the source function and is expected to be very much the same for both types of seismic events. These two characteristics of the amplitude spectra, the peak frequency and the slope of the amplitude spectra in the low range of frequencies ($f < f_o$), are potential tools in the discrimination between natural and manmade seismic events.

None of the theoretical amplitude spectra corresponding to the existing models for an explosive source have peaks and valleys in counterpoint with those from actual events, a fact that indicates the existence of modulations (Knopoff and Pilant, 1963). The causes of these modulations can be numerous but among the most

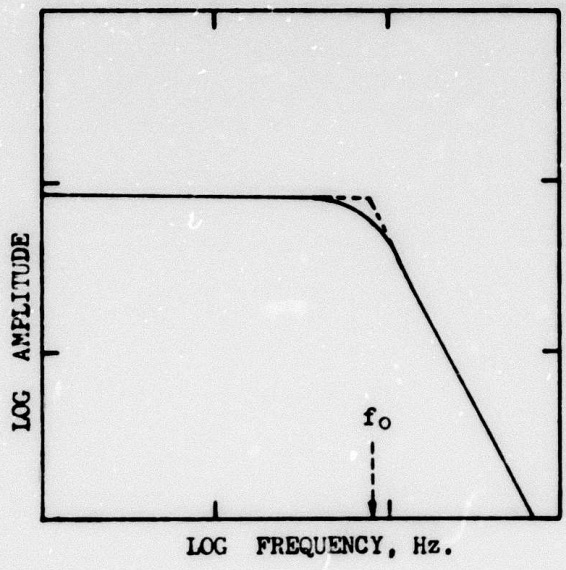

Figure 1. Theoretical P-wave displacement spectrum of an earthquake. f_o = corner frequency. (from Hanks and Wyss, 1972).

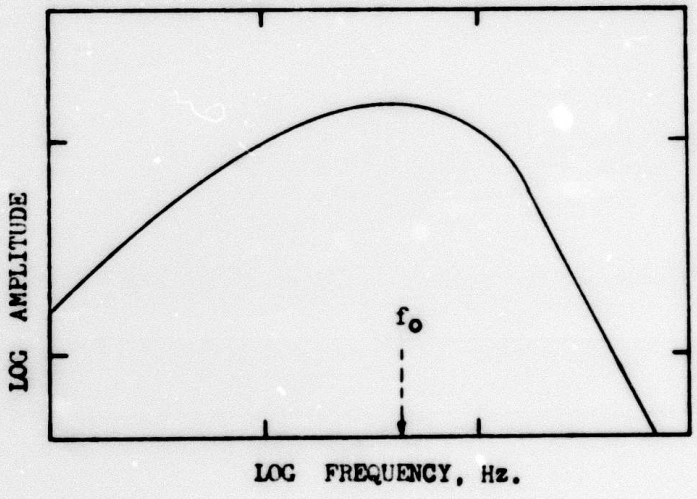

Figure 2. Theoretical P-wave displacement spectrum of an explosive source. f_o = corner frequency. (from Wyss and others, 1971).

effective are the difference in the path due to the layered nature of the earth's crust, and the reverberation of the near-station and the near-source. In the case of a multiple explosion with spatial separation of the shot points and/or firing time delay, a modulation effect would also result from the geometry or time delays.

The last modulating effect of those mentioned above is the one that has received primary attention in this work. The multiplicity of a nuclear explosion will be theoretically investigated in several possible situations under the following five assumptions:

1. The maximum order of multiplicity is two.
2. Both explosions are considered to be of the same order of magnitude.
3. The earth and the recording stations behave as linear functions in terms of the radiated energy.
4. The focuses of all nuclear explosions are sufficiently close that the near-source conditions are equivalent.
5. The source area is transparent to propagation following detonation.

Let e(t) and s(t) be the impulse response of the earth and recording station, respectively, and $r_1(t)$, the time function that represents the recorded seismogram. It follows that:

$$r_1(t) = p(t) * e(t) * s(t) \qquad (2)$$

where p(t) is the mathematical expression in the time domain of the signal emitted by the source, and * denotes convolution.

For a double explosion, p(t) can be expressed as follows:

$$p(t) = f(t) + f(t-\Delta T_1) - Kf(t-\Delta T_2) - Kf(t-\Delta T_3) \qquad (3)$$

where f(t) is the mathematical expression of the signal emitted by a single explosion; $f(t-\Delta T_1)$, accounts for the signal emitted by the second explosion with a delay time ΔT_1; $Kf(t-\Delta T_2)$ and $Kf(t-\Delta T_3)$ are the time functions that represent the reflected pulse or waves in the free surface of the first and second explosions, respectively; K is the scaling factor and ΔT_2 and ΔT_3 are the delay times such that $\Delta T_3 = \Delta T_2 + \Delta T_1$.

Therefore, combining (2) and (3), it follows:

$$r_1(t) = [f(t) + f(t-\Delta T_2) - Kf(t-\Delta T_2) - Kf(t-\Delta T_3)] * e(t) * s(t) \qquad (4)$$

and equation (4) in the Fourier transform domain is given by:

$$R_1(\omega) = F(\omega)\cdot E(\omega)\cdot S(\omega)(1 + e^{j\omega\Delta T_1} - Ke^{j\omega\Delta T_2}) - Ke^{j\omega\Delta T_3}) \qquad (5)$$

where $E(\omega)$ and $S(\omega)$ are the transfer functions of the earth and the recording station; $R_1(\omega)$ and $F(\omega)$ are the

Fourier transforms of $r_1(t)$ and $f(t)$; and ω is the angular frequency.

The amplitude spectra of $R_1(\omega)$ is then:

$$|R_1(\omega)| = |F(\omega)| \cdot |E(\omega)| \cdot |S(\omega)| [2 + 2K^2 + (1 + K^2 - 2K \cos \omega\Delta T_2) \cdot 2 \cos \omega\Delta T_1 - 4K \cos \omega\Delta T_2]^{1/2} \quad (6)$$

The factor

$$[2 + 2K^2 + (1 + K^2 - 2K \cos \omega\Delta T_2)\ 2 \cos \omega\Delta T_1 - 4K \cos \omega\Delta T_2]^{1/2} \quad (7)$$

in (6) is the modulating factor of the amplitude spectra $|R_1(\omega)|$ due to the second explosion and the two pP waves. It should be noted that the absence of ΔT_3 in the modulating function is due to the linear relation that has been assumed between ΔT_3, ΔT_2 and ΔT_1.

In the case of a single explosion, the other effects being equal

$$r_2(t) = [f(t) - Kf(t-\Delta T_2)] * e(t) * s(t) \quad (8)$$

and the Fourier transform of (8):

$$R_2(\omega) = F(\omega) \cdot E(\omega) \cdot S(\omega) [1 - K^{ej\omega\Delta T_2}] \quad (9)$$

and the amplitude spectra is:

$$|R_2(\omega)| = |F(\omega)| \cdot |E(\omega)| \cdot |S(\omega)| [1 + K^2 - 2K \cos \omega\Delta T_2]^{1/2} \quad (10)$$

From (10), it can be seen that a modulating effect also exists and is due to the reflected waves pP in the free surface.

As initially pointed out in this section, the near-source and the near-station reverberations will have modulation effects upon the amplitude spectra which are rather difficult to eliminate using the record of only one shot (whether multiple or single). An alternative procedure to overcome this difficulty is to use the spectral ratio of two explosions whose focuses lie at the same location and which have been recorded at the same stations with the same equipment. Under these conditions, the effect of the near-source and the near-stations will be the same on both amplitude spectra and therefore cancelled in the ratio. This method has been used by Healy and others (1971) and King and others (1972, 1974). In the case of two double explosions, the amplitude spectra ratio will have the form:

$$\text{RATIO}(\omega) = \frac{[2 + 2K^2 + (1 + K^2 - 2K \cos \omega\Delta T_2) 2 \cos \omega\Delta T_1 -}{[2 + 2K^2 + (1 + K^2 - 2K \cos \omega\Delta T_2^1) 2 \cos \omega\Delta T_1 -}$$

$$\frac{4K \cos \omega\Delta T_2]^{1/2}}{4K \cos \omega\Delta T_2^1]^{1/2}} \qquad (11)$$

In the case of a multiple detonation and a single one, the corresponding ratio will be:

$$\text{RATIO}(\omega) = \frac{[2 + 2K^2 + (1 + K^2 - 2K \cos \omega\Delta T_2) 2 \cos \omega\Delta T_1 - 4K \cos \omega\Delta T_2]^{1/2}}{1 + K^2 - 2K \cos \omega\Delta T_2)^{1/2}} \tag{12}$$

When both explosions are single, the corresponding ratio of the amplitude spectra will have the following form:

$$\text{RATIO}(\omega) = \frac{(1 + K^2 - 2K \cos \omega\Delta T_2)^{1/2}}{(1 + K^2 - 2K \cos \omega\Delta T_2^1)^{1/2}} \tag{13}$$

Correlation

The cross-correlation function is a coherency measure that gives in a quantitative manner the similarity between two sequential sets of data. For data in a continuous form, the cross-correlation function Φ_{XY} between two time series X(t) and Y(t) is given by:

$$\Phi_{XY}(\tau) = \frac{1}{T} \int_0^T X(t)Y(t + \tau)\alpha\tau \tag{14}$$

where τ is the time lag. When the data are in discrete form, the cross-correlation is given as:

$$\Phi_{XY} = \frac{\sum_{J=1}^{NX} (X_{NX-J} - \bar{X})(Y_J - \bar{Y})}{\left| \sum_{J=1}^{NX} |X_J - \bar{X}|^2 \sum_{J=1}^{NY} |Y_J - \bar{Y}|^2 \right|^{1/2}} \tag{15}$$

where: NX = the number of points in data set X

NY = the number of points in data set Y

$$\bar{X} = \frac{\sum_{J=1}^{NX} X_J}{NX} \qquad \text{and} \qquad \bar{Y} = \frac{\sum_{J=1}^{NY} Y_J}{NY}$$

The cross-correlation function is used in this study as a measure of similarity between two seismic signals recorded at the same station from events which are theoretically located at the same point. Due to the difference in the source mechanism of shallow earthquakes and nuclear explosions, the signal shape and its frequency content produced by these two different sources will differ somewhat. It then appears reasonable to expect a higher value of the cross-correlation for the zero lag when comparing two nuclear shots than when an earthquake and a nuclear detonation are correlated. By the same line of reasoning, a higher correlation will be expected for two double detonations than when a double and a single one are compared.

Maintaining the same assumption for the nuclear explosions enumerated on the amplitude spectra theory, let us examine in analytical form the resulting cross-correlation function for several cases.

Let $r(t)$ be the time function that represents the P coda of an earthquake's recorded signal at some station composed of the direct P-waves $r_1(t)$ and the pP phase $kr_1(t - \Delta T_1)$, such that:

$$r(t) - r_1(t) - kr_1(t_1 - \Delta T_1) \tag{16}$$

where ΔT_1 is the time delay of the pP waves, and k, a scaling factor.

In a similar manner, if $q_1(t)$ and $kq_1(t - \Delta T_1)$ represent the direct P and the pP phases, respectively, from a single nuclear explosion, its recorded signal $q_s(t)$ can be represented as follows:

$$q_s(t) = q_1(t) - kq_1(t - \Delta T_1) \tag{17}$$

and assuming that ΔT_2 is the delay time for a second explosion with characteristics identical to the first one, the time expression $q_d(t)$ of a recorded signal for a double shot will be represented as follows:

$$q_d = q_1(t) - kq_1(t - \Delta T_1) + q_1(t - \Delta T_2) - kq_1(t - \Delta T_1 - \Delta T_2) \tag{18}$$

Now consider the correlation function for the following cases:

1. Earthquake and single nuclear explosion
2. Earthquake and double nuclear explosion
3. Single nuclear explosion and double nuclear explosion.

Earthquake-single shot:

$$\phi rq_s(\tau) = \frac{1}{T_0}\int^{T} [r_1(t) - kr_1(t - \Delta T_1)]$$

$$[q_1(t + \tau) - kq_1(t + \tau - \Delta T_1)]d\tau \tag{19}$$

$$\phi rq_s = (1 + k^2)\cdot\varepsilon(\tau) - k[\varepsilon(\tau + \Delta T_1) + \varepsilon(\tau - \Delta T_1)] \qquad (20)$$

where

$$\varepsilon(\tau) = \frac{1}{T_0}\int^{T} r_1(t)\cdot q_1(t + \tau)d\tau$$

Earthquake-double shot:

$$\phi rq_d(\tau) = \frac{1}{T_0}\int^{T} [r_1(t) - kr_1(t - \Delta T_1)][q_1(t + \tau) -$$

$$kq_1(t + \tau - \Delta T_1) + q_1(t + \tau - \Delta T_2) - kq_1(t + \tau - \Delta T_1 - \Delta T_2)]d\tau \qquad (21)$$

$$\phi rq_d = (1 + k^2)\varepsilon(\tau) - k[\varepsilon(\tau + \Delta T_1) + \varepsilon(\tau - \Delta T_1) +$$

$$\varepsilon(\tau + \Delta T_1 + \Delta T_2) + \varepsilon(\tau + \Delta T_2 - \Delta T_1)] +$$

$$(1 + k^2)\varepsilon(\tau + \Delta T_2) \qquad (22)$$

Single shot-double shot:

$$\phi q_s q_d(\tau) = \frac{1}{T_0}\int^{T} [q_1(t) - kq_1(t - \Delta T_1)][q_1(t + \tau) -$$

$$kq_1(t + \tau - \Delta T_1) + q_1(t + \tau - \Delta T_2) -$$

$$kq_1(t + \tau - \Delta T_1 - \Delta T_2)]d\tau \qquad (23)$$

$$\phi q_s q_d(\tau) = (1 + k^2)a(\tau) - k[a(\tau + \Delta T_1) + a(\tau - \Delta T_1) +$$

$$a(\tau + \Delta T_1 + \Delta T_2) + a(\tau + \Delta T_2 - \Delta T_1)] + (1 + k^2)a(\tau + \Delta T_2) \qquad (24)$$

where

$$a(\tau) = \frac{1}{T_0}\int^{T} q_1(t)q_1(t + \tau)d\tau$$

There are three other trivial cases: earthquake-earthquake, single shot-single shot and double shot-double shot, for which obviously, due to our theoretical frame, the cross-correlation function is coincident with the auto-correlation function, and, consequently, the value of the correlation function for zero lag is +1 for all of them.

From expressions (20) and (22), the following relation can be written:

$$\phi rq_d = \phi rq_s - k[\varepsilon(\tau + \Delta T_1 + \Delta T_2) + \varepsilon(\tau + \Delta T_2 - \Delta T_1)] + (1 + k^2)\varepsilon(\tau + \Delta T_2) \qquad (25)$$

which clearly indicates the difference that exists in the value for any τ of the cross-correlation function for the earthquake-single shot and the earthquake-double shot cases.

The difference of the cross-correlation function, that results when comparing single-shot and double-shot with the first two cases presented, is obvious by inspection of the expressions (20), (22), and (24). Expressions (20) and (22) both contain $\varepsilon(\tau)$, which is the cross-correlation of the direct P-waves time function from the earthquake and the direct P-waves time function of the single nuclear shot; and (24) contains the auto-correlation of the P-waves time function of a single shot.

Theoretical Source Models

The source dimension for the Massachusetts Mountain earthquake was calculated using a relation similar to that given by Brune (1970, 1971) and in which the velocity of the P-waves has been substituted for the S-waves velocity. The actual expression used was:

$$r = \frac{2.34v}{2\pi f_o} \qquad (26)$$

where v is the velocity of the P-waves in the immediate vicinity of the source and f_o is the corner frequency of the P-waves spectrum. This approach for the estimation of the source dimension has been utilized by Wyss and others (1971) and Hanks and Wyss (1972). While widely used, in application the validity of (26) is dependent upon the following assumptions:

1. The earthquake is produced by the dislocation of a strike-slip fault.
2. The dislocation is produced by a tangential stress applied to the interior of the fault area, which is stimulated in an infinite, homogeneous, perfectly elastic and isotropic medium.
3. The rupture is initiated instantaneously and simultaneously over the total fault area.
4. The rupture velocity is always subsonic.

5. During the time that the rupture takes place, the fault surface reflects perfectly the shear waves, or in other words, each block of the fault behaves as a liquid with respect to the other.
6. The stress pulse only produces shear waves which propagate in a direction perpendicular to the fault surface.

Sharpe's (1942) model for an explosive source was used for the estimation of the source dimension of the nuclear detonations. In Sharpe's model, the corner frequency is related to the P-waves velocity v of the media near the source and the source radius r as follows:

$$f_o = \sqrt{2}\, v/3\pi r \qquad (27)$$

The validity of this equation is dependent upon the following assumptions:

1. The explosion takes place in a spherical cavity.
2. The medium surrounding the spherical cavity is infinite, homogeneous and perfectly elastic.
3. No net displacement occurs beyond the equivalent elastic cavity.
4. An arbitrary pressure function of time is applied uniformly to the interior of the cavity.

Geological Setting

The Nevada Test Site (NTS) lies between the east boundary of the Cordilleran eugeosyncline and the east boundary of the miogeosyncline, close to the Las Vegas Valley shear zone (Figures 3 and 4), within the Basin and Range province.

The rocks that constitute the Late Precambrian and Early Cambrian are typically clastic, chert being the most representative lithologic unit. Silurian and Lower Devonian rocks are mainly dolomites with depositional characteristics of broad shallow-subtidal, intertidal environments as documented by Matti and others (1974). The Roberts Mountain thrust plate, formed northwest of the NTS, was the source of part of the clastic material that constitutes the Eleana Formation deposited during Late Devonian and Mississippian. The rest of the Paleozoic is characterized by carbonate deposition.

Mesozoic sediments and volcanic rocks are almost absent in the area of study, being represented only by a few granitic plutons dated in that period.

Ash-flow tuffs, mainly of rhyolitic composition dominated the lithology of the more than 3,700 foot section which constitutes the Tertiary and has been used as a test media for many of the underground nuclear detonations carried out in the NTS. Given in Table 1 are the principal Tertiary volcanic units at NTS and the surrounding

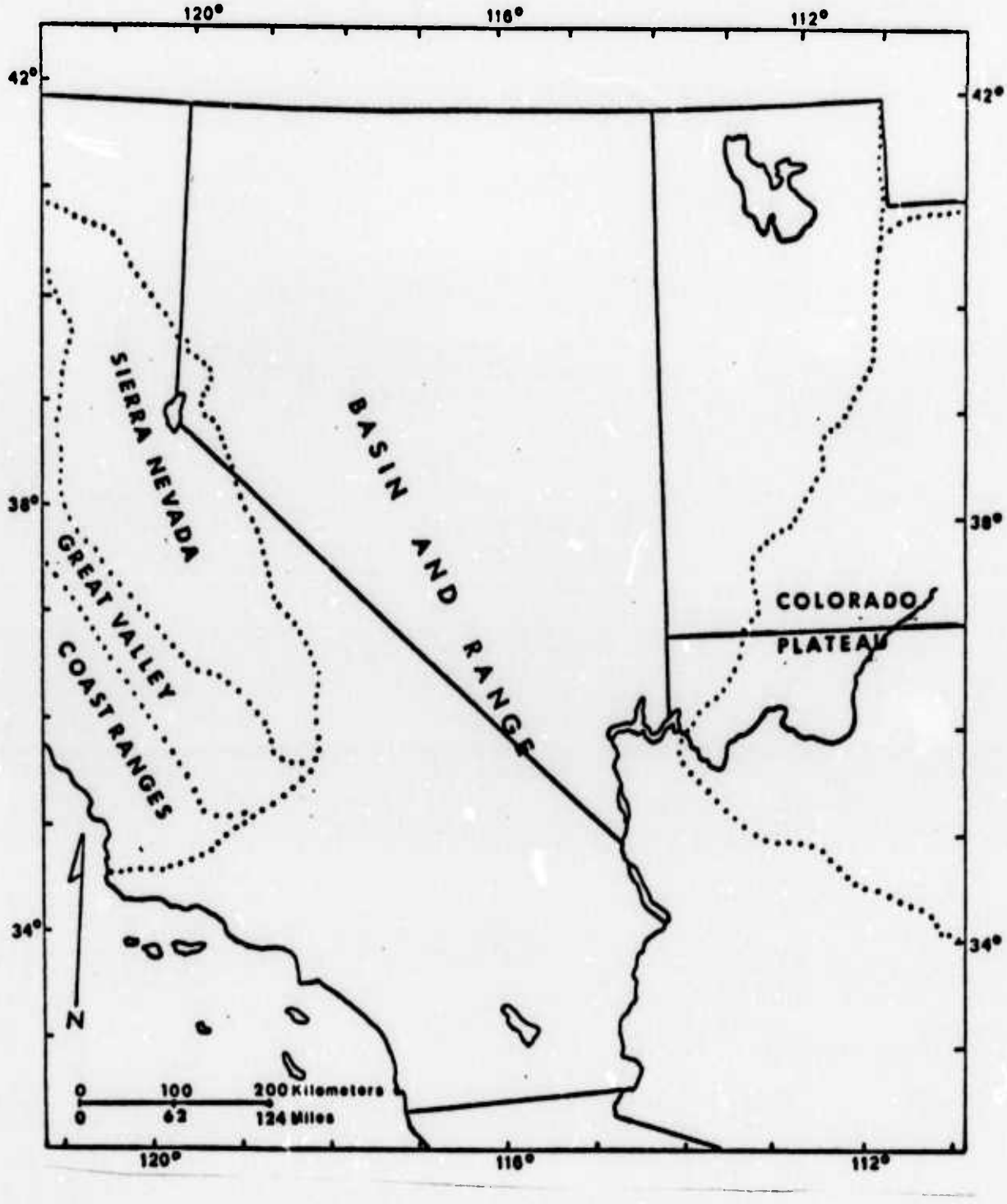

Figure 3. Physiographic provinces of the Nevada, California, and Utah area.

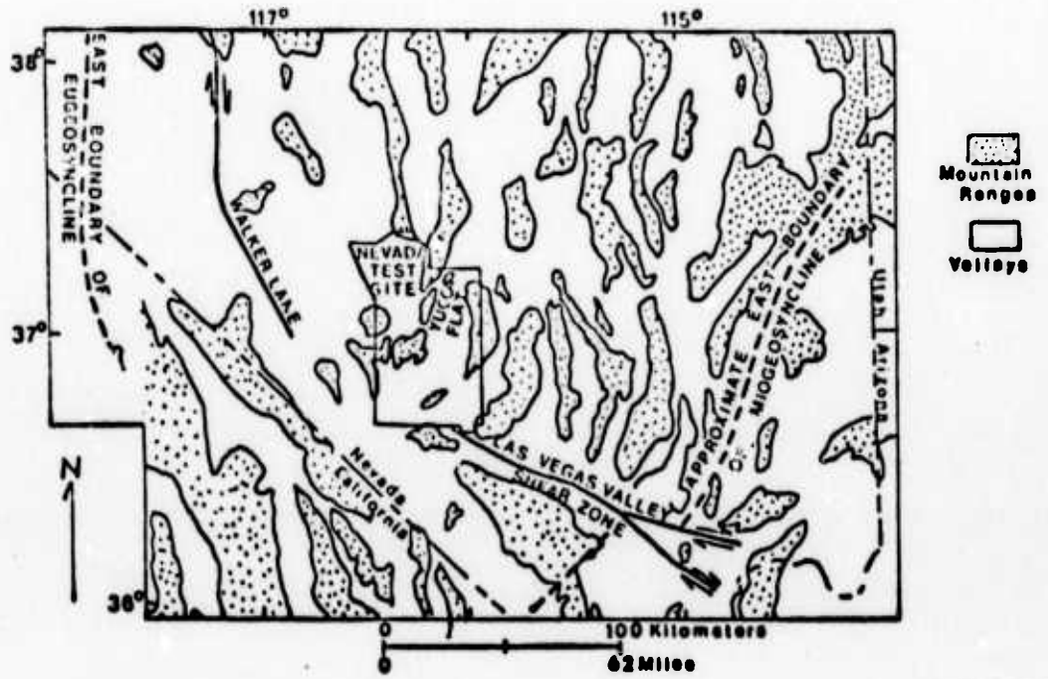

Figure 4. Index map of the geologic and physiographic features of the Nevada Test Site and surrounding area. (modified from Ekren, 1968, p. 12).

TABLE 1

Principal Tertiary Volcanic Units at NTS, K/Ar Dates, Areal Extent, and the Estimated Volume of Each Unit

Age	K/Ar Date	Unit	Lateral Extent, In Miles	Volume In Cubic Miles
TERTIARY	7.5 m.y.	Thirsty Canyon tuff	80	50
	11.0 m.y.	Timber Mountain tuff	100	500
		Paintbrush tuff	70	120
	13.8 m.y.	Belted Range tuff	60	70-100
	17.5 m.y.	Fraction tuff	120+	500
		White Blotch Spring tuff	120+	500
	26.5 m.y.	Monotony Valley tuff	120+	1000+

(Modified from E. B. Ekren, 1968)

area, the K/Ar dates, the areal extent, and the estimated volume of each unit.

The structural features of the NTS are those of the Basin and Range province, characterized by a north-south trend of mountain ranges and intermontane basins due to an intense faulting. Shown in Figure 4 are the major thrust faults and other physiographic features of the NTS.

All the seismic events used in this study have been fired or have occurred in the Yucca Flat area, which is in an intermontane basin mainly covered with Tertiary (volcanic) and Quaternary (alluvium) deposits, and which is bordered by mountains consisting of Precambrian and Paleozoic rocks and a few Mesozoic intrusives in the northern region. A general geologic map of the Yucca Flat area is presented in Figure 5.

A sound knowledge of the geology of the area, not only where the observed seismic events take place but also along the propagation path separating the source and the recording station, is of prime importance. Much of what is contained on a seismogram is the result of the geological structure and major lithologic units that constitute the path traveled by the seismic energy. It is not difficult to realize the complexity of these effects and the arduousness of their evaluation. Much of the work along this line for the NTS area has been done by the United States Geological Survey (USGS). Yacoub and others

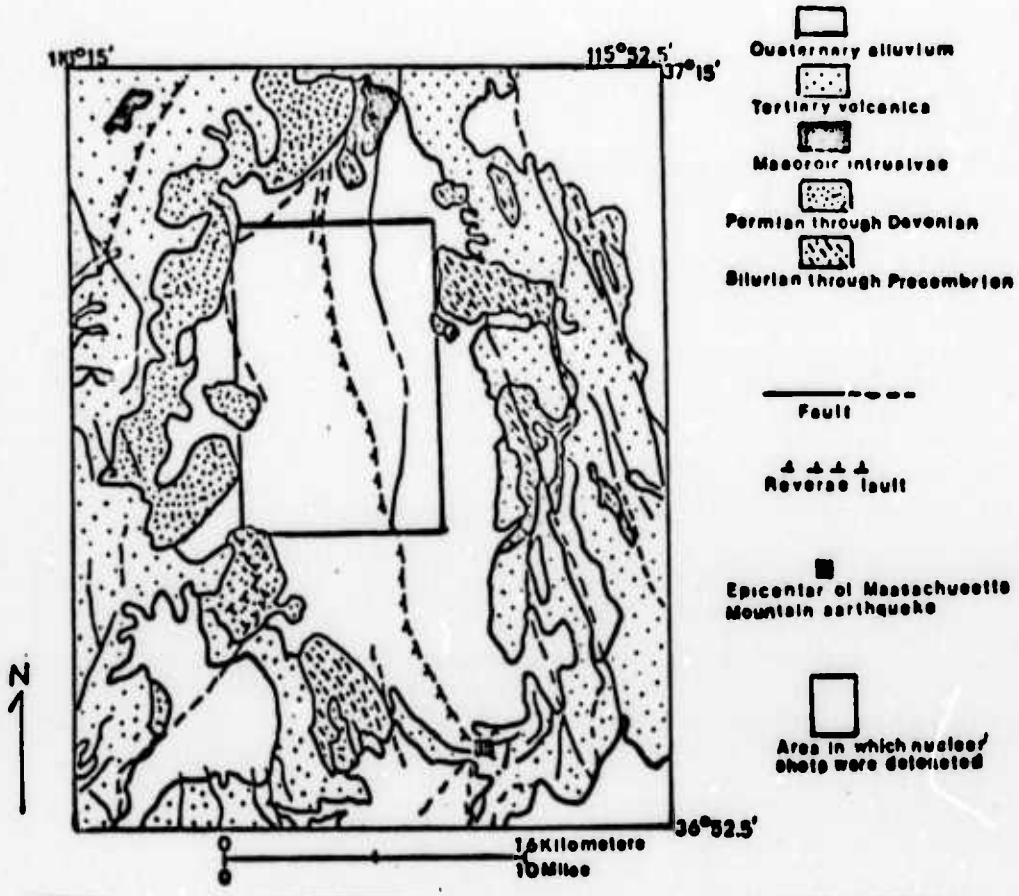

Figure 5. Generalized geologic map of Yucca Flats area with epicenter of Massachusetts Mountain earthquake and area in which nuclear events were detonated. (modified from Hinrichs, 1968, p. 242).

(1968, 1970), have studied the effects of the subsurface geology on the ground motion due to underground nuclear detonations at the NTS by using computer ray tracing techniques on two complex two-dimensional geological models. Since the two mentioned models include the sites of the Tonopah and Nelson stations (which are two of the data sources used in this thesis), a brief review of the results from the models concerning the seismic stations is presented.

Yacoub and others (1970) applied the ray tracing computer program to the two geological models indicated by lines AB and BC, respectively, in Figure 6 with a seismic source for both models located at point B which is coincident with drill hole UE20f. Shown in Figures 7 and 8 are the geological model and the program output that correspond to model AB. In Figure 8, the high ray density that can be observed between distances of 330,000 and 350,000 feet bracketing the Tonopah station site and its immediate vicinity has been suggested to be a possible partial explanation of the large ground motion recorded at this station for many events in the NTS. The high concentration of rays (Figure 8) seems to be controlled mainly by the lithological unit (Figure 7) to the Conrad and Moho discontinuity. An important observation (pointed out by Yacoub and others, 1970) is that if the source, rather than being located in UE20f, were located at a point between Tonopah and

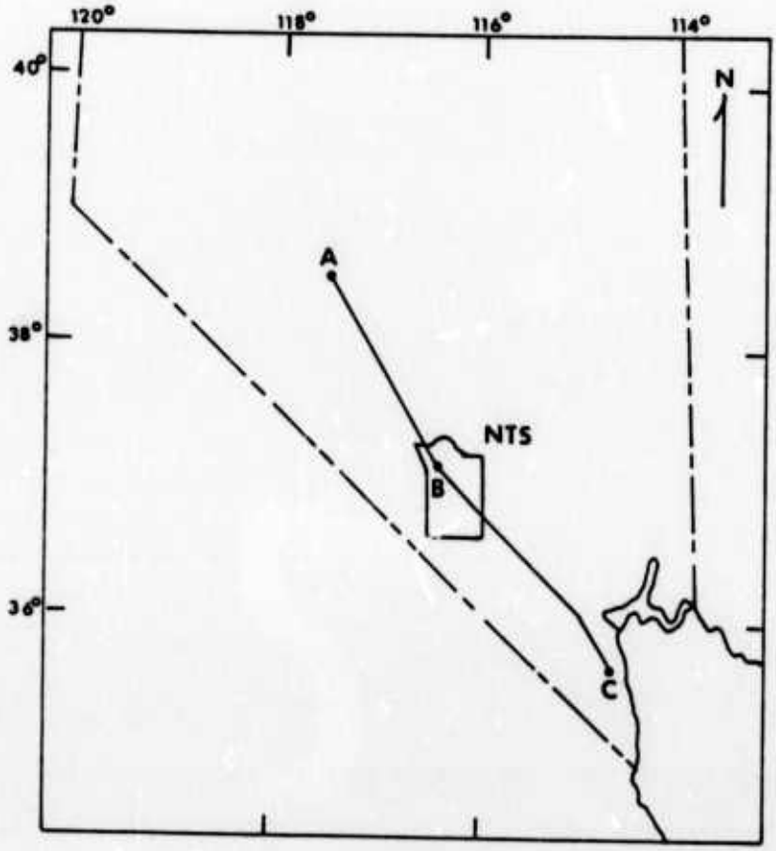

Figure 6. Index map of geological models AB and BC. (modified from Yaucoub and others, 1970, p. 589).

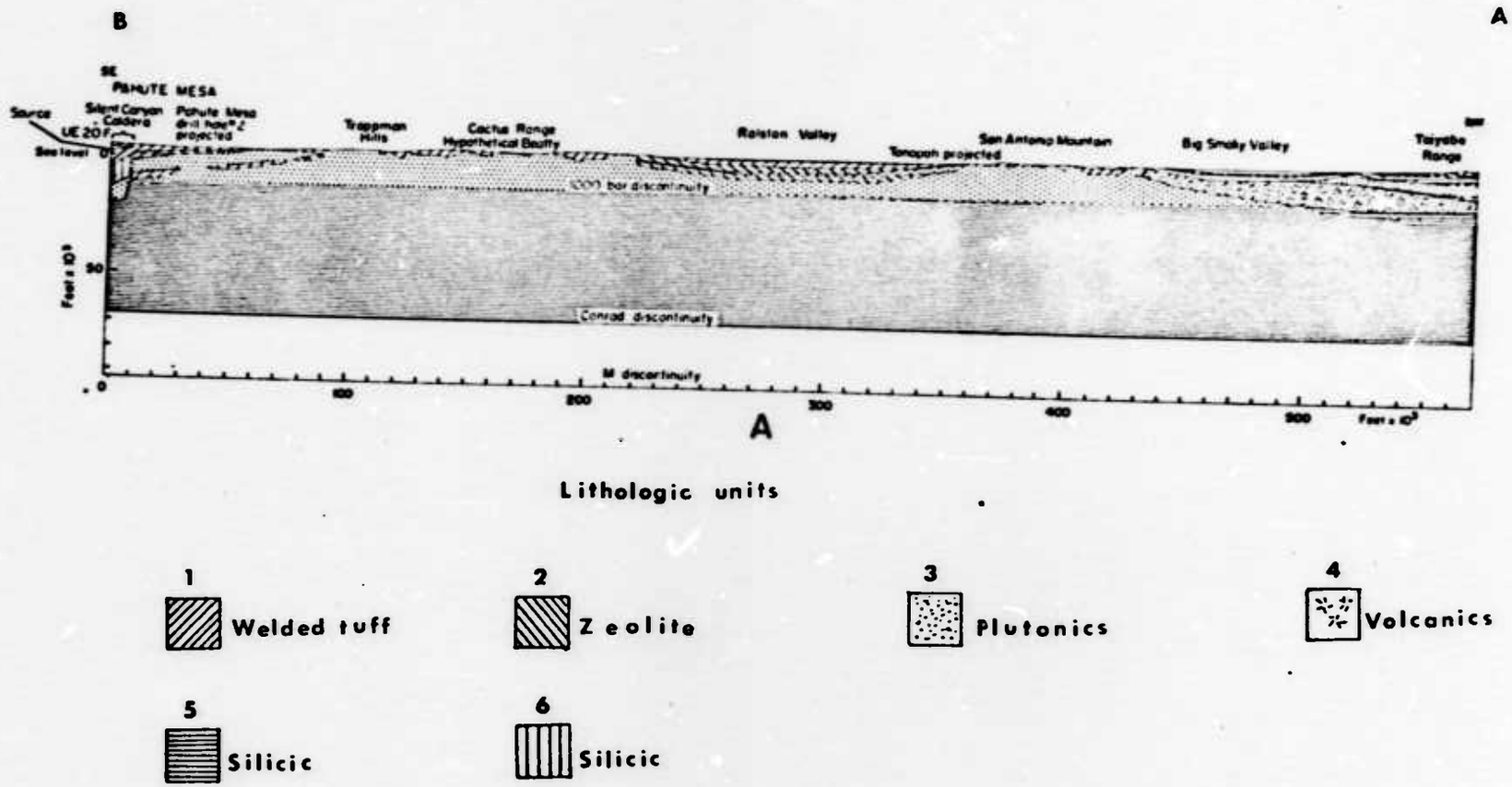

Figure 7. Geological model of Line AB. (from Yaucoub and others, 1970, p. 591).

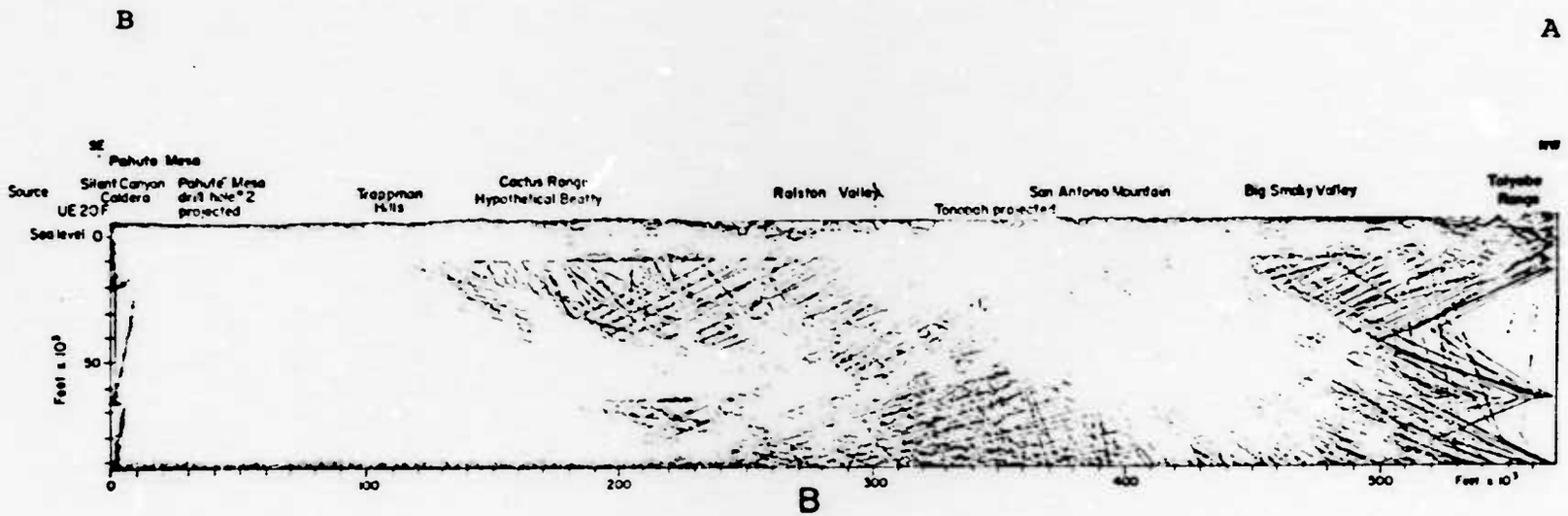

Figure 8. Seismic ray plot corresponding to the geological model of Line AB shown in Figure 7. (from Yacoub and others, 1970, p. 591).

UE20f, the station would probably fall in a "shadow zone" (low density of rays) similar to that of the Ralston Valley and Cactus Range shown in Figure 8. This point is particularly important with respect to the emplacement of the stations in an unmanned monitoring system.

The model for line BC is not as detailed as that for line AB. Hence, the corresponding geological model and output have not been presented here. It appears that the majority of the emerging rays at the Nelson station have undergone many refractions in the crust prior to reaching the area close to the station which is underlain by intrusive and extrusive rocks with a small number of elastic interfaces.

In Table 2, the average values are listed for the longitudinal velocity, density and Poisson's ratio for the major lithologic units in the NTS. These values are used in this study and were taken from Yacoub and others (1970).

TABLE 2

Longitudinal Velocity, Density and Poisson's Ratio of the Major Lithologic Units in the NTS

Longitudinal Velocity km/sec	Density gr/cc	Poisson's Ratio	Rock Types
1.2	1.80	.405	Alluvium; vitric bedded tuff
3.4	2.30	.330	Welded tuff
2.4	2.00	.270	Zeolitic bedded tuff; calcareous sedimentary rocks
4.6	2.40	.300	Silicic volcanic rocks
5.5	2.65	.250	Silicic plutonic and hypoabyssal rocks at shallow depths; quartzite and argillite
6.0	2.70	.250	Limestone
6.7	2.75	.250	Dolomite

(Modified from N. K. Yacoub and others, 1970)

Data

Nine seismic events from the NTS comprise the data used in this study. The Massachusetts Mountain earthquake that occurred August 5, 1971, on the NTS between the Yucca and Frenchman Flats (Fischer and others, 1972; Rohrer and Springer, 1972) is the only natural event. The rest are nuclear explosions. The nuclear explosion BLENTON/THISTLE is known to be a double detonation and DIDO QUEEN, a single one; the remaining shots from A to F are of unknown multiplicity. The arrivals from an earthquake with an epicenter at teleseismic distance from the shot point of Event F occurred almost simultaneously with the firing of this nuclear detonation and both events were recorded together. In Table 3, the data for all events are summarized.

The seismographic coverage of the area is comprised of the Lawrence Livermore Laboratories (LLL) stations, ELK, KNB, LAC and MNV and the Sandia Laboratories stations, BMN, DAC, ELY, LEE, NEL and TPH. The approximate locations of these stations are shown in Figure 9, and their geodetic coordinates given explicitly in Table 4. The azimuth and distance of each event from BLENTON, which serves as somewhat of a reference for this study, are also given in Table 4. The recordings at the LLL and Sandia stations were obtained with Sprengnether and Benioff instruments, respectively. The amplitude of the velocity

TABLE 3

Summary of the Data of the Seismic Events Used in this Study

Name	Shot Time (GMT)	Depth (km.)	Coordinates	Shot Medium	Azimuth with Respect to BLENTON	Magnitude (m_b)	Date
BLENTON	1700:00.04	.56	37°04'53.4"N 116°00'52.2"W	Tuff	0°00'00.0"	5.3	4/30/69
THISTLE	1700:00.04	.56	37°05'25.0"N 116°00'20.3"W	Tuff	36°53'55.6"		4/30/69
DIDO QUEEN	1700:00.00	.39	37°11'06.1"N 116°12'54.5"W	Tuff		5.1	6/5/73
EVENT A		.24		Alluvium		4.7	
EVENT B		.56		Tuff		5.6	
EVENT C		.31		Tuff		5.0	
EVENT D		.44		Tuff		5.3	
EVENT E		.39		Alluvium		5.3	
EVENT F		.24		Alluvium			
Mass. Mt. (earthquake)		4.6	36°55'00.0"N 115°59'27.0"W			4.3	8/5/71

*Events A through F are all located at distances less than 20 km from BLENTON/THISTLE.

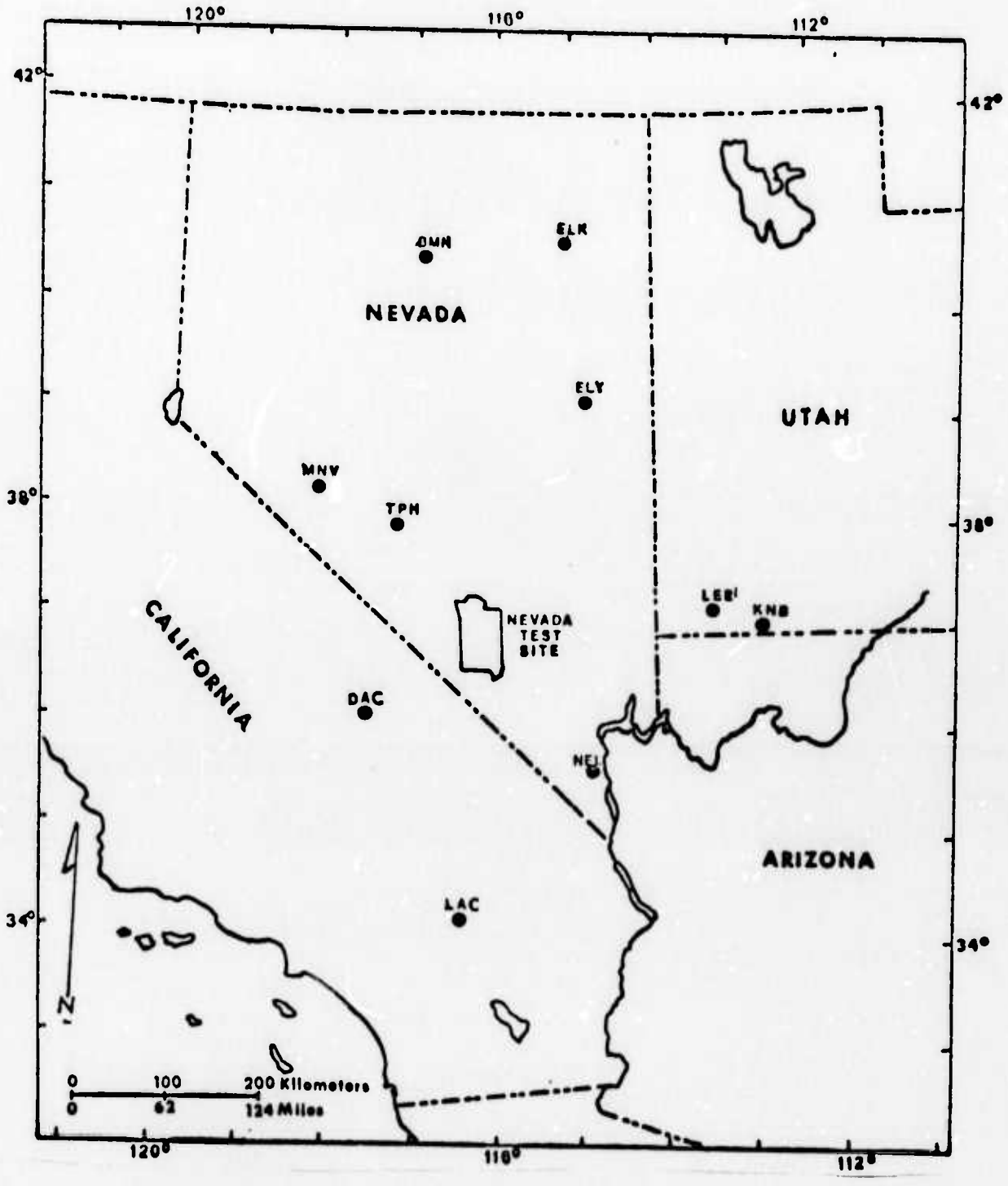

Figure 9. Location of Nevada Test Site and Lawrence Livermore (ELK, KNB, MNV, and LAC) and Sandia (BMN, DAC, ELY, LEE, NEL, and TPH) stations.

TABLE 4

Geodetic Coordinates of the LLL and Sandia Laboratories Seismic Stations Used in this Study and their Azimuth and Distance with Respect to the Nuclear Explosion BLENTON/THISTLE

STATION	CODE	GEODETIC COORDINATES	AZIMUTH WITH RESPECT TO BLENTON	DISTANCE TO BLENTON (km.)
Elko, Nevada	ELK	40°44'41.4"N 115°14'19.6"W	09°08'59.7"	412.24
Kanab, Utah	KNB	37°00'59.8"N 112°49'20.7"W	90°29'18.9"	283.91
Lander, California	LAC	34°23'23.2"N 116°22'36.0"W	186°59'13.2"	300.79
Mina, Nevada	MNV	38°25'56.0"N 118°09'15.8"W	309°06'42.7"	240.95
Battle Mountain, Nevada	BMN	40°25'53.3"N 117°13'18.4"W	344°36'46.2"	386.45
Darwin, California	DAC	36°16'37.2"N 117°35'37.2"W	238°09'25.3"	167.05
Ely, Nevada	ELY	39°07'52.8"N 114°53'31.2"W	23°02'41.9"	247.95
Leeds, Utah	LEE	37°14'34.8"N 113°22'36.0"W	84°49'03.1"	234.94
Nelson, Nevada	NEL	35°42'44.0"N 114°50'37.0"W	145°00'34.6"	184.75
Tonopah, Nevada	TPH	38°04'29.0"N 117°13'21.0"W	316°16'34.6"	153.54

response for each of these instruments is given in Figure 10. A summary of the records used in this study is given in Table 5. The records indicated by this table were selected on the basis of record quality and availability.

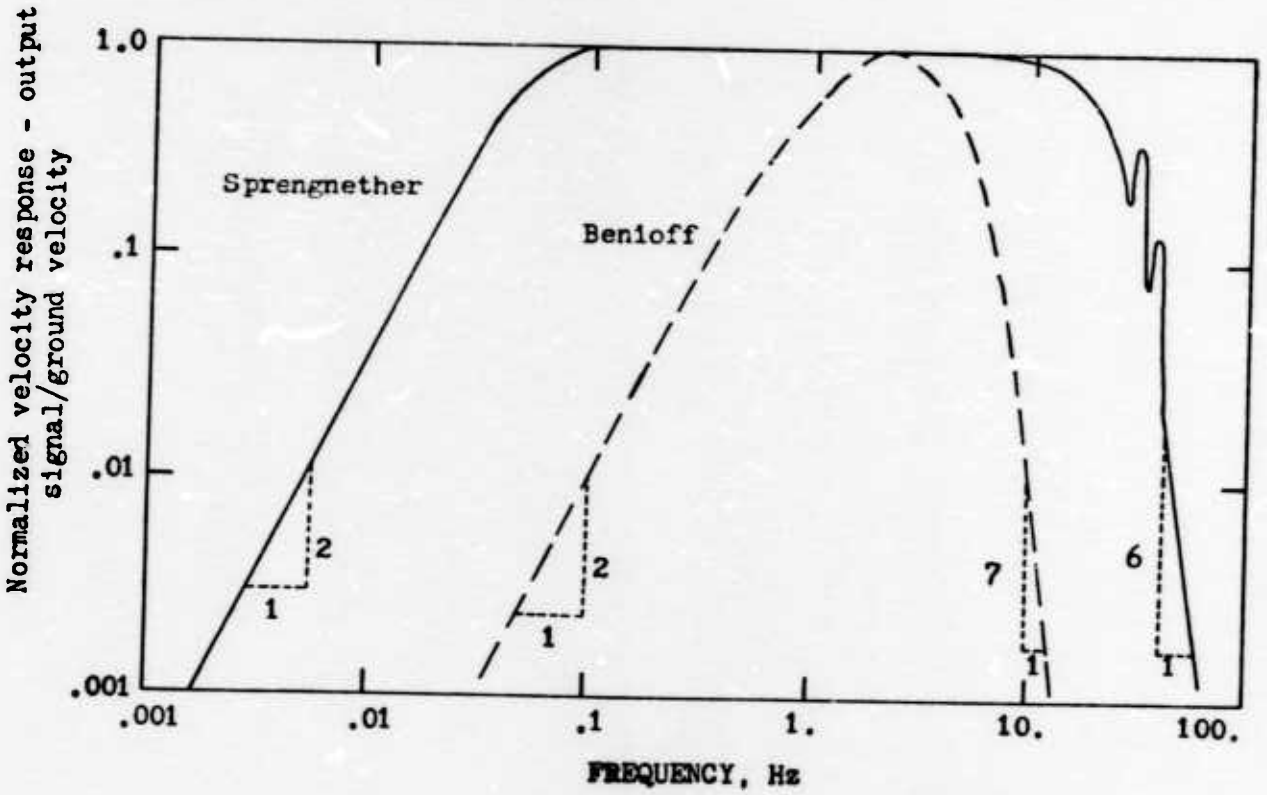

Figure 10. Amplitude response of the Sprengnether and Benioff seismic systems. (from Powel and Fries, 1964).

TABLE 5

Summary of the Records Used in this Study

	Massachusetts Mountain Earthquake	BLENTON/THISTLE	DIDO QUEEN	EVENT A	EVENT B	EVENT C	EVENT D	EVENT E	EVENT F
ELK	X				X		X		
KNB	X	X				X	X	X	
LAC	X	X		X	X	X	X	X	X
MNV	X			X	X	X	X	X	X
BMN		X		X	X				
DAC		X	X	X	X	X	X	X	
ELY		X		X	X	X	X	X	
LEE		X	X		X	X	X	X	
NEL		X		X	X	X	X	X	
TPH		X			X		X	X	

Digital Analysis

Approximately 30 seconds of the P-wave and P-wave coda for all records were digitized with a Computer Equipment Corporation digitizer. The initial digitization was performed at unequally spaced intervals in order to obtain maximum information from the records while minimizing digitizing efforts. The unequally spaced data was then linearly interpolated at equal 0.05 second increments to facilitate computer processing. This uniform rate of sampling yields a folding (or Nyquist) frequency f_N of

$$f_N = \frac{1}{2\Delta t} = \frac{1}{2(.05)} = 10 \text{ Hz.} \tag{28}$$

On the basis of electrical and material considerations, this Nyquist frequency is satisfactory.

The amplitude spectra, amplitude spectral ratios and the natural logarithm of the amplitude spectra of the data were calculated using a computer program which performs the operations schematized in Figure 11. The tapering operation was applied to smooth the ends of the data vector and is equivalent to the application of a tapered time window to the data set. The taper used is given by

$$T(J) = \begin{cases} \frac{1}{2}\left(1 + \cos \frac{\pi(J+2)}{3}\right), & J = 1,3 \\ 1, & J = 4, NP-3 \\ \frac{1}{2}\left(1 + \cos \frac{\pi(NP+3-J)}{3}\right), & J = NP-2, NP \end{cases} \tag{29}$$

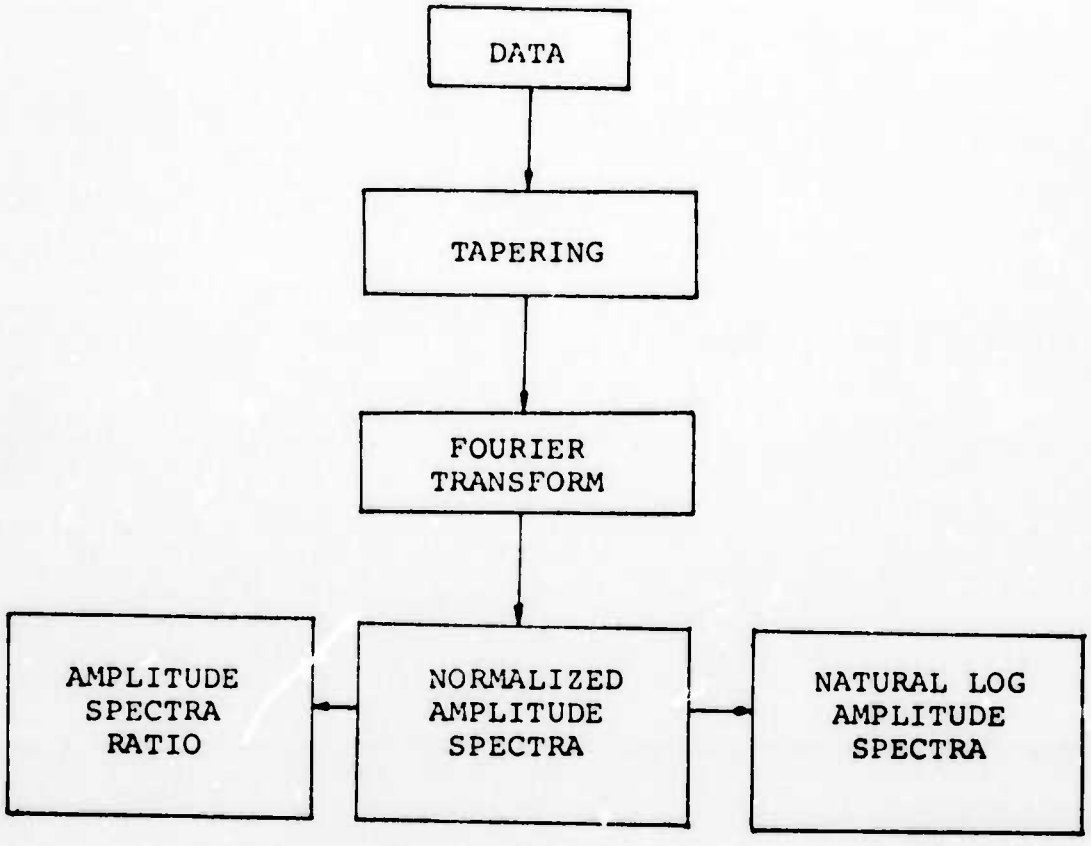

Figure 11. General flow chart of the spectral analysis computer program.

where NP is the number of points in the input data set. The Fourier transformation was accomplished with a FFT (Fast Fourier Transform) package due to Cooley and Tukey (1965).

The cross-correlations were calculated in the time domain with a computer program due to Taylor (1974). The cross-correlation program is conventional in all respects and utilizes the following definition of the cross-correlation at lag $N\Delta t$.

$$\phi_{XY}(N D\tau) = \frac{\left(\sum_{K=1}^{NX-N} X_{NX-N-K} - \bar{X} \times Y_K - \bar{Y} \right)}{\left| \sum_{K=1}^{NX} [X_K - \bar{X}]^2 \sum_{K=1}^{NY} [Y_K - \bar{Y}]^2 \right|^{1/2}} \qquad (30)$$

where

ϕ_{XY} = the cross-correlation

NX = the number of points in data set X

NY = the number of points in data set Y

$\bar{X}$ = the mean of data set X

$\bar{Y}$ = the mean of data set Y

Results

Spectral Analyses

For an $m_b = 5$ explosion with an assumed source radius of 0.6 km, detonated in material with a P-wave velocity of 2.5 km/sec, equation (27) yields a peak frequency of 0.63 Hz. The above parameters are typical of the events employed in this study and peak frequencies on the order of 0.63 Hz are, therefore, expected. From Figure 10 it is evident that this frequency falls within the pass-band of the Sprengnether system, used by the LLL stations, and no instrument correction is required. For the Benioff system, used by the Sandia Laboratories stations, Figure 10 indicates the expected frequency of approximately 0.63 Hz falls outside the -6 db point of the pass band. The slope of the amplitude spectra at frequencies less than f_o for the Sandia stations would clearly be determined by the low frequency roll-off of the sensing system and would be unrelated to signal characteristics. The system roll-off, thus, invalidates the use of low frequency displacement spectra slope, for the Benioff system, as a criterion of differentiation. While corrections for instrument response in these cases may have been possible, it was felt that the corrections over the required part of the band would enhance noise to an unacceptable level. For this reason only the LLL stations with their broad pass-bands were employed in the spectral characteristics portion of this study.

In order to clearly define the corner frequencies in the displacement spectra, broad band frequency information is required. The amplitude spectra of all events considered here were determined for frequencies from DC to 10 Hz. This band, however, exceeds the signal band and the spectra are, therefore, presented over the range from .04 Hz to 3 Hz.

The natural logarithm of the amplitude spectra, uncorrected for instrument effects, versus the natural logarithm of the frequency for five typical events are shown in Figures 12 to 16. The spectra for all other remaining event-station combinations are included in Appendix A. The single nuclear event, DIDO QUEEN, was not used here since LLL records were not available for this event. The corner frequencies obtained from these spectra are summarized in Table 6. The apparent source radii were calculated from the observed corner frequencies for spectra and assumed P-wave velocities of 3.4 km/sec for the Massachusetts Mountain earthquake, 1.4 km/sec for the nuclear explosions fired in alluvium, and 2.4 km/sec for those detonated in tuff. The calculated source radii for all events are summarized in Table 7. The average radius for each event, obtained from the data of Table 7, is shown with the corresponding depth and magnitude of the event in Table 8. It is evident from Table 8 that although the magnitude of the Massachusetts Mountain earthquake is less

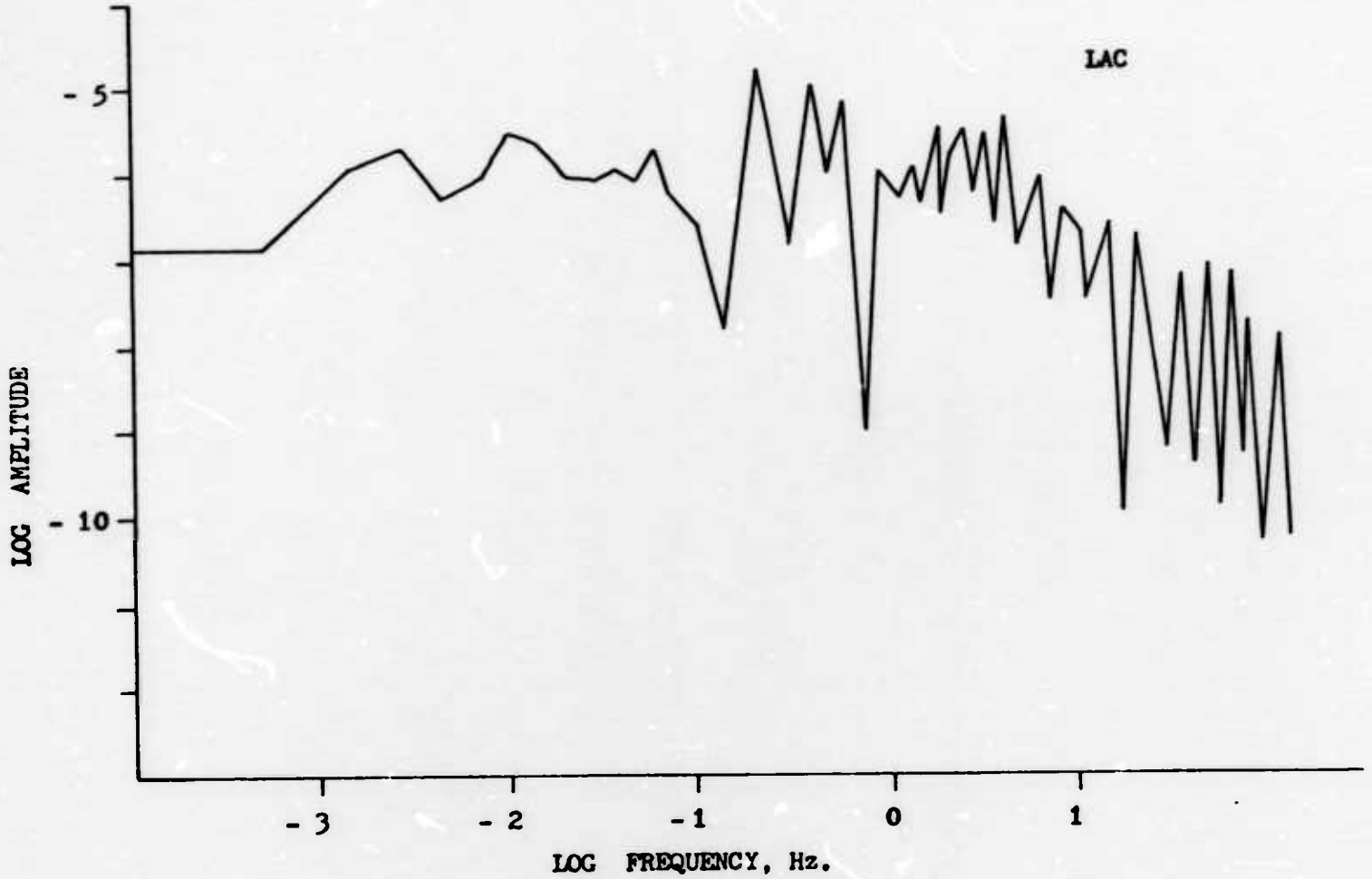

Figure 12. Displacement spectrum of Massachusetts Mountain earthquake for KNB station ($\log_e$ 2.7, Hz = 0).

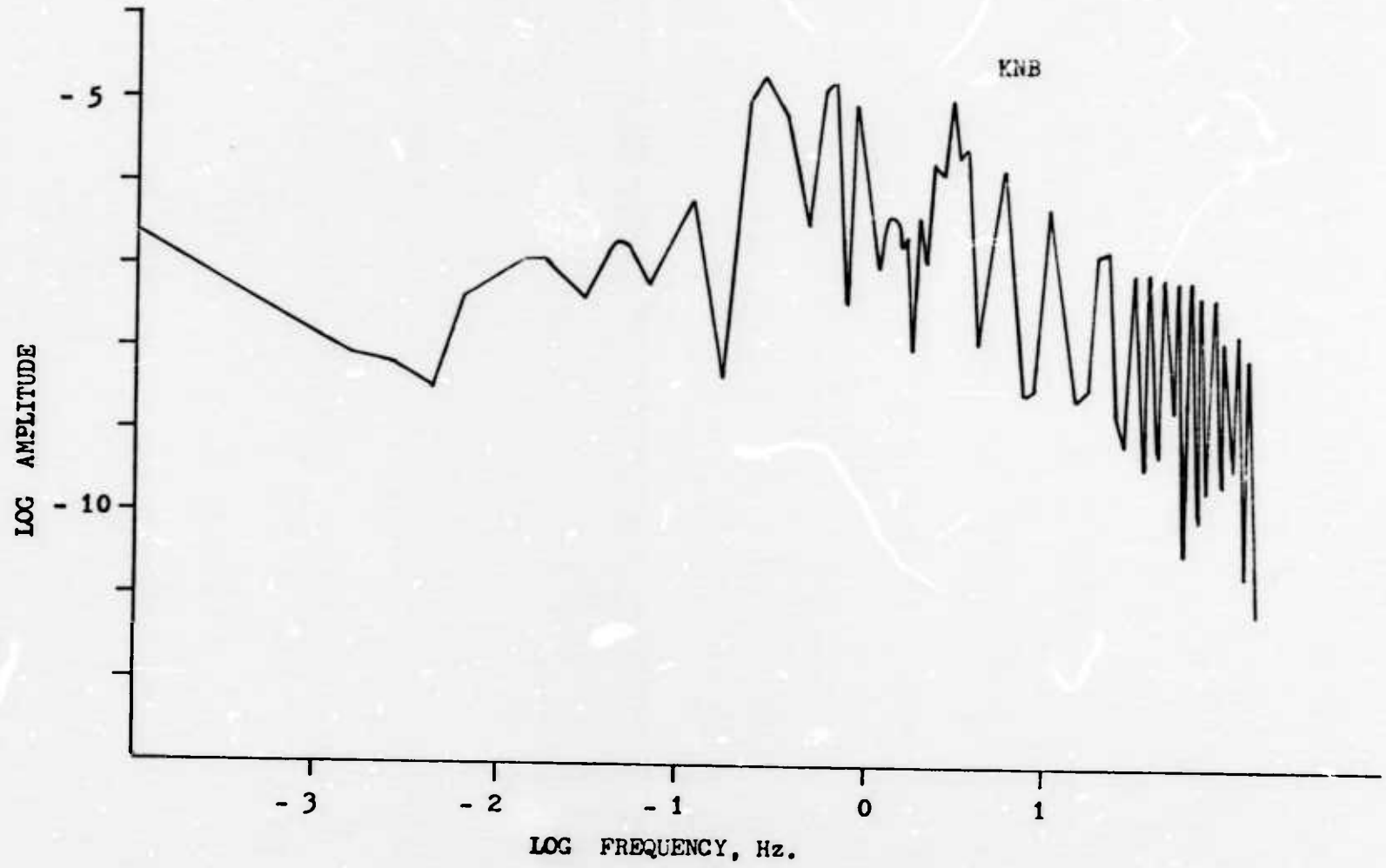

Figure 13. Displacement spectrum of BLENTON/THISTLE explosion for KNB station ($\log_e$ 2.7, Hz = 0).

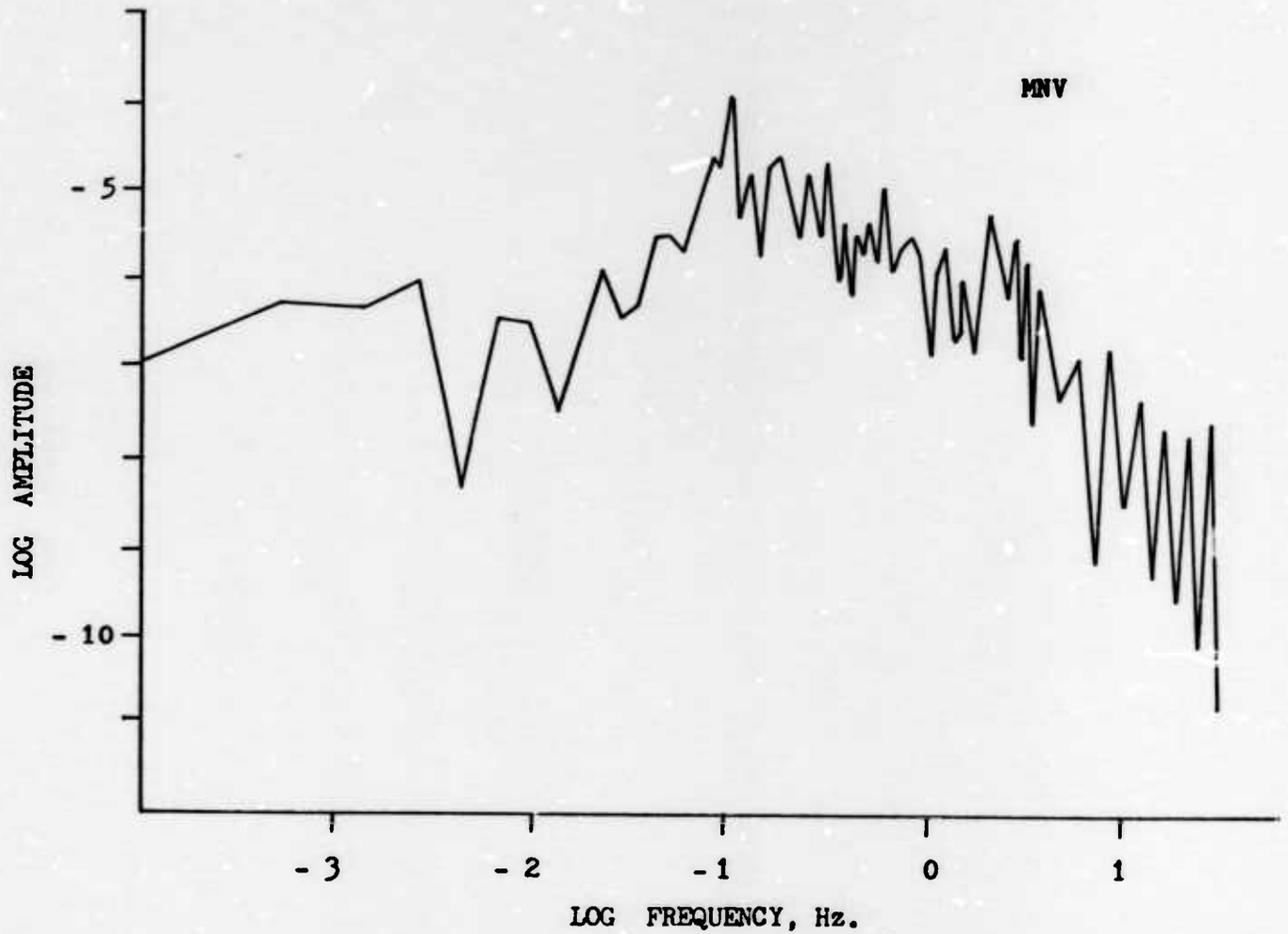

Figure 14. Displacement spectrum of Event A for MNV station ($\log_e$ 2.7, Hz = 0).

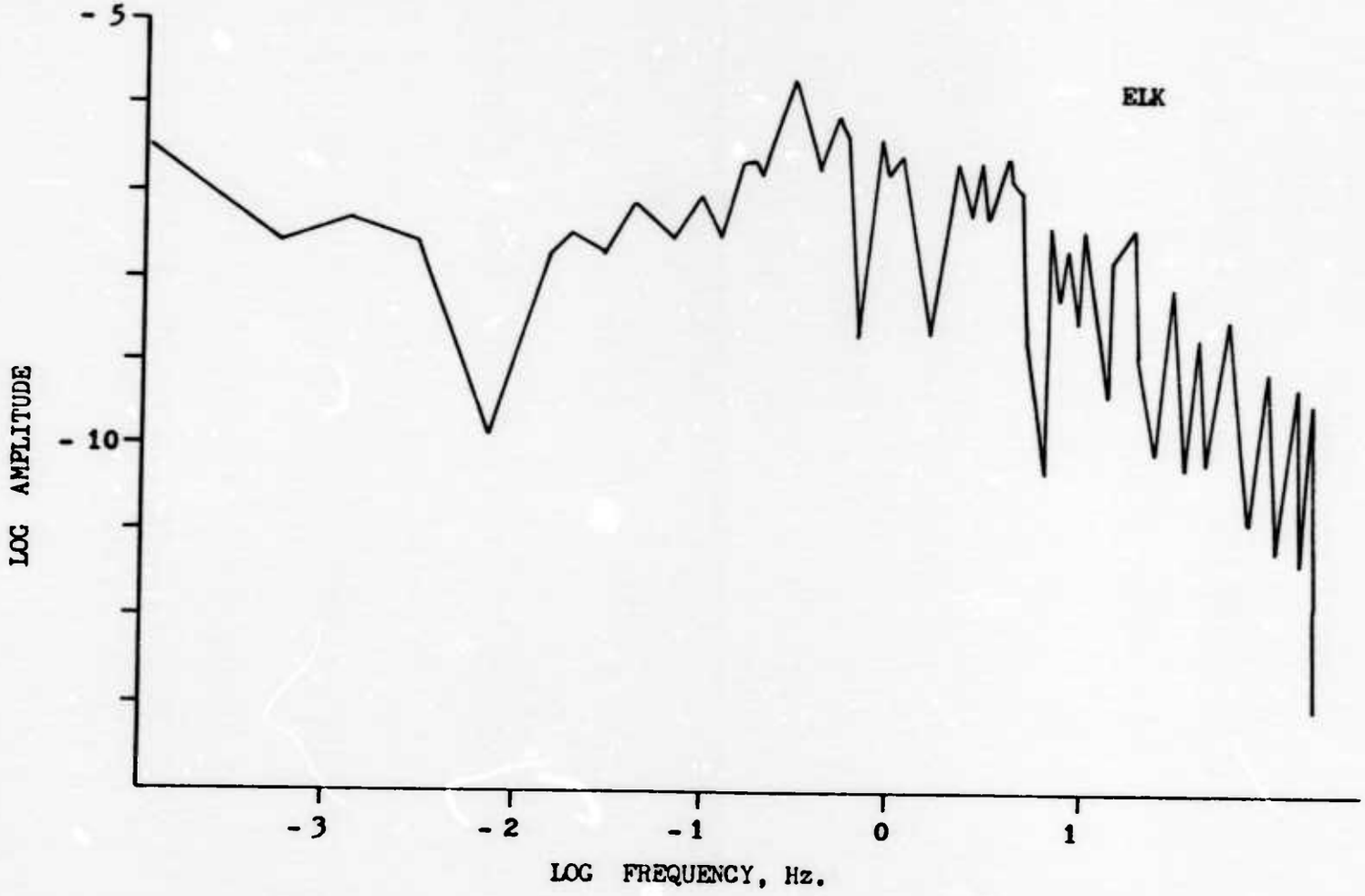

Figure 15. Displacement spectrum of Event B for ELK station ($\log_e$ 2.7, Hz = 0).

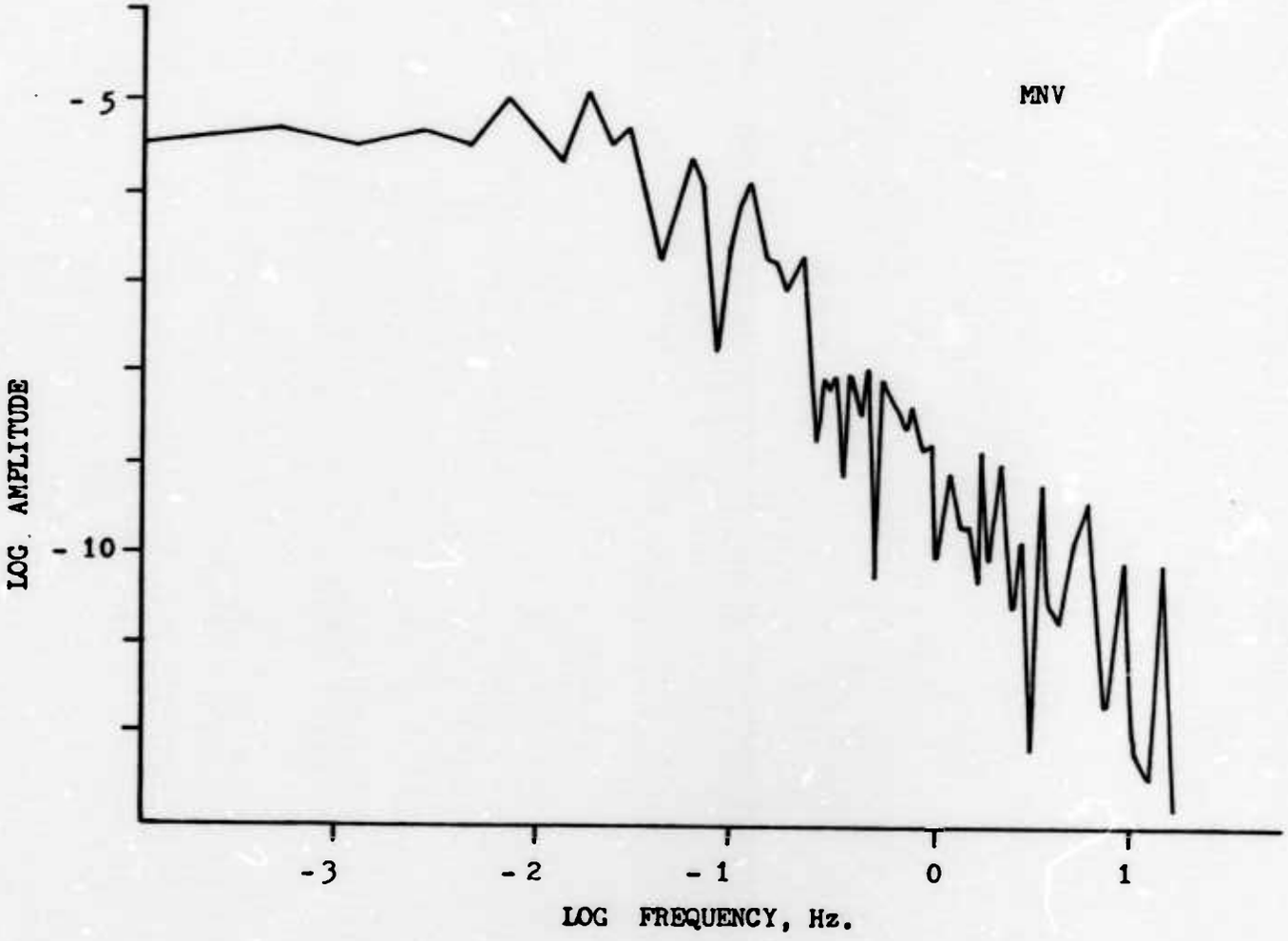

Figure 16. Displacement spectrum of Event F for MNV station ($\log_e$ 2.7, Hz = 0).

TABLE 6

Corner Frequency of Massachusetts Mountain Earthquake and Nuclear Explosions BLENTON/THISTLE, A, B, C, D, E and F for the LLL Stations

	f_o (Hz)								
Station	Mass. Mt.	BLENTON/ THISTLE	Event A	Event B	Event C	Event D	Event E	Event F	Event F*
ELK	1.08	-	-	.56	-	.60	-	-	-
KNB	1.08	.84	-	-	1.80	.80	.80	-	-
LAC	1.00	.72	.76	.76	1.32	.80	.96	.36	.36
MNV	1.12	-	.76	.76	1.04	1.00	1.00	.36	.36

* This result has been obtained considering Event F as an earthquake.

TABLE 7

Source Radius of Events Massachusetts Mountain Earthquake, Nuclear Explosions BLENTON/THISTLE, A, B, C, D, E and F for the LLL Stations

	r (km.)								
Station	Mass. Mt.	BLENTON/ THISTLE	Event A	Event B	Event C	Event D	Event E	Event F	Event F*
ELK	1.1	-	-	.64	-	.60	-	-	-
KNB	1.1	.433	-	-	.28	.45	.26	-	-
LAC	1.2	.506	.28	.48	.35	.45	.22	1.00	3.33
MNV	1.0	-	.28	.48	.45	.36	.21	1.00	3.33

* This result has been obtained considering Event F as a nuclear explosion.

TABLE 8

Average Source Radius, Depth, and Magnitude (m_b)
of Massachusetts Mountain Earthquake and Nuclear Explosions
BLENTON/THISTLE, A, B, C, D, E and F

Event	Average Source Radius (km.)	Depth (km.)	Magnitude (m_b)
Massachusetts Mountain	1.1	4.6	4.3
BLENTON/THISTLE	.47	.56	5.3
EVENT A	.28	.24	4.7
EVENT B	.50	.56	5.6
EVENT C	.36	.31	5.0
EVENT D	.47	.44	5.3
EVENT E	.23	.39	5.3
F (as an explosion)	1.00	.24	?
F (as an earthquake)	3.33	?	?

than the magnitude of the nuclear explosions, its average source radius is clearly greater. It was previously noted that Event F consisted of a natural earthquake arrival preceding the shot arrival. This is clearly suggested in Table 8, indicating a source radius too large for a nuclear event of this magnitude.

The source radii versus depth and magnitude are plotted in Figures 17 and 18. It is interesting to note that for all explosions with the exception of Event E, the average source radius and the corresponding depth are of the same magnitude. The same relation has been found by Wyss and others (1971) for the MILROW nuclear explosion which was fired at a depth of 1.2 km in a calculated source radius of 1.25 km. These authors have suggested that the coincidence between the elastic source radius and the depth of the event could be due to a restraining effect that the free surface exerted upon the elastic source dimension. It is also apparent by inspection of Figure 18, in which the calculated elastic source radius of events BLENTON/THISTLE, A, B, C, D and E are plotted versus the corresponding magnitudes, that with the exception of Event E, an increase in the magnitude of the event is associated with an increase of the calculated equivalent elastic source radius.

A difference in the slope of the displacement spectra for the band from .20 Hz to the corresponding peak

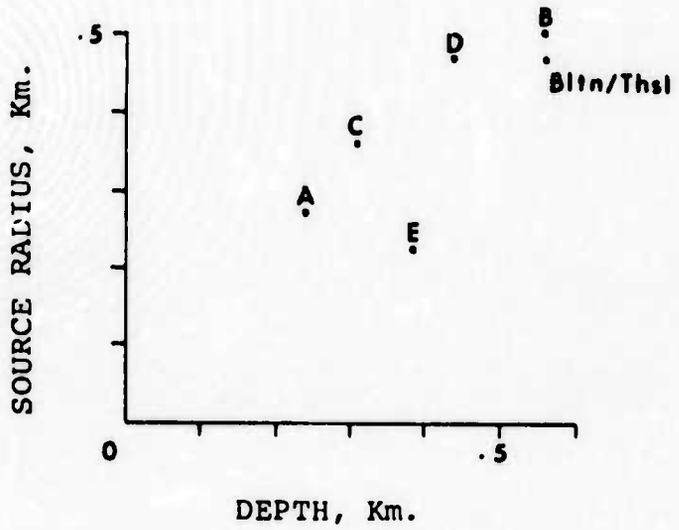

Figure 17. Average source radius of BLENTON/THISTLE, A, B, C, D and E events versus depth of each event.

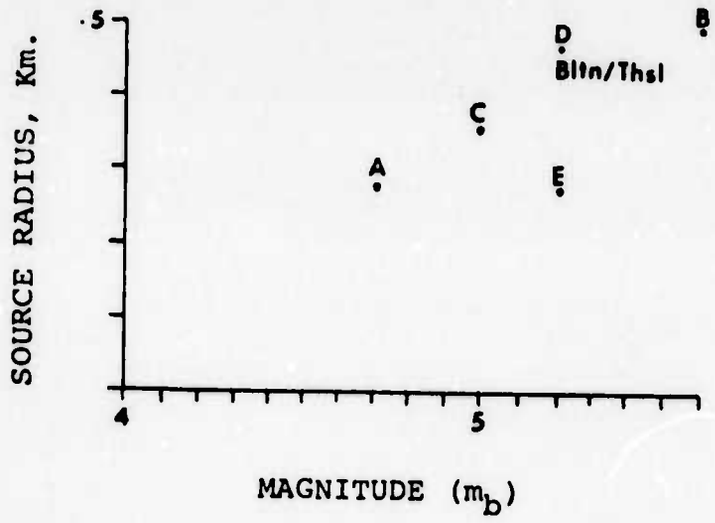

Figure 18. Average source radius of BLENTON/THISTLE, A, B, C, D and E events versus magnitude of each event.

frequency for the Massachusetts Mountain earthquake and the nuclear explosions is evident from Figures 12 to 16. An inspection of the remaining displacement spectra in Appendix A clearly establishes the consistency of this difference. The mean slope of the earthquake in the .04 to peak frequency band is near zero, while the slopes of the nuclear shots are clearly positive. Event F is again an exception to this but, as previously noted, the initial arrivals for the event were the result of an earthquake. This difference in the behavior of the displacement spectra for long periods has been observed by Wyss and others (1971). Those authors suggested that the flatness of the displacement spectrum of an earthquake at low frequencies is indicative of a step function at the source, while the faster deterioration of the explosion's displacement spectra could be related to the depth of the source and its time function. On the basis of these limited cases, the slope of the low frequency part of the displacement spectra is clearly a differentiating quantity.

Special attention has been given to Event F due to the fact that it is a "mixture" of an earthquake that occurred at teleseismic distance and a nuclear detonation. It is evident from the displacement spectra of this event (Figure 16) that its low frequency behavior is that of a typical earthquake. The source dimension for Event F was calculated considering its dual nature as a nuclear

explosion and earthquake. The results are given in Tables 7 and 8. Since the earthquake occurred at teleseismic distance, correction for attenuation should be applied, and the 3.33 km obtained for its source radius is of an approximate nature. Nevertheless, its calculated source radius clearly indicates an earthquake. The source dimension obtained by considering the event as being only a nuclear explosion is 1.1 km and although its magnitude was not known, this radius appears to be too large for an explosion with a depth of .24 km, therefore suggesting an earthquake.

With the techniques considered here, it does not appear possible to detect the presence of the shot, although it should be noted that no attempt was made in this study to extract the nuclear explosion from the record. A possible explanation of the earthquake-type behavior of the displacement spectra of Event F can be made by assuming the low frequencies result primarily from the earthquake. In this sense the event should be considered an earthquake rather than an underground explosion. On this basis, the event lends significance to the use of spectral slope and source radii as methods of identification.

A careful examination of the spectra for all nuclear events will show that a strong peak occurs consistently at about .16 Hz. In the few exceptions which do exist, a strong peak does appear in the neighborhood of .16 Hz.

This peak is probably unrelated to any characteristic of the events and is due instead to the seismic background noise. . The existence of a peak in the spectrum of ground noise at a frequency of .16 Hz has been established by Brune and Oliver (1959) and Brune (1971).

Records of the single explosion DIDO QUEEN from the LLL stations were unfortunately not available and comparative studies of the behavior in terms of the logarithm of the spectra of single and double explosive sources could not be accomplished. For the sake of completeness, the logarithm of the spectra of some nuclear detonations from the Sandia Laboratories stations, BMN, ELY, NEL and TPH are shown in Figures 19 to 22. These spectra exhibit a positive slope in the long period range, but due to the narrow band of the recording equipment, much of the behavior of the spectra in the lower range of frequencies is conditioned by the amplitude response of the seismic system. Therefore, no consideration has been given to these spectra in the calculation of the source radius.

In an attempt to investigate the possibility of a multiple explosive nature for Events A to E, the expressions of the modulation factor given in the Theory section by equations (7) and (10) were calculated for various assumed values of the delay times ΔT_1, ΔT_2, and ΔT_3. Typical forms of the resulting modulation function are shown in Figure 23. It is evident from this figure that

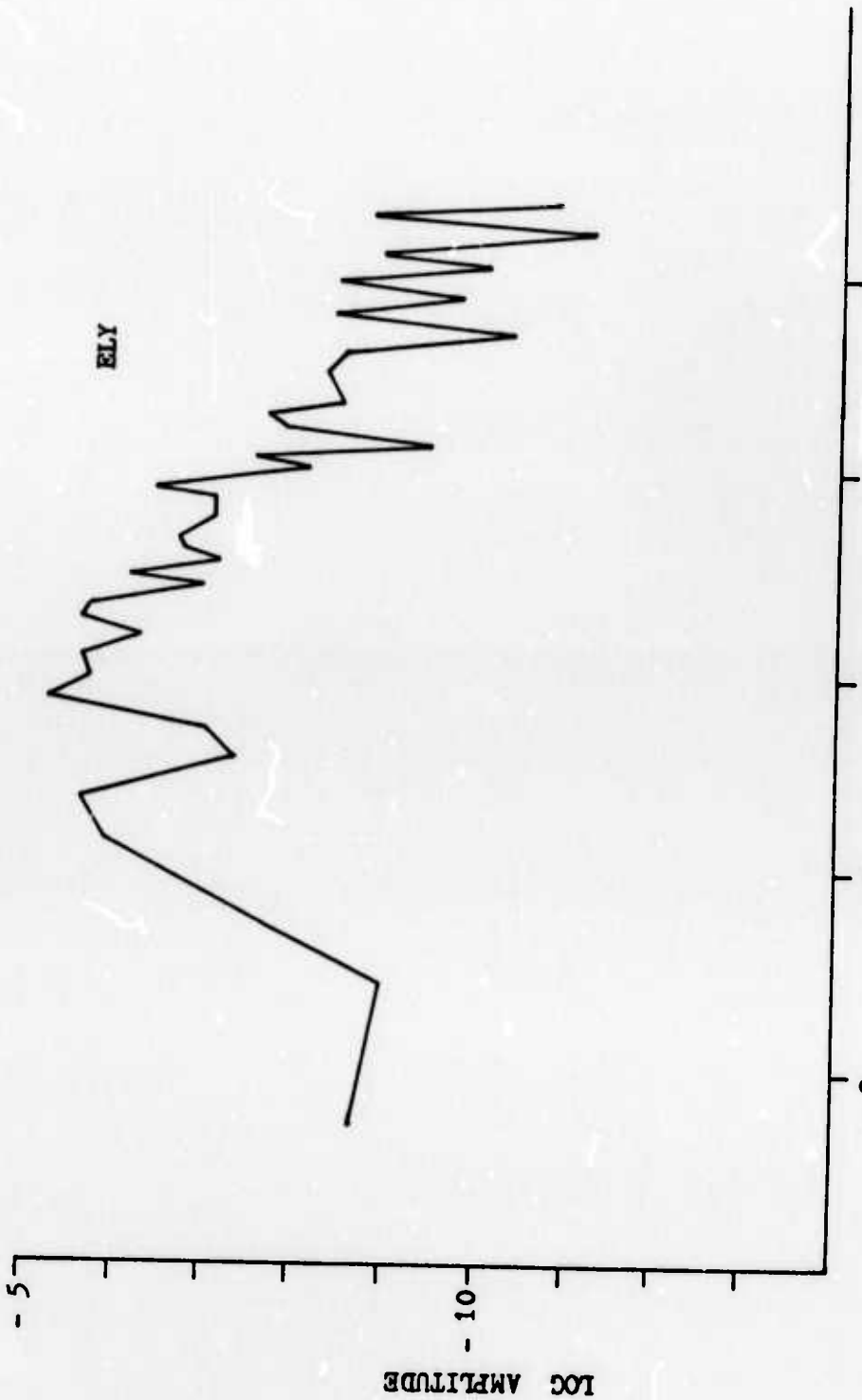

Figure 19. Displacement spectrum of Event A for ELY station ($\log_e$ 2.7, Hz = 0).

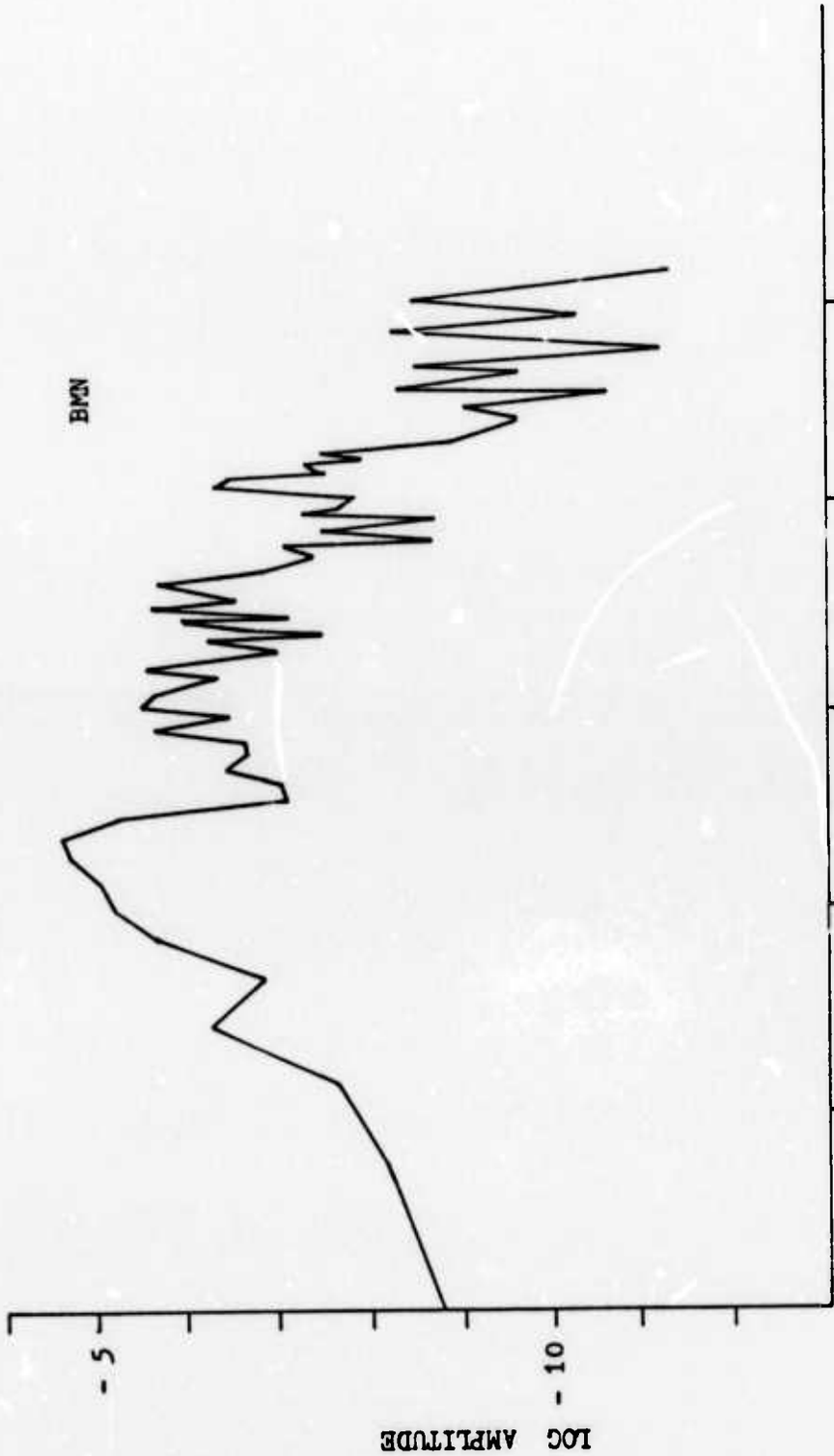

Figure 2[illegible]. Displacement spectrum of Event B for BMN station ($\log_e$ 2.7, Hz = 0).

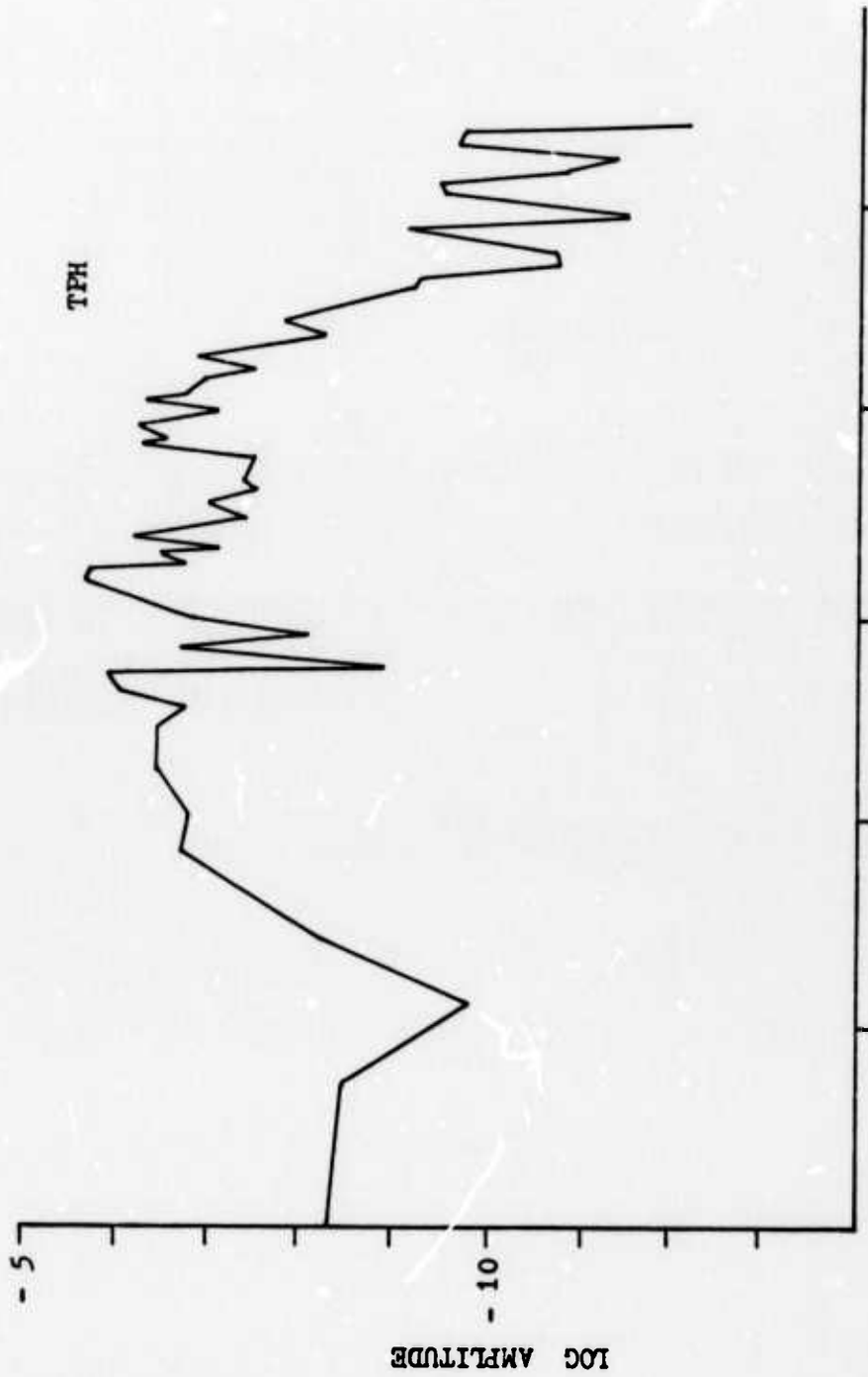

Figure 21. Displacement spectrum of Event D for TPH station ($\log_e$ 2.7, Hz = 0).

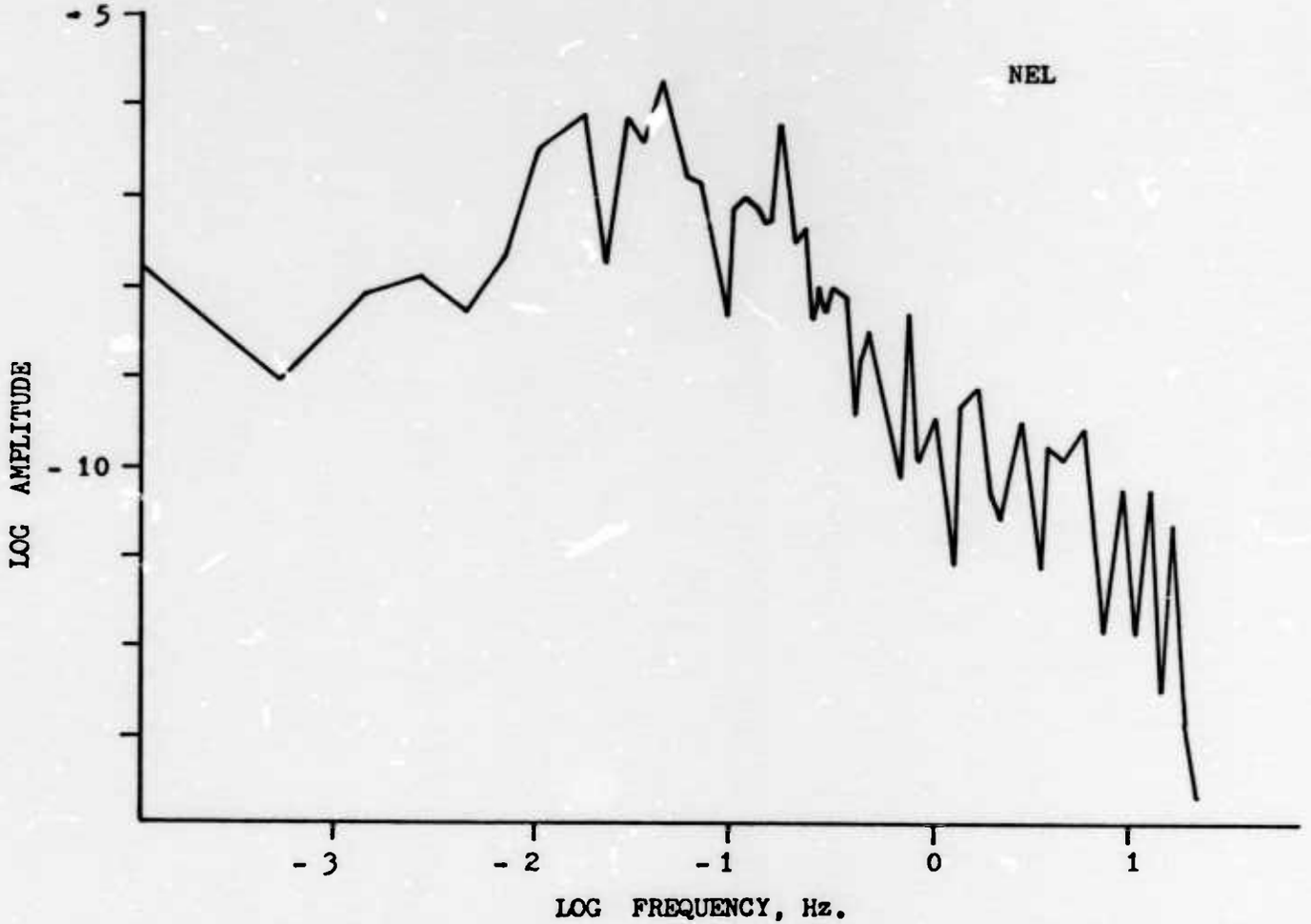

Figure 22. Displacement spectrum of Event E for NEL station ($\log_e$ 2.7, Hz = 0).

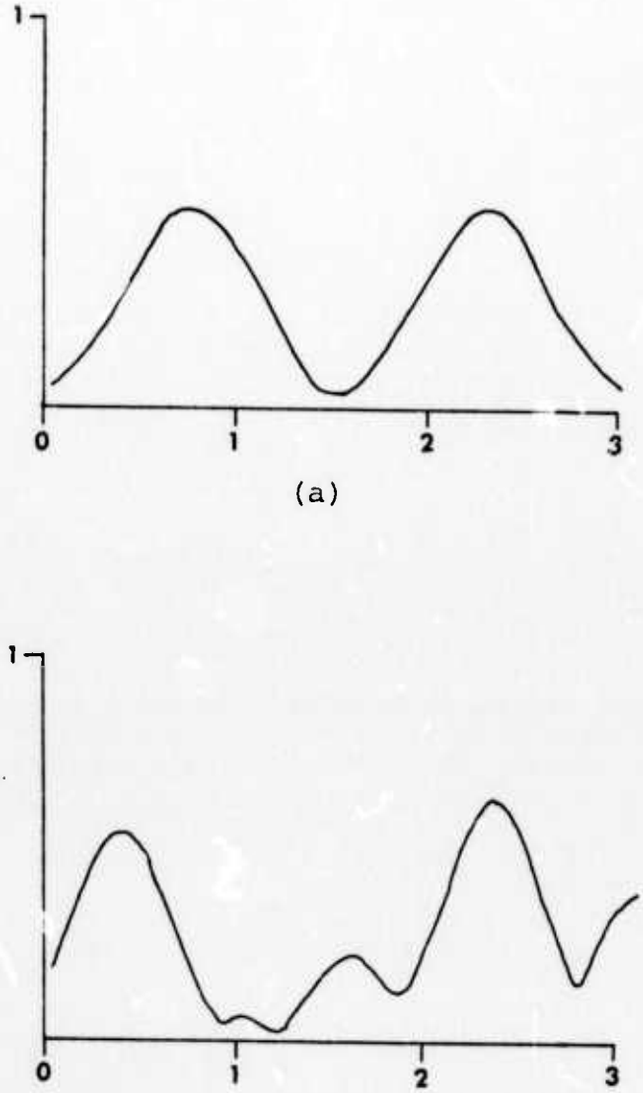

Figure 23. Typical form of the theoretical modulation functions. (a) single explosion; (b) double explosion.

the modulation function is highly dependent on the delay times and is not a slowly varying function. The theoretical modulation function was then compared to the actual amplitude spectra of each event. Attempts were then made to match the peaks and troughs of the modulation function with the envelope of the signal spectra by trial and error changes in the assumed values of ΔT_1, ΔT_2 and ΔT_3.

Examples of the amplitude spectra for which a seemingly suitable modulation function was found are shown in Figures 24 to 33. In the remaining cases no reasonable modulation function could be found. In Table 9, the times of the different arrivals are given and also their character found with the modulation functions which, in general, appear to be consistent with those found by Cepstrum Analysis (Zimdars, 1974). It is obvious from Figures 24 to 33 that complex modulation effects are contained in the amplitude spectra. As discussed in the Theory section of this investigation, the causes of the modulations are varied and difficult to evaluate, if not impossible. This, coupled with the first order approach that constitutes the empirical models for the modulation functions used in this study, makes the assumed times and their polarity highly speculative. Nevertheless, the results of this approach complement the other results.

The amplitude spectra considered here result from the combined actions of the source function and propagation

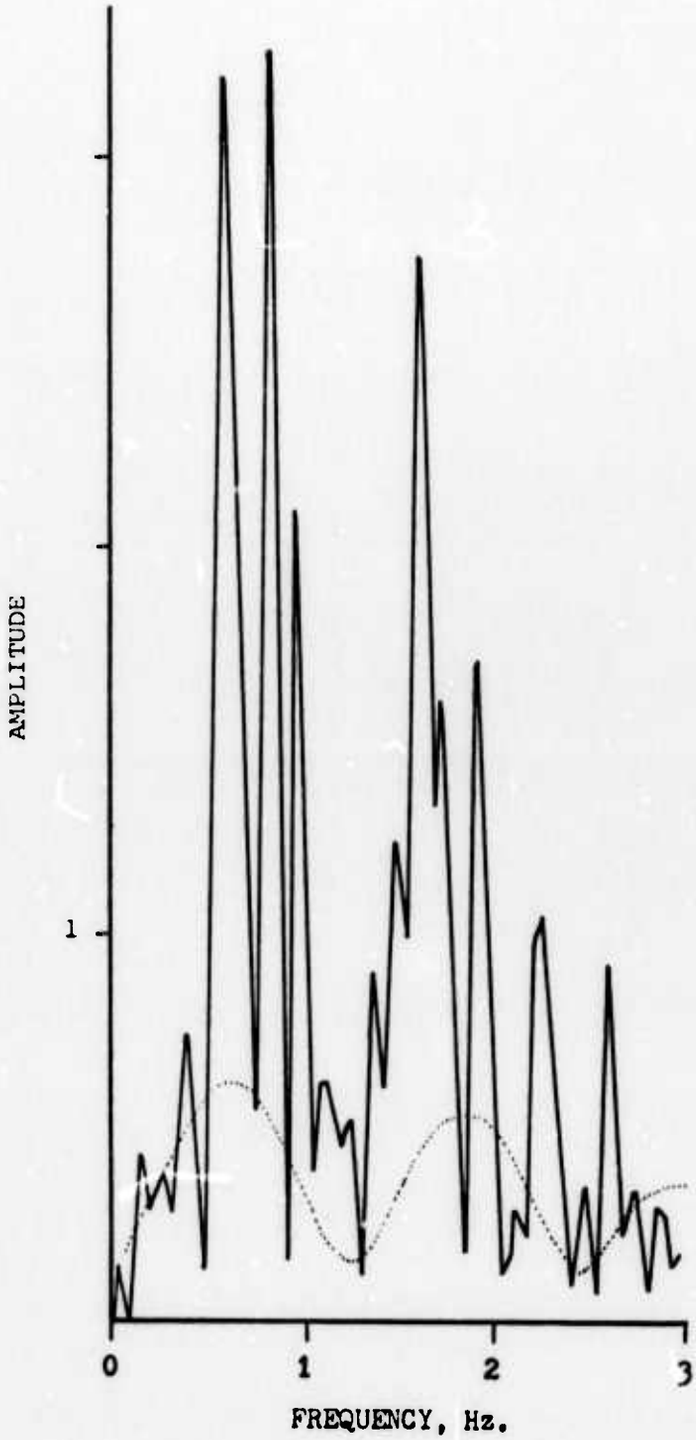

Figure 24. Amplitude spectrum of BLENTON/THISTLE explosion (solid line) and modulation function (dotted line) for KNB station.

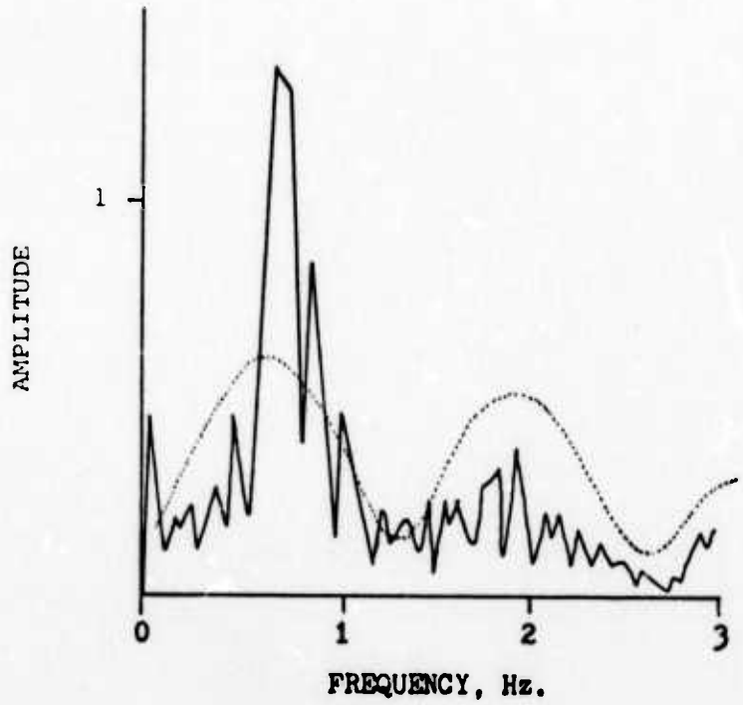

Figure 25. Amplitude spectrum of BLENTON/THISTLE explosion (solid line) and modulation function (dotted line) for LAC station.

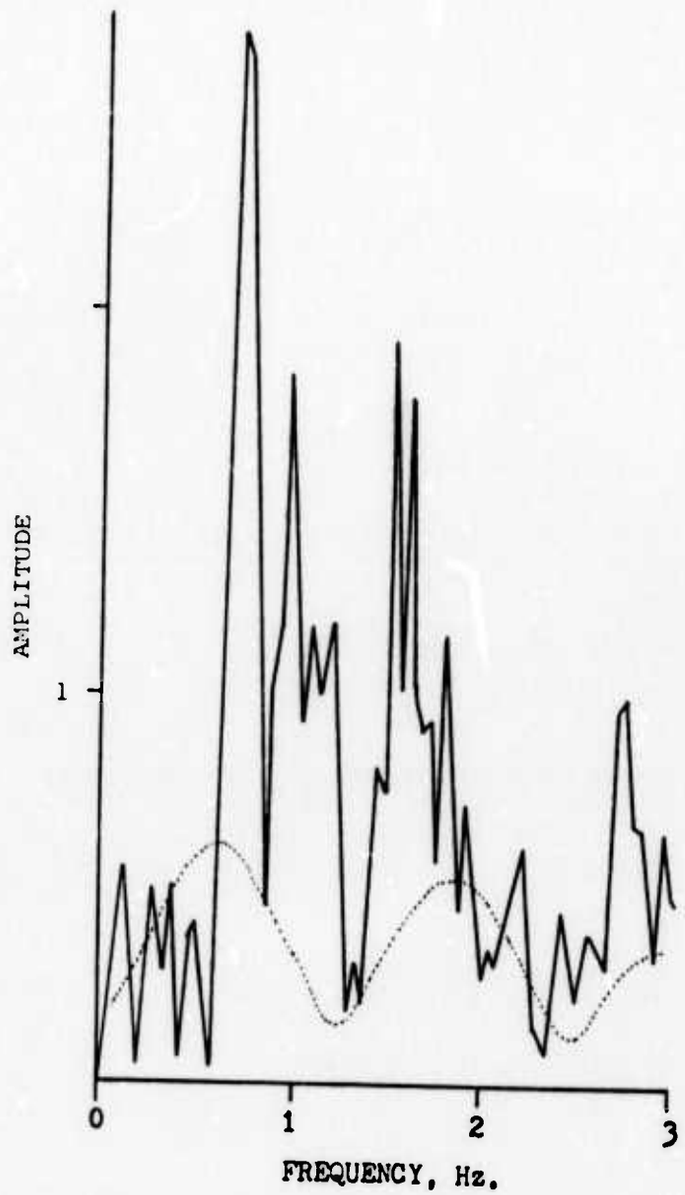

Figure 26. Amplitude spectrum of Event A (solid line) and modulation function (dotted line) for MNV station.

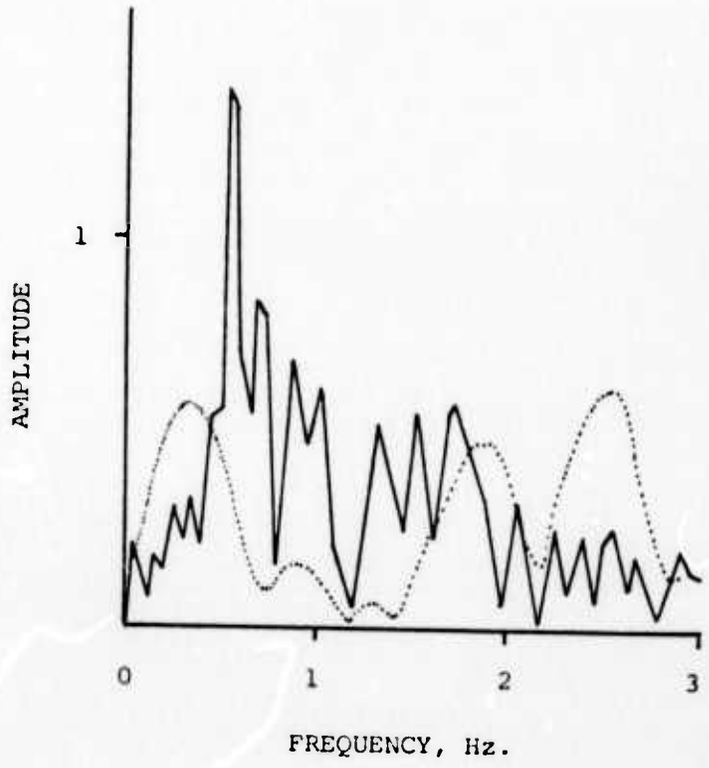

Figure 27. Amplitude spectrum of Event B (solid line) and modulation function (dotted line) for ELK station.

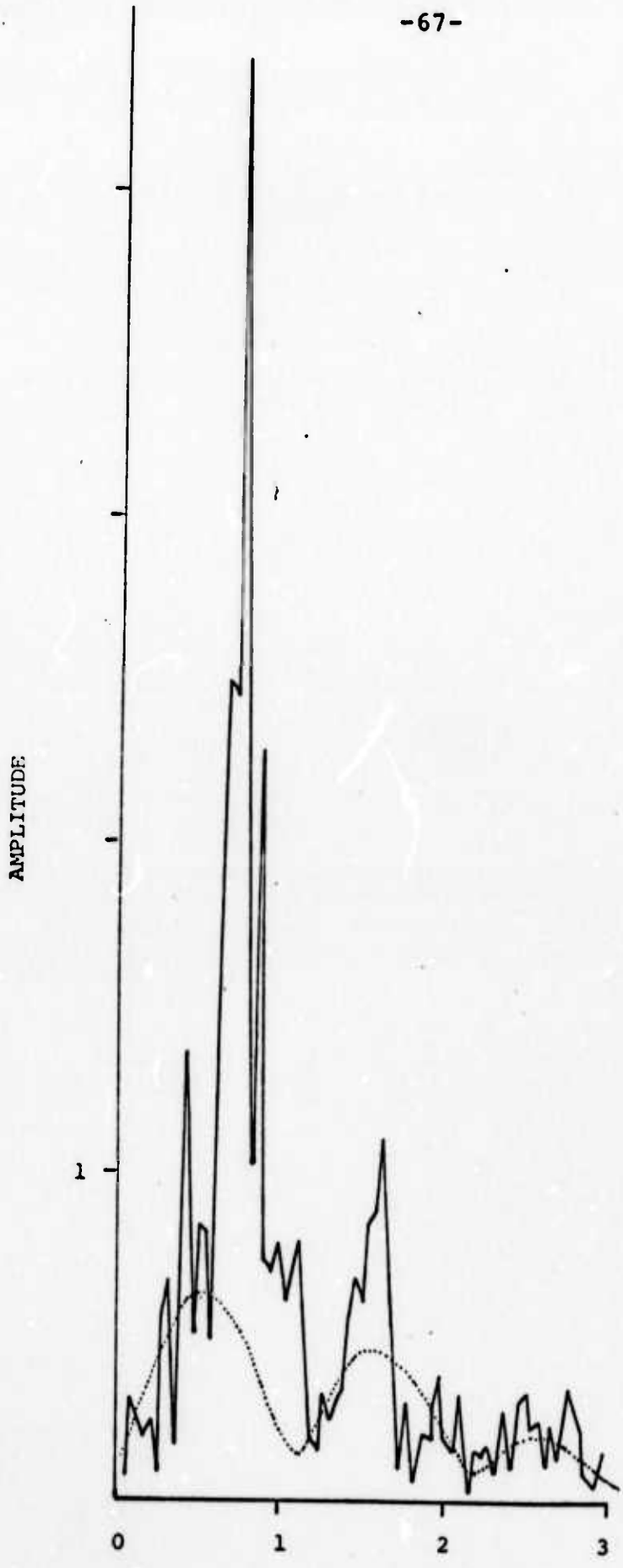

Figure 28. Amplitude spectrum of Event B (solid line) and modulation function (dotted line) for LAC station.

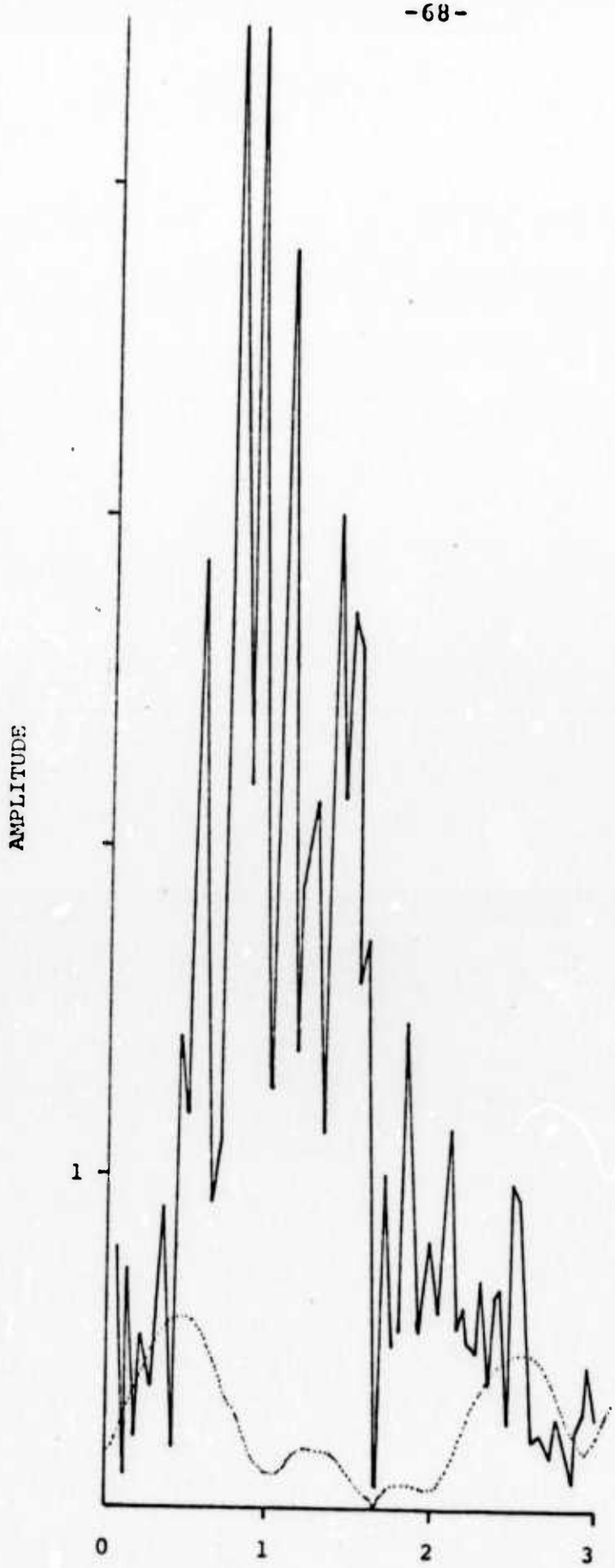

Figure 29. Amplitude spectrum of Event B (solid line) and modulation function (dotted line) for MNV station.

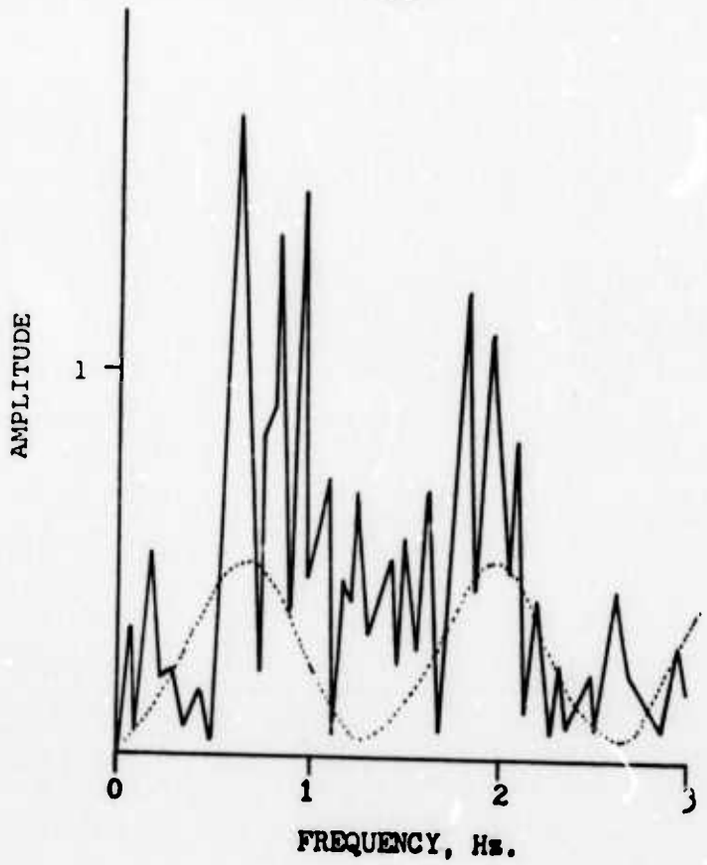

Figure 30. Amplitude spectrum of Event C (solid line) and modulation function (dotted line) for KNB station.

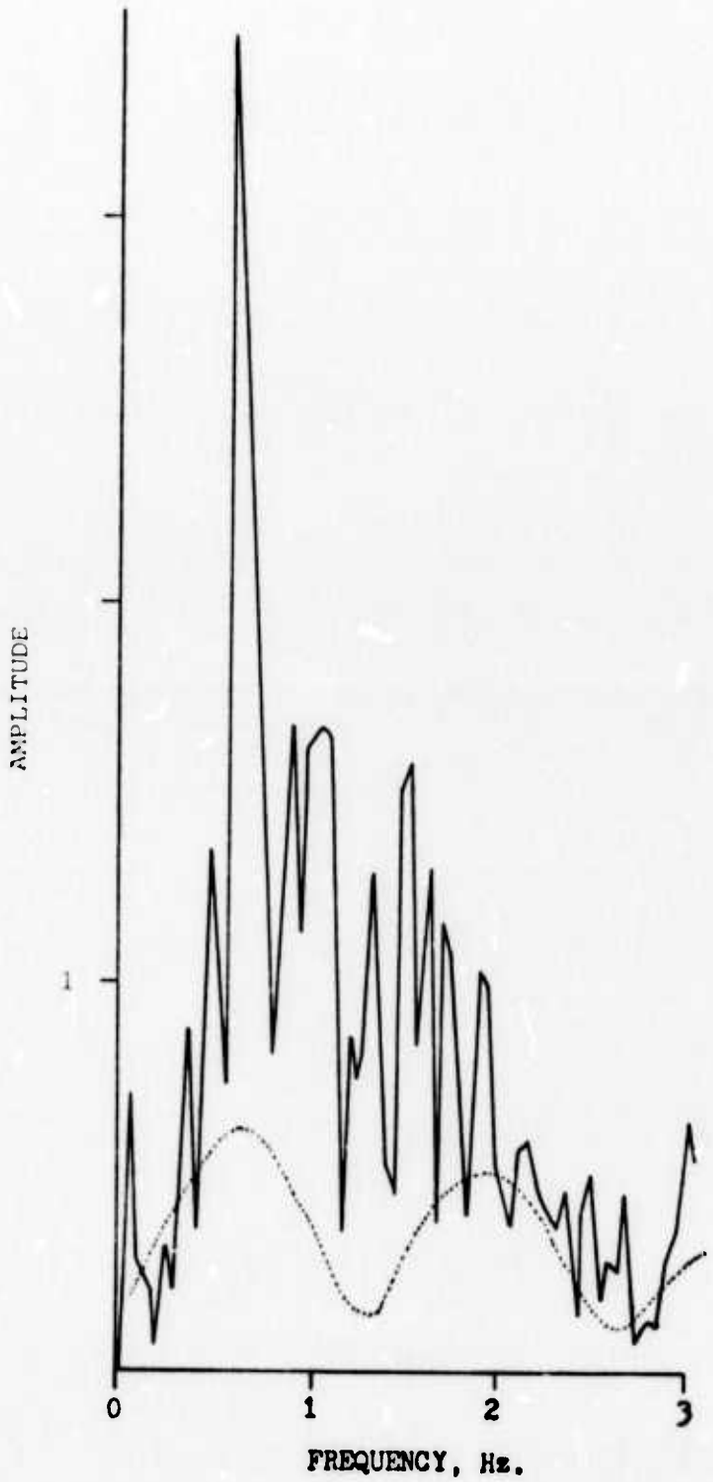

Figure 31. Amplitude spectrum of Event D (solid line) and modulation function (dotted line) for ELK station.

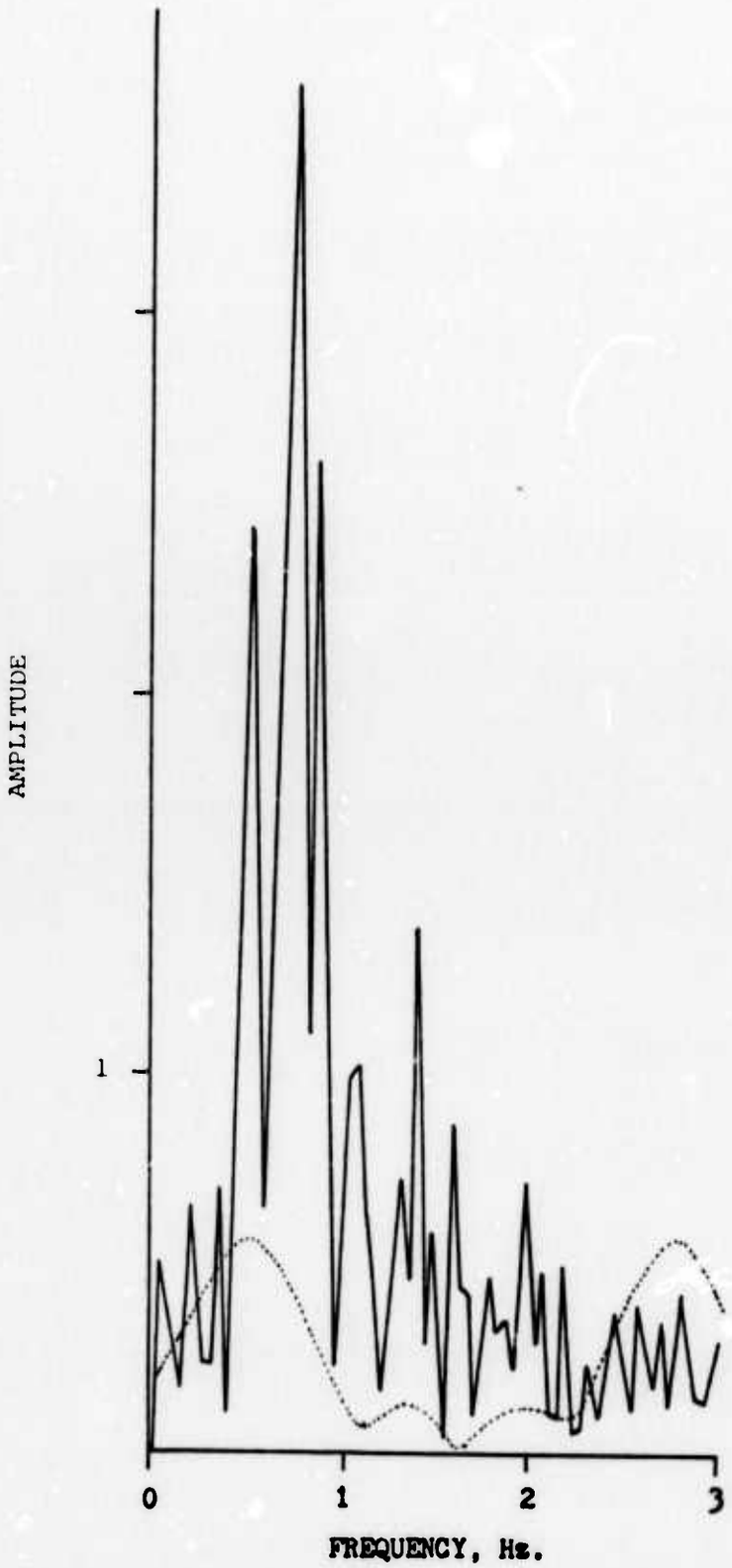

Figure 32. Amplitude spectrum of Event D (solid line) and modulation function (dotted line) for LAC station.

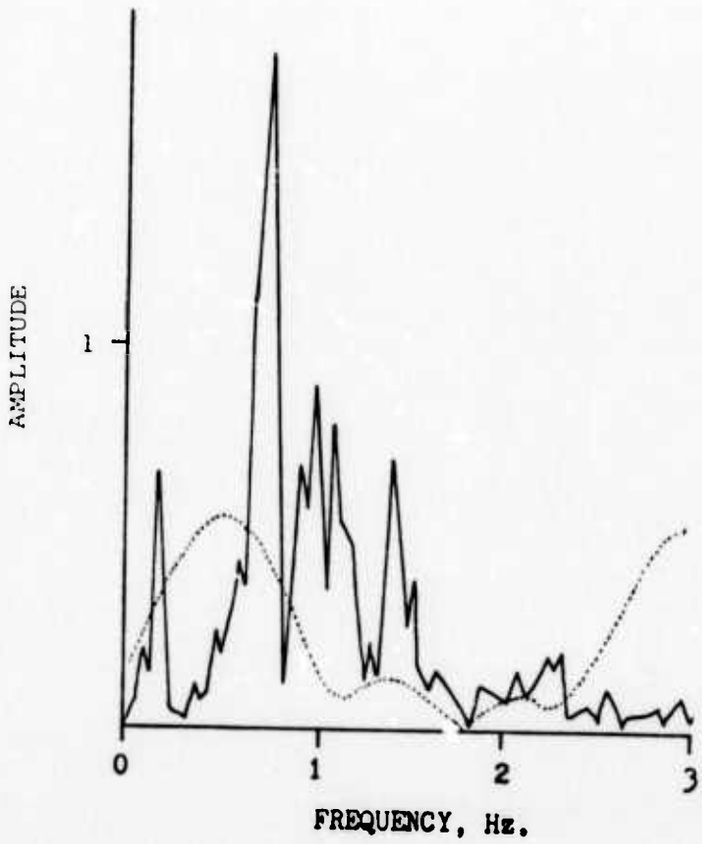

Figure 33. Amplitude spectrum of Event E (solid line) and modulation function (dotted line) for LAC station.

TABLE 9

Delay Time Values of the Arrivals and Their Polarities for Some Nuclear Detonations Found Using Theoretical Modulation Functions. The Times Given Are in Seconds.

	EVENTS														
	BLENTON/THISTLE			A			B			C			D			E		
STATION	P_2	pP_1	pP_2	P_2	pP_1	pP_2	P_2	pP_1	pP_2	P_2	pP_1	pP_2	P_2	pP_1	pP_2	P_2	pP_1	pP_2
ELK							.42	1.38	1.80				.1	.75	..85			
KNB	.1	.8	.9							.75								
LAC	.1	.75	.85				.15	.90	1.05				.3	.9	1.2	.27	.85	1.12
MNV				.1	.8	.9	.30	1.0	1.30									

P_2 = direct P-wave arrival due to a secondary explosion

pP_1 = reflected P-wave arrival from the first explosion

pP_2 = reflected P-wave arrival from the seconda.y explosion

path effects. It is, therefore, possible that spectral characteristics attributed to the source actually result from propagation path effects. In the Theory section it was shown that forming the spectral ratio for two events would remove propagation effects and, thus, yield additional information concerning the source functions. Typical examples of the calculated spectral ratios are shown in Figures 34 to 36. It is evident from Figure 34 that the spectral contents of the signals from events BLENTON and D as seen at Kanab were nearly identical. This would suggest an equivalent nature for the two events. The spectral ratio for the same two events as seen at Nelson is shown in Figure 35. On the basis of this figure it appears that the spectral contents of the two events are unrelated. In general, the spectral ratios were characterized by this lack of consistent results and the strong dependence on frequency which is obvious in Figure 36.

Using equations (11) and (12), attempts were made to determine the theoretical envelopes of calculated spectral ratios. Because of the number of parameters involved, no reasonable results were obtained.

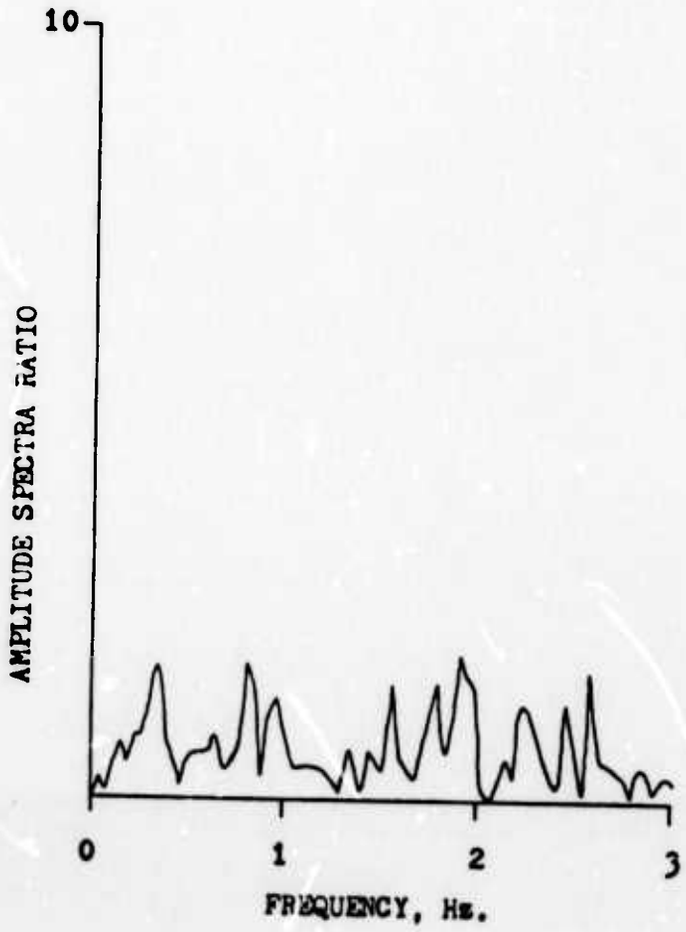

Figure 34. Amplitude spectral ratio of event BLENTON/THISTLE to Event D for KNB station.

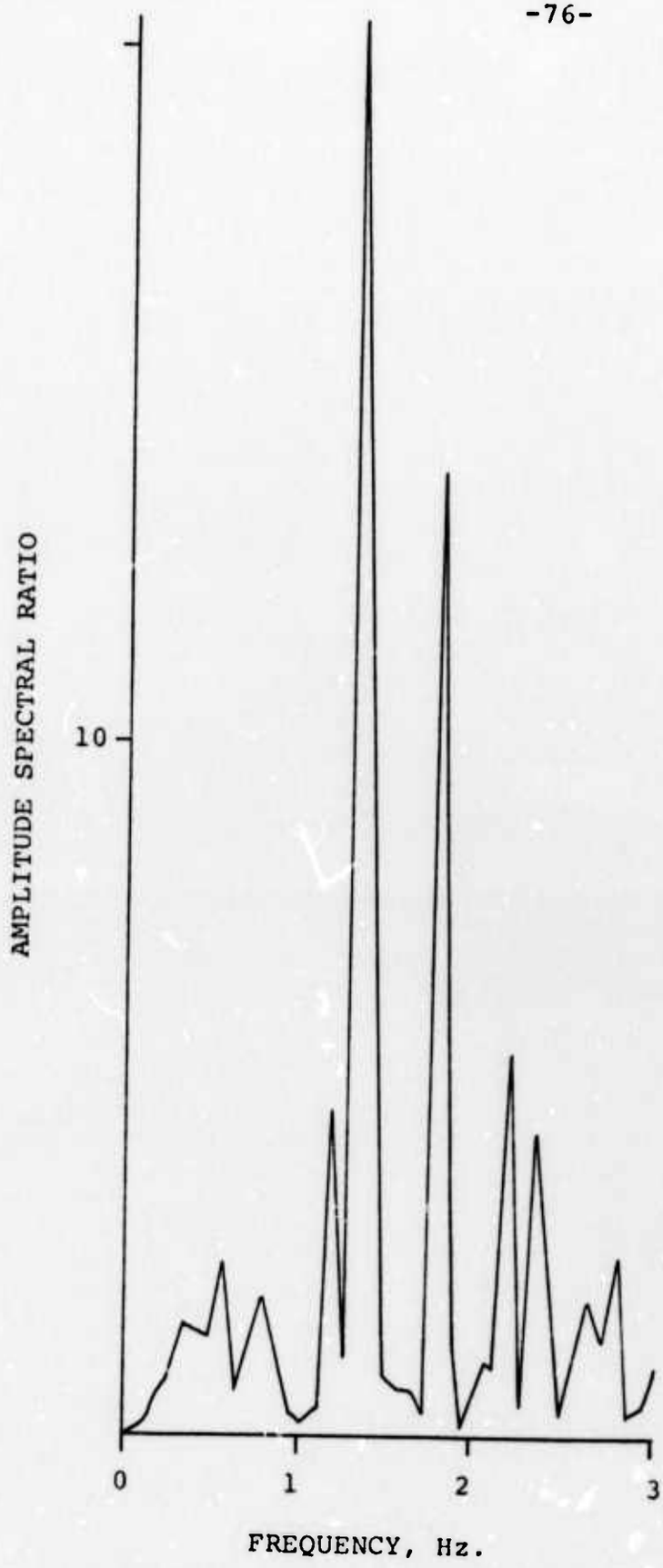

Figure 35. Amplitude spectral ratio of event BLENTON/ THISTLE to Event D for NEL station.

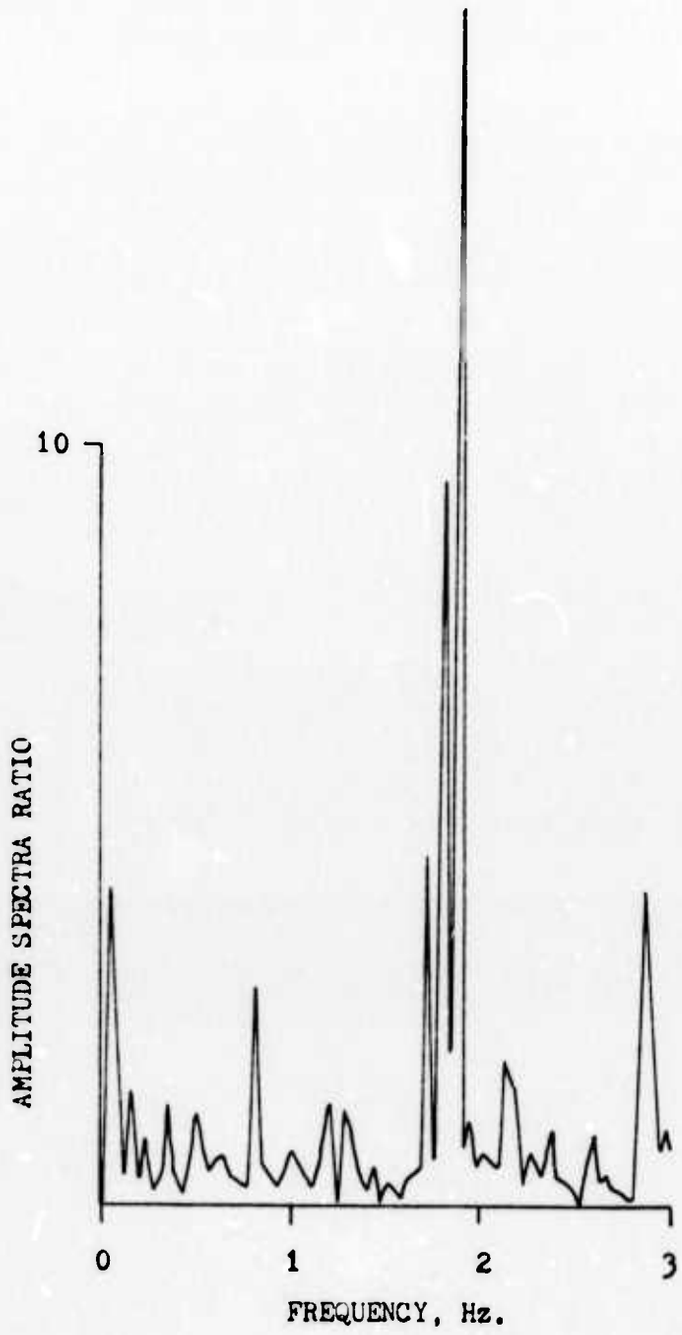

Figure 36. Amplitude spectral ratio of event BLENTON/ THISTLE to Event B for LAC station.

Correlation Analyses

In keeping with the theoretical development previously considered, it is desirable to consider the correlation of the following four cases; cross-correlation of natural events with nuclear events, known single explosion with known double explosion, shots of unknown multiplicity with single detonation, and known double explosion with detonations of unknown multiplicity. These four cases are represented respectively by the cross-correlation of all nuclear explosions with the Massachusetts Mountain earthquake; the cross-correlation of event BLENTON/THISTLE with single explosion DIDO QUEEN; the cross-correlation of DIDO QUEEN with explosions B, D and E; and finally the cross-correlation of BLENTON/THISTLE with events A to E.

The actual cross-correlations are time dependent functions having durations of approximately 60 seconds. A typical example is shown in Figure 37 for 20 percent of the lags or ± 6 seconds. In view of the geographical proximity of all the events, however, the significant part of the correlation should exist near a lag of zero seconds. On this basis the correlation functions presented here are given for only 7 percent of the total lags or ± 2 seconds. Since the correlations are conducted in the time domain and the two events are recorded at the same station, the narrow band-pass of the Benioff seismic system used in the

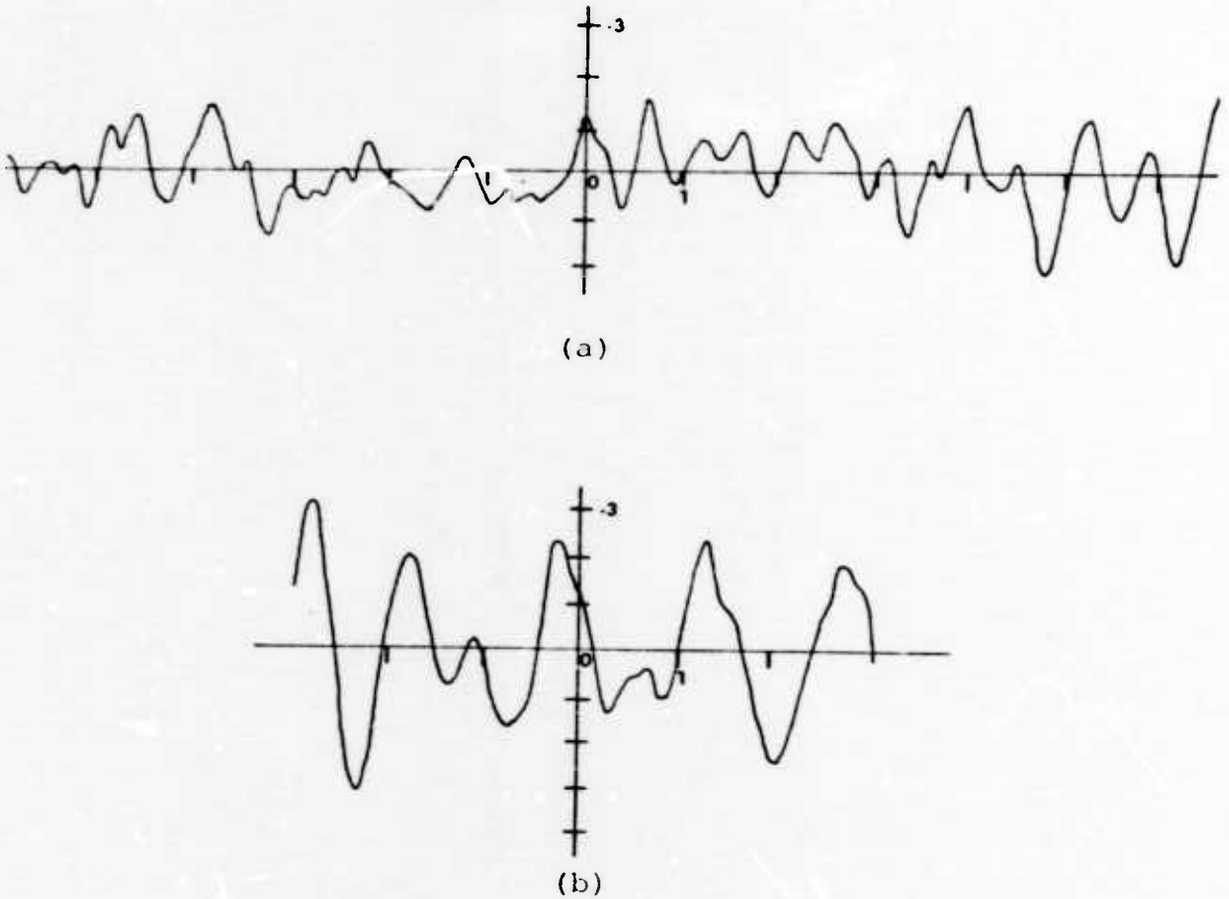

Figure 37. Cross-correlations of Massachusetts Mountain earthquake wi h Event A for stations (a) LAC and (b) MNV. Abscissa: Time lag in sec. Ordinate: Correlation

Sandia Laboratories stations, has no detrimental consequences and, therefore, the records of these stations may be used.

The results of the correlation of the explosions with the Massachusetts Mountain earthquake are presented in Figures 37 to 43. By inspection of these figures, one can notice that in general an increase of the correlation occurs for values of the time lag other than zero. It is also interesting to note the poor correlation obtained for Event F despite its partial earthquake nature. This probably results from the difference in distance from the respective epicenters to the recording stations and also is due to the fact that Event F is not a "pure" earthquake but a "mixture" of an earthquake and a nuclear detonation. The correlation values at zero lag for the Massachusetts Mountain earthquake and each of the nuclear explosions are summarized in Table 10. From this table it can be seen that in general a wide variation exists in the values of the cross-correlation at zero lag. Despite this wide variation, the maximum value obtained was 0.29 and typical values were on the order of 0.1.

The cross-correlation function of event BLENTON/THISTLE with the single explosion DIDO QUEEN is illustrated in Figure 44, from which it is apparent that a low correlation exists. The correlation value at zero lag of .08, given in Table 11, is much lower than the expected value

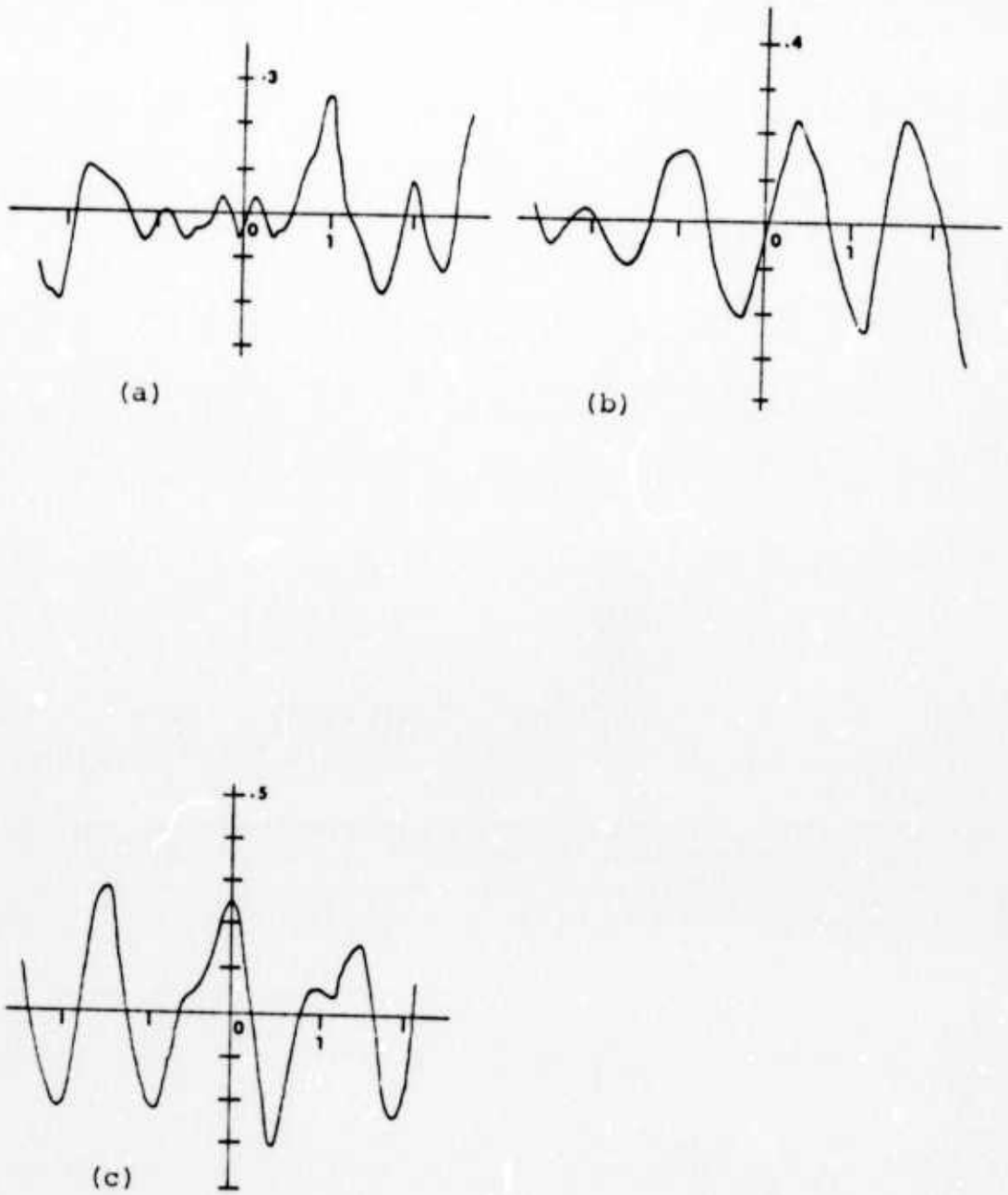

Figure 38. Cross-correlations of Massachusetts Mountain earthquake with Event B for stations (a) ELK, (b) LAC, and (c) MNV. Abscissa: Time lag in sec. Ordinate: Correlation

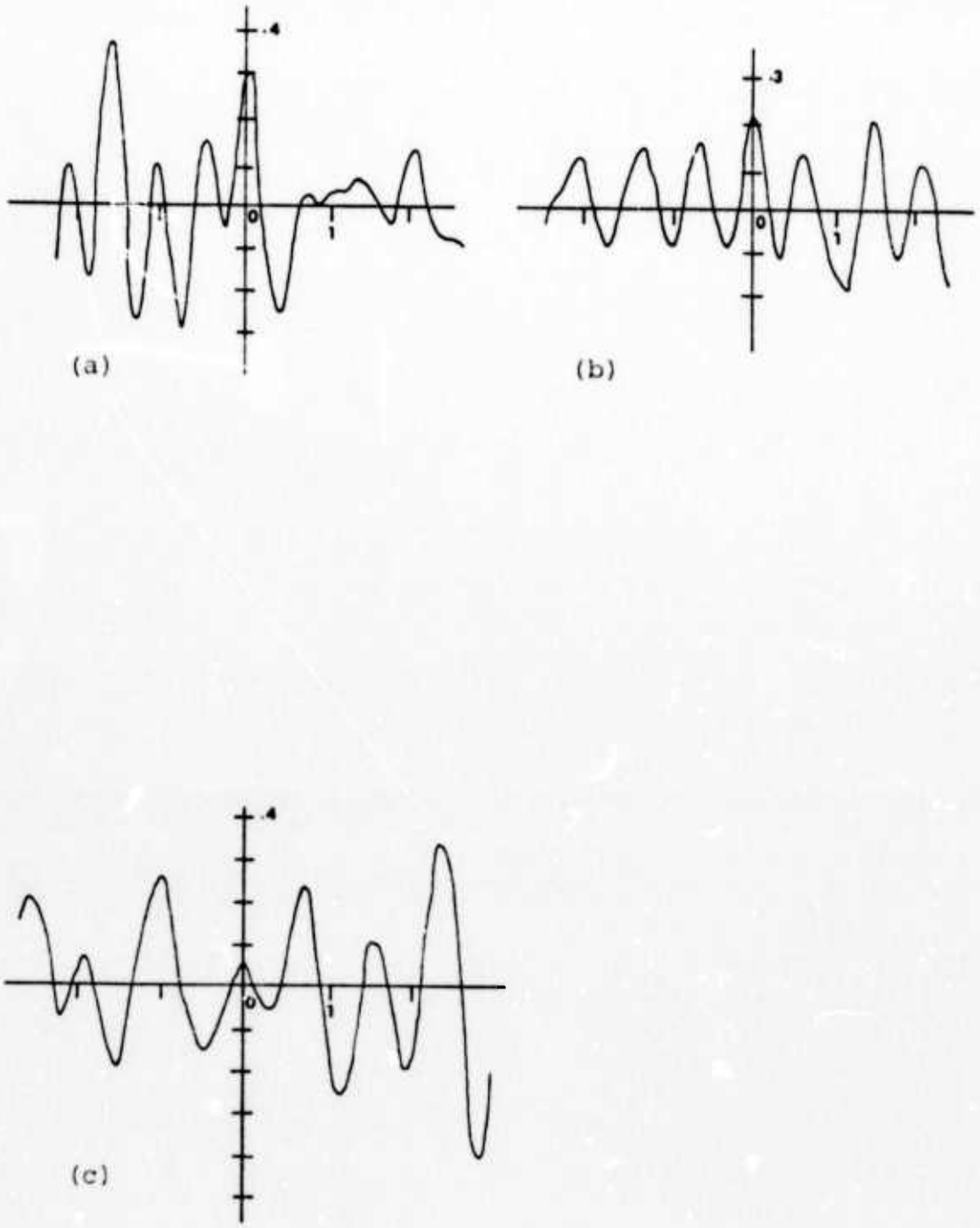

Figure 39. Cross-correlation of Massachusetts Mountain earthquake with Event C for stations (a) KNB, (b) LAC, and (c) MNV. Abscissa: Time lag in sec. Ordinate: Correlation

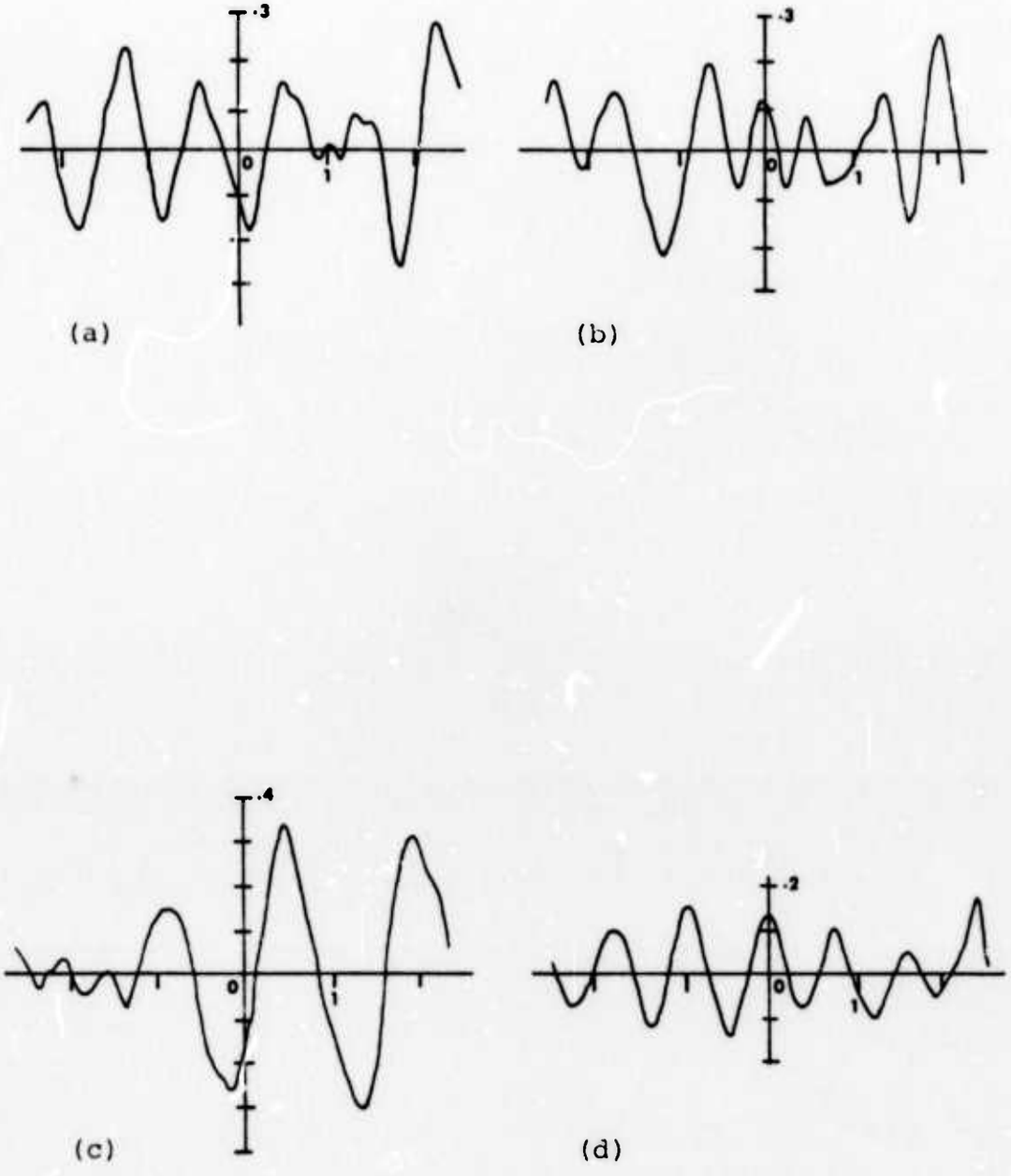

Figure 40. Cross-correlation of Massachusetts Mountain earthquake with Event D for stations (a) ELK, (b) KNB, (c) LAC, and (d) MNV. Abscissa: Time lag in sec. Ordinate: Correlation

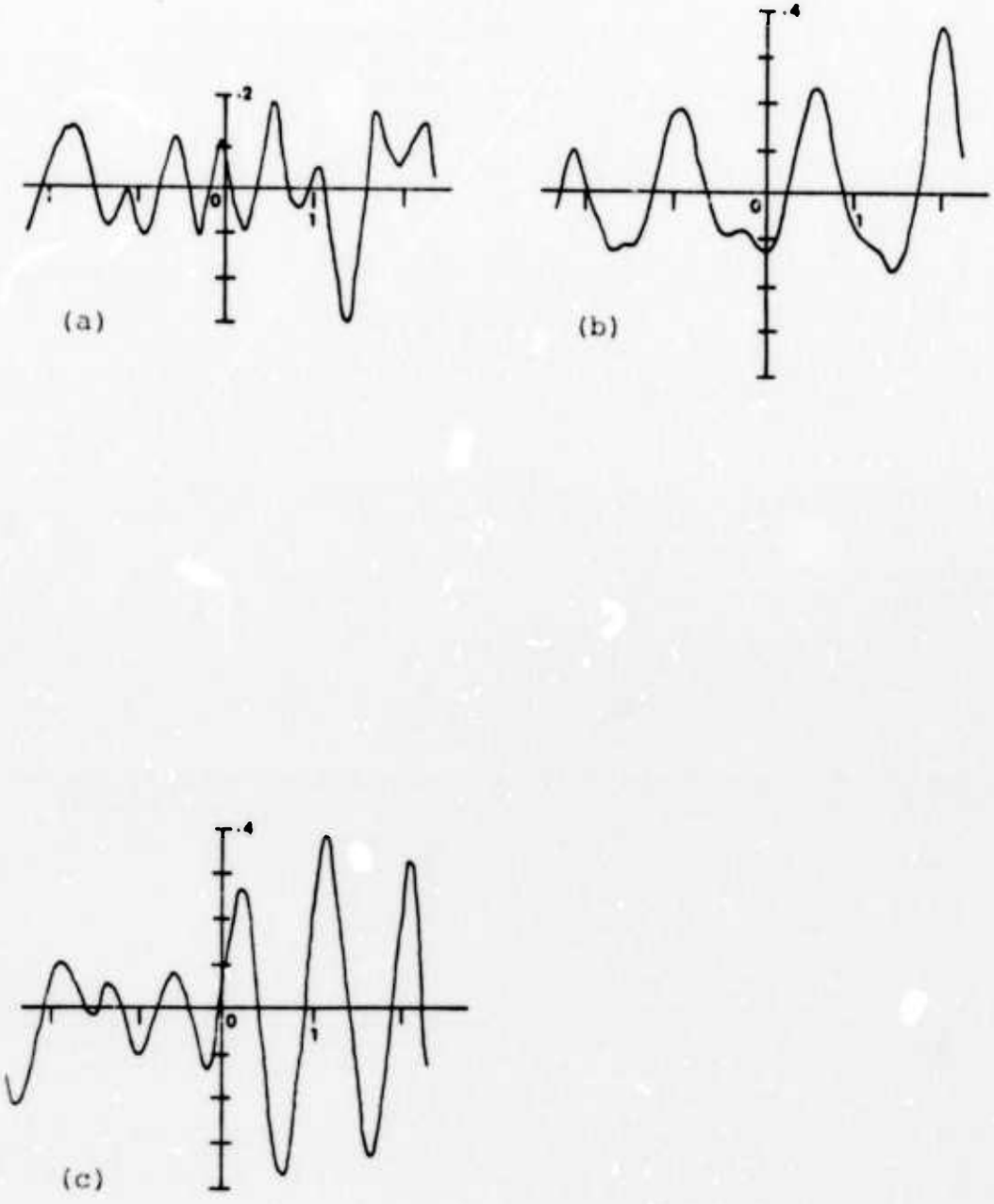

Figure 41. Cross-correlation of Massachusetts Mountain earthquake with Event E for stations (a) KNB, (b) LAC, and (c) MNV. Abscissa: Time lag in sec. Ordinate: Correlation

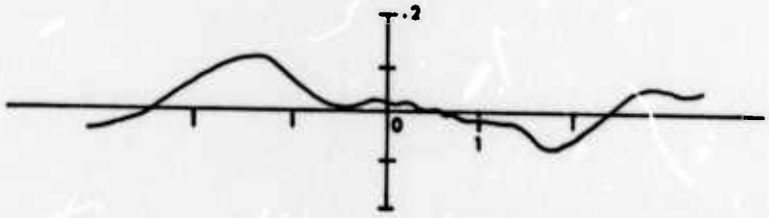

(a)

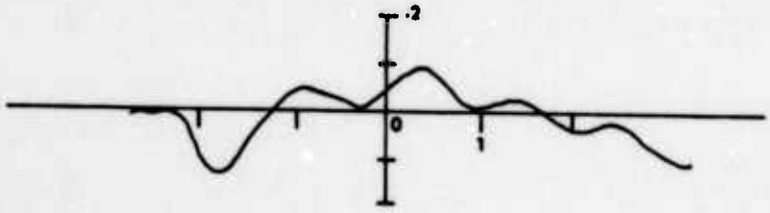

(b)

Figure 42. Cross-correlation of Massachusetts Mountain earthquake with Event F for stations (a) LAC and (b) MNV.
Abscissa: Time lag in sec. Ordinate: Correlation

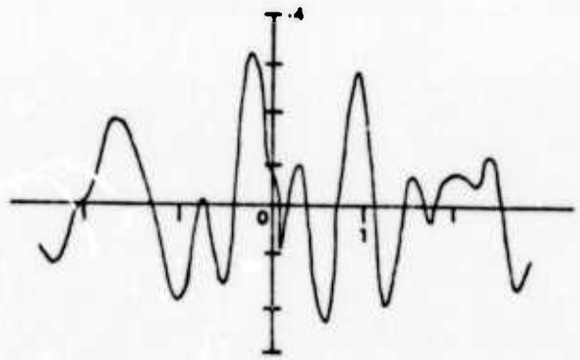

(a)

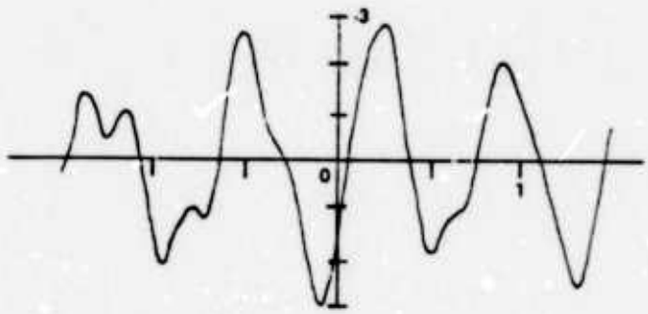

(b)

Figure 43. Cross-correlation of Massachusetts Mountain earthquake with BLENTON/THISTLE for stations (a) KNB and (b) LAC. Abscissa: Time lag in sec. Ordinate: Correlation

TABLE 10

Correlation Values at Zero Lag of Massachusetts Mountain Earthquake with Nuclear Explosions BLENTON/THISTLE, A, B, C, D, E and F for the LLL Stations

	ELK	KNB	LAC	MNV
Mass. Mt. BLENTON/THISTLE		.09	-.15	
Mass. Mt. Event A			.12	.12
Mass. Mt. Event B	-.03		-.04	.24
Mass. Mt. Event C		.29	.21	.05
Mass. Mt. Event D	-.12	.10	-.17	.13
Mass. Mt. Event E		.08	-.14	.04
Mass. Mt. Event F			.01	.04

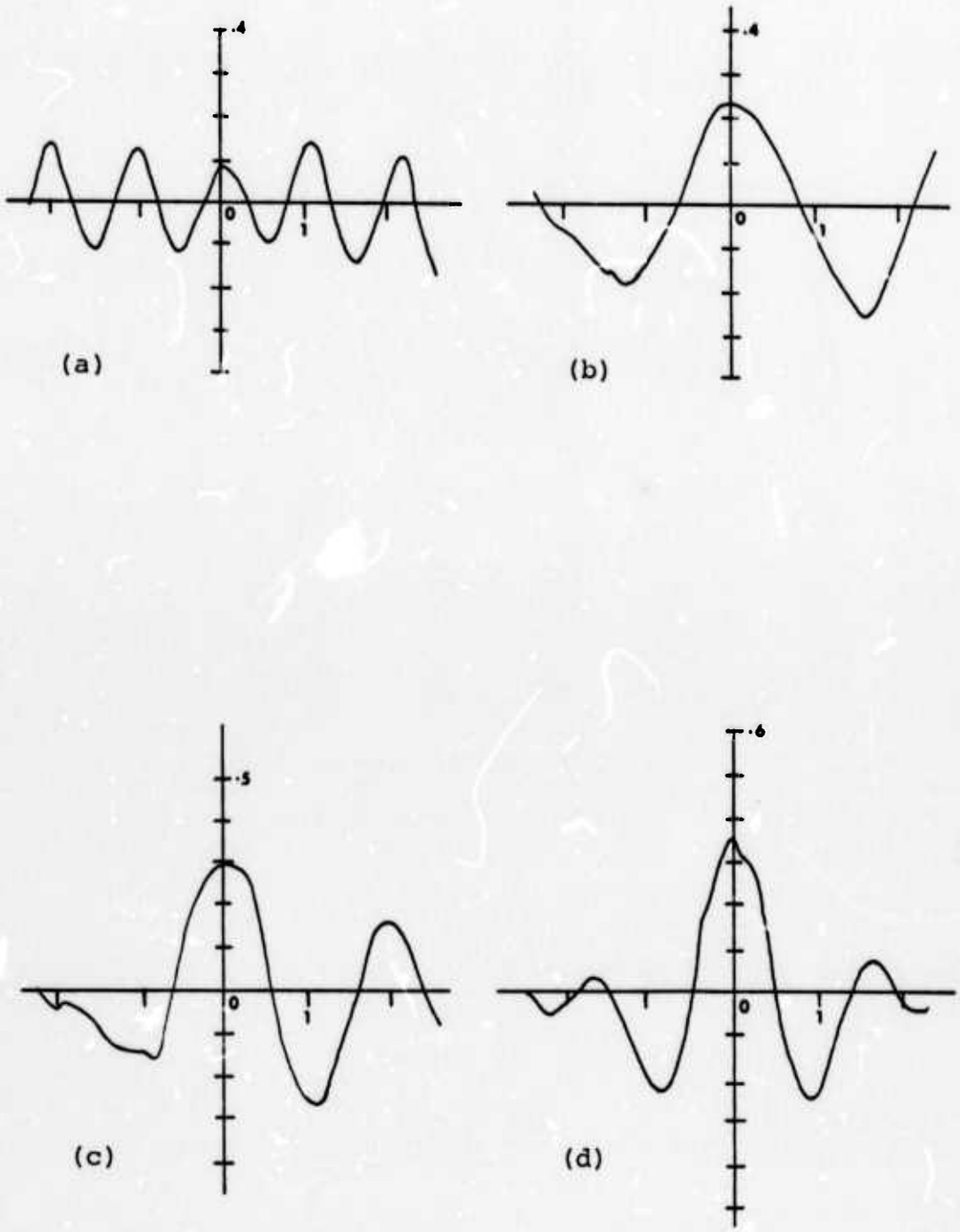

Figure 44. Cross-correlation of event DIDO QUEEN with event:
(a) BLENTON/THISTLE for station LEE
(b) A for station DAC
(c) D for station DAC
(d) E for station DAC

Abscissa: Time lag in sec. Ordinate: Correlation

TABLE 11

Correlation Value at Zero Lag of Single Nuclear Explosion DIDO QUEEN with Double Explosion BLENTON/THISTLE and Unknown Explosions B, D and E for the LLL Stations

Events	Station	Correlation
DIDO QUEEN - BLENTON/THISTLE	LEE	.08
DIDO QUEEN - EVENT B	DAC	.23
DIDO QUEEN - EVENT D	DAC	.28
DIDO QUEEN - EVENT E	DAC	.35

for the correlation of two nuclear detonations. However, little significance can be given to the results of only one station. The results of the correlation of Events B, D and E with DIDO QUEEN are also shown in Figure 44. By simple inspection of this figure, it is apparent that higher correlations exist for these events than for BLENTON/THISTLE. The corresponding correlation values at zero lag, which are summarized in Table 11, indicate that higher correlation values have been obtained than when the same events B, D and E were correlated with the Massachusetts Mountain earthquake. Nevertheless, the same assertion that was made regarding the correlation of BLENTON/THISTLE and DIDO QUEEN applies here and not much meaning can be derived from the results of only one station.

The correlations of Events A to E with the double detonation BLENTON/THISTLE are shown in Figures 45 to 52, and the corresponding zero lag values are itemized in Table 12. Of particular interest are the correlation values obtained for BLENTON/THISTLE and Event B given in Table 12. These values are on the order of 0.6 and indicate a strong similarity of both events. The values obtained in the cross-correlation of BLENTON/THISTLE and Events D and E for the stations LAC and KNB are also high. The similarity of the events indicated by the cross-correlation values at zero lag for the mentioned cases is strongly supported by visual comparison of their records

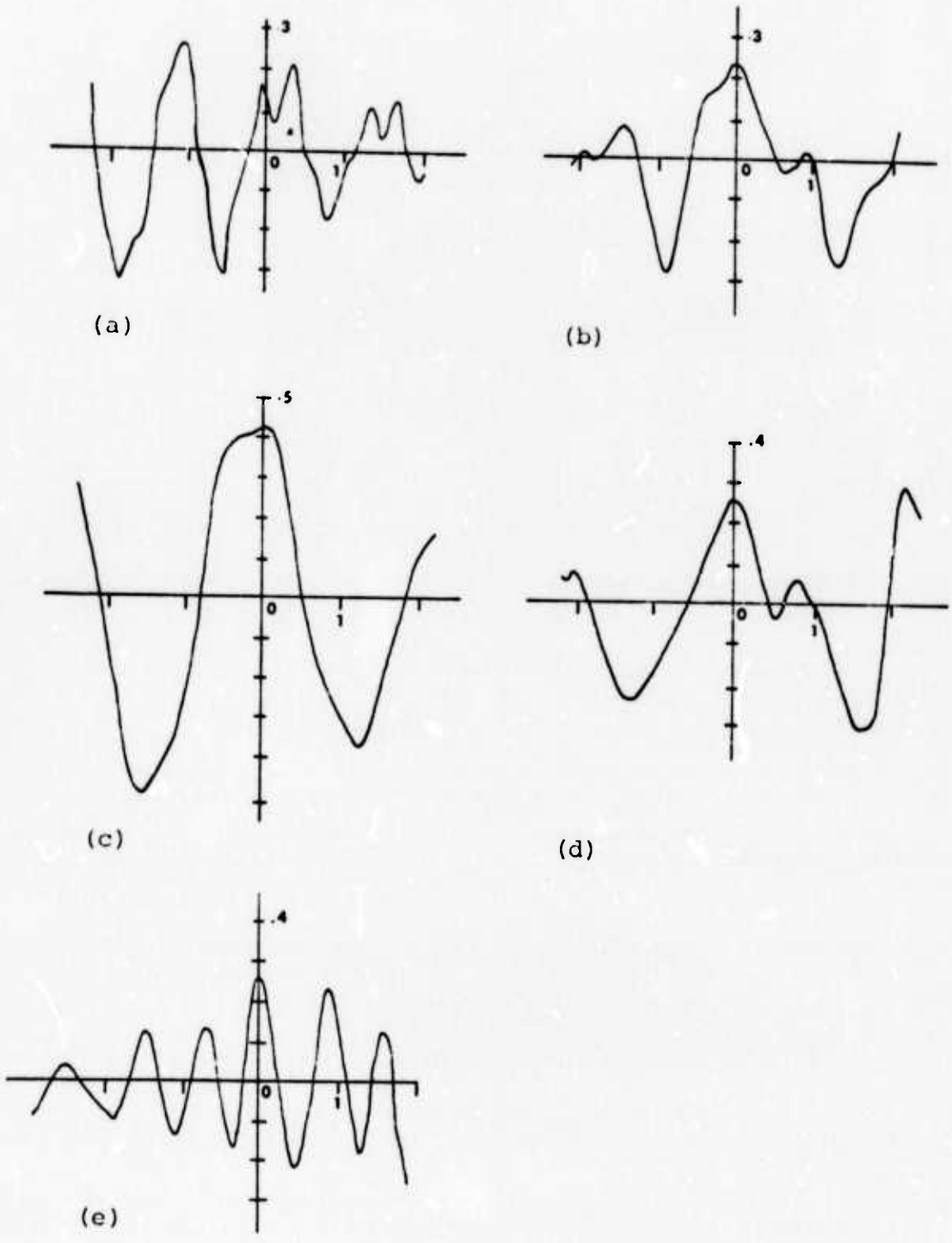

Figure 45. Cross-correlation of Event A with the double detonation BLENTON/THISTLE for stations (a) LAC, (b) NEL, (c) DAC, (d) ELY, and (e) BMN.
Abscissa: Time lag in sec. Ordinate: Correlation

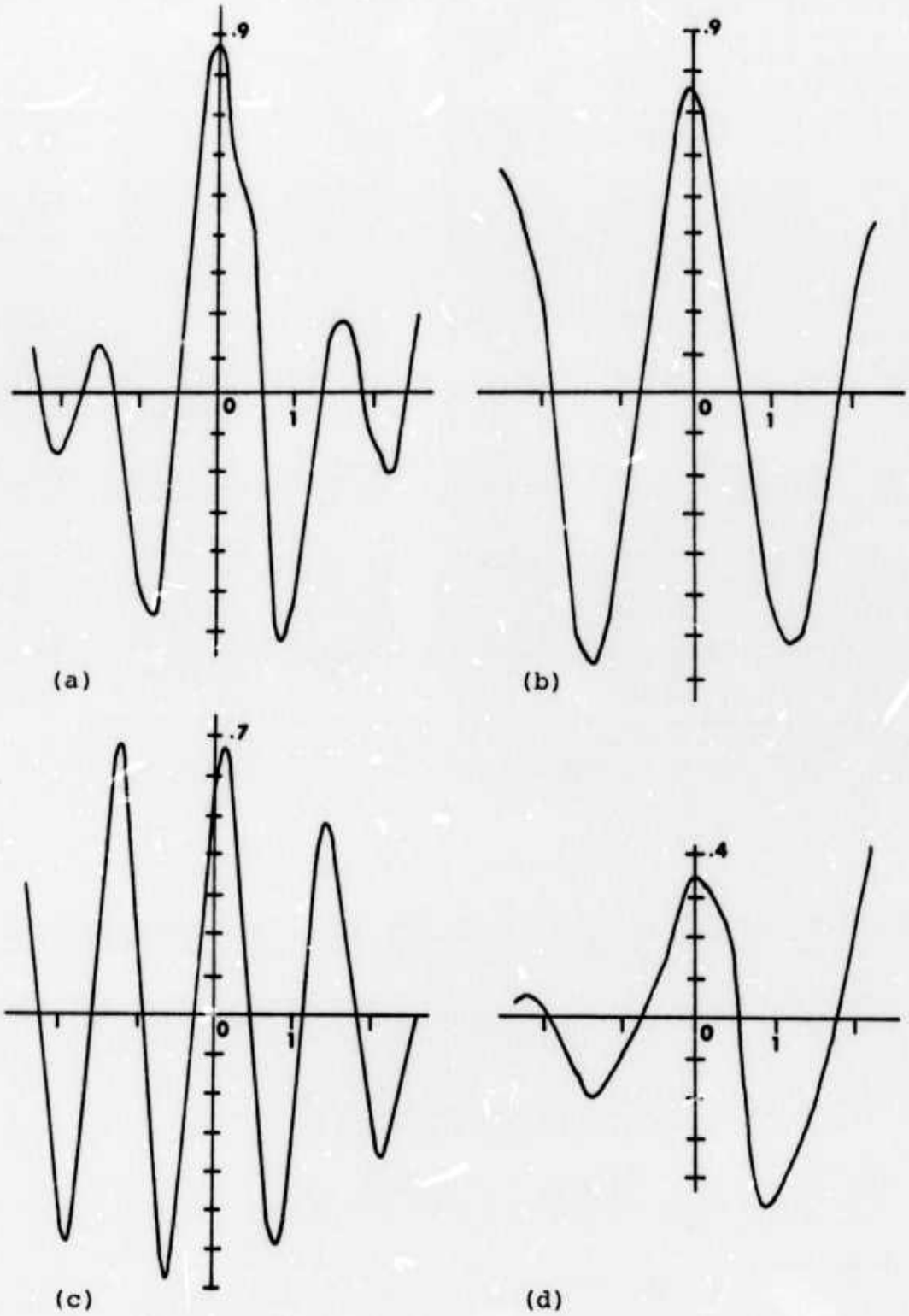

Figure 46. Cross-correlation of Event B with the double detonation BLENTON/THISTLE for stations (a) TPH, (b) DAC, (c) LAC, and (d) NEL.
Abscissa: Time lag in sec. Ordinate: Correlation

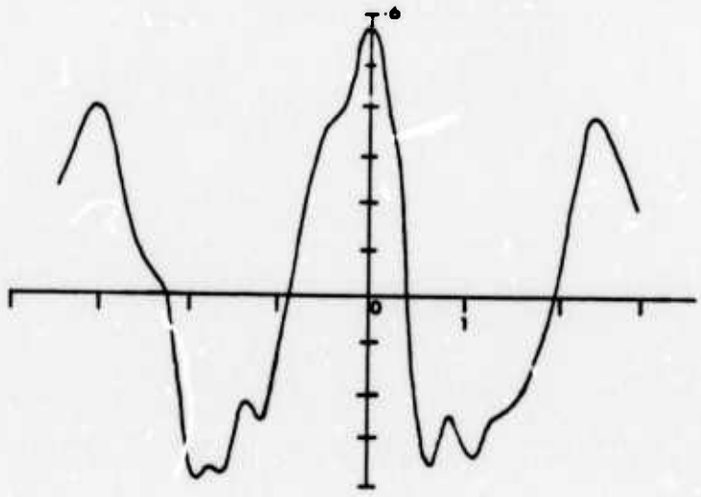

Figure 47. Cross-correlation of Event B with the double detonation BLENTON/THISTLE for station BMN.

Abscissa: Time lag in sec.
Ordinate: Correlation

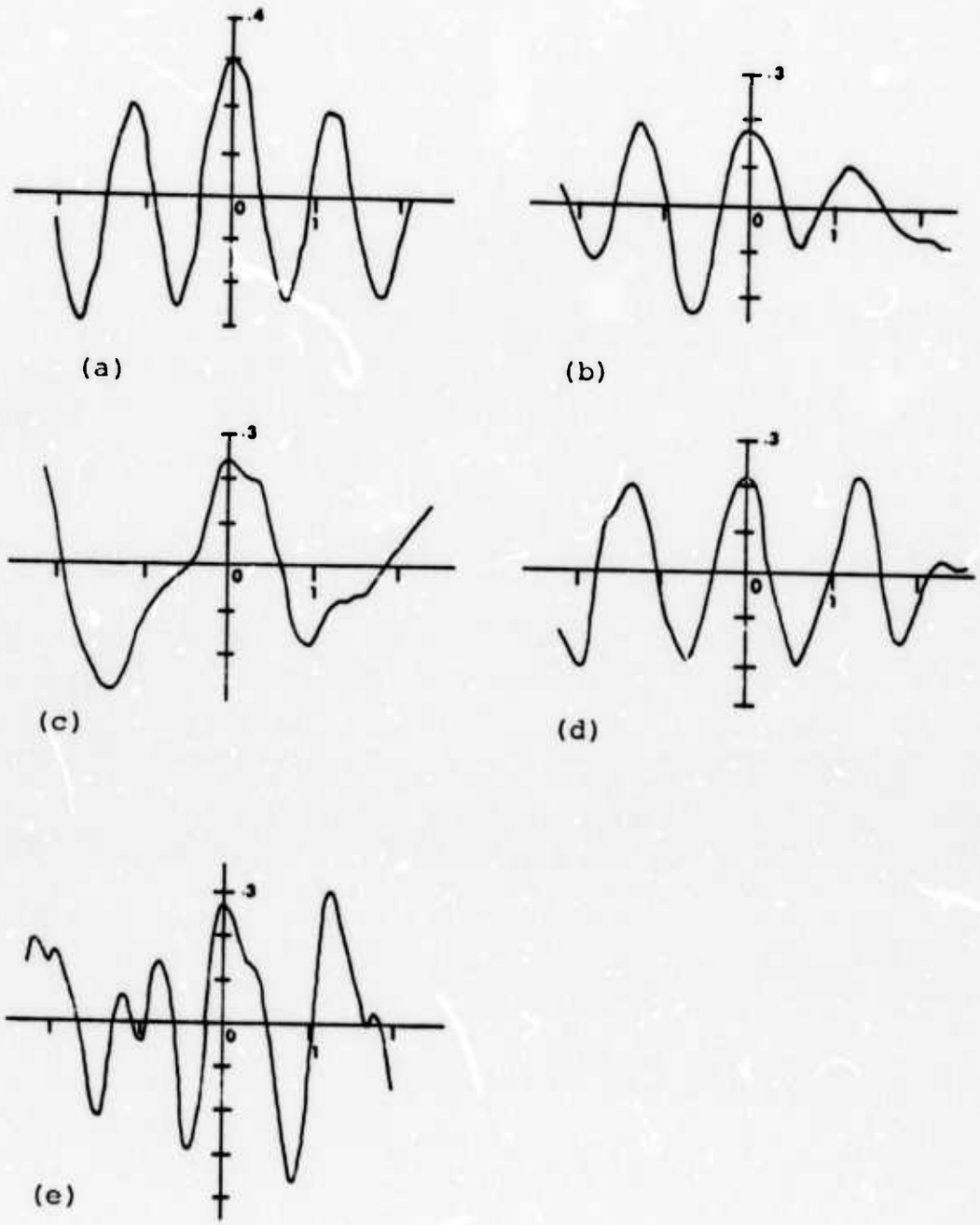

Figure 48. Cross-correlation of Event C with the double detonation BLENTON/THISTLE for stations (a) LEE, (b) ELY, (c) NEL, (d) LAC, and (e) KNB.
Abscissa: Time lag in sec. Ordinate: Correlation

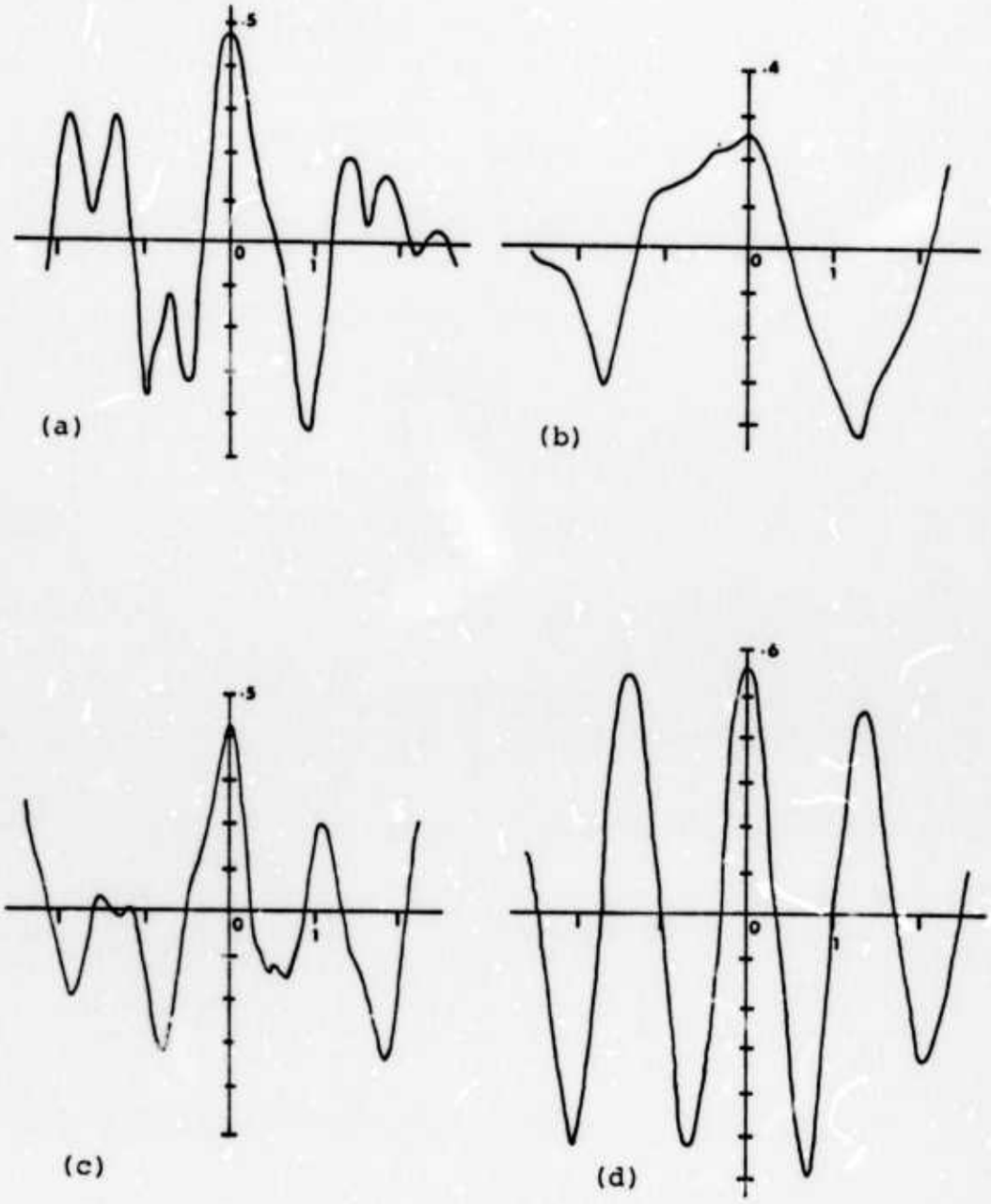

Figure 49. Cross-correlation of Event D with the double detonation BLENTON/THISTLE for stations (a) KNB, (b) NEL, (c) TPH, and (d) LAC.
Abscissa: Time lag in sec. Ordinate: Correlation

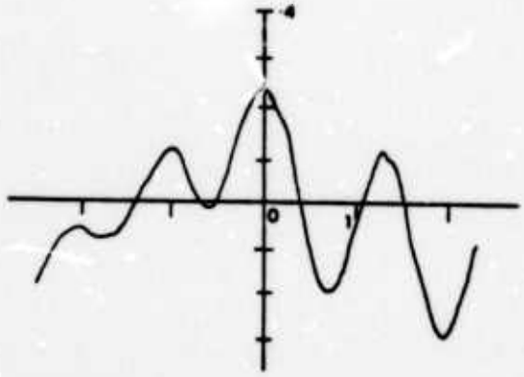

Figure 50. Cross-correlation of Event D with the double detonation BLENTON/THISTLE for station ELY.

Abscissa: Time lag in sec.
Ordinate: Correlation

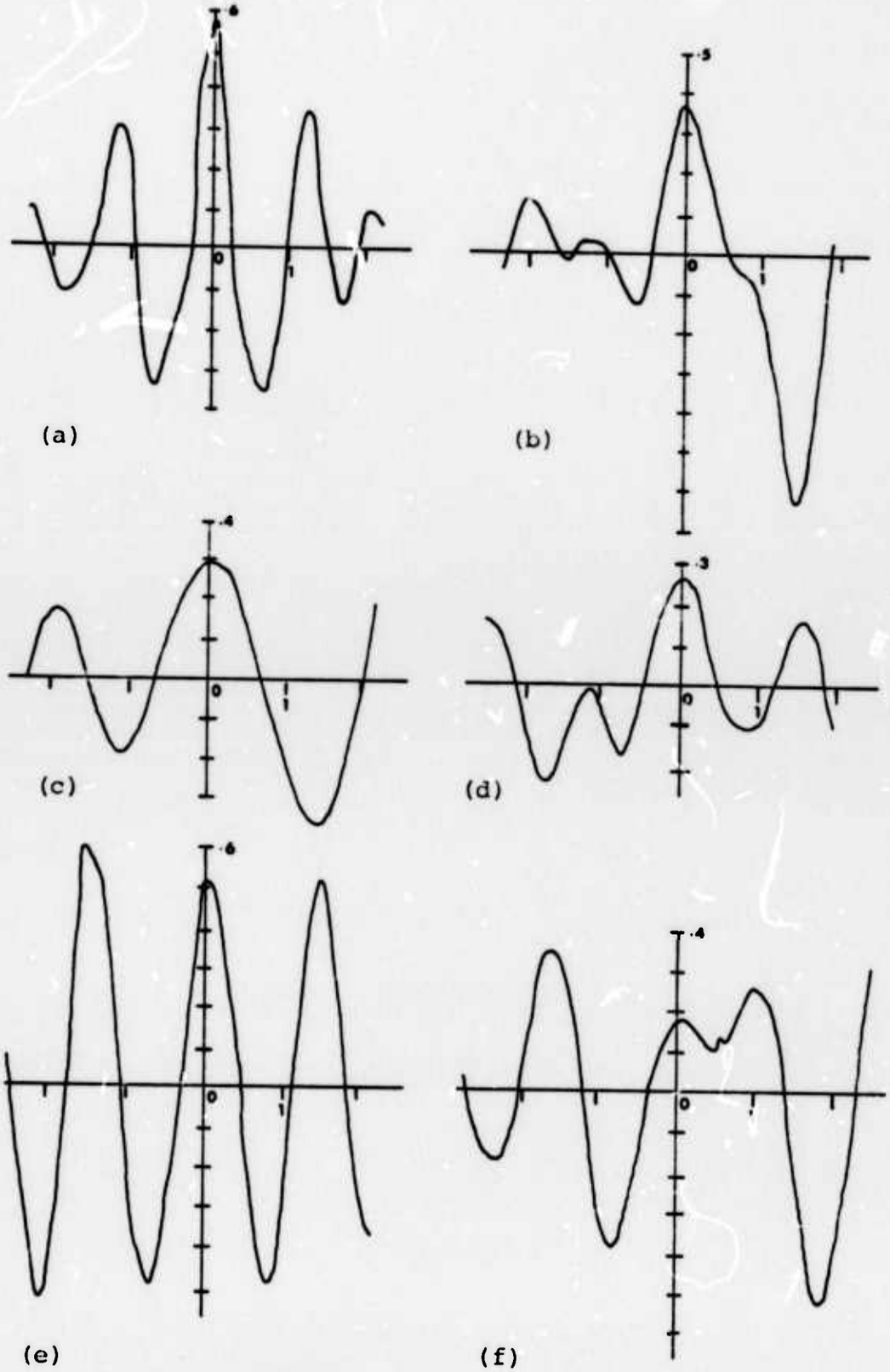

Figure 51. Cross-correlation of Event E with the double detonation BLENTON/THISTLE for stations (a) KNB, (b) NEL, (c) DAC, (d) ELY, (e) LAC, and (f) TPH.
Abscissa: Time lag in sec. Ordinate: Correlation

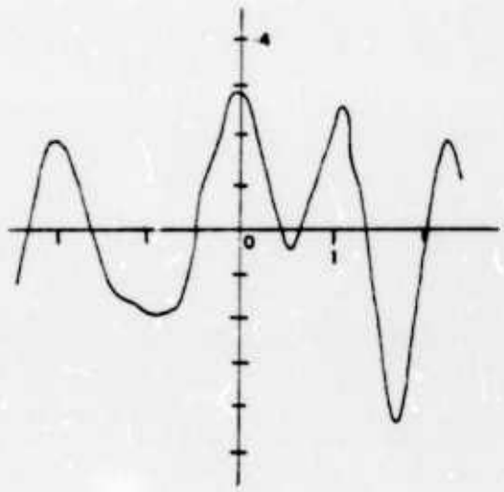

Figure 52. Cross-correlation of Event E with the double detonation BLENTON/THISTLE for station LEE.

Abscissa: Time lag in sec.
Ordinate: Correlation

TABLE 12

Correlation Values at Zero Lag of Double Explosion BLENTON/THISTLE with Unknown Explosions A, B, C, D, and E for LLL and Sandia Laboratories Stations

	BMN	DAC	ELY	KNB	LAC	LEE	NEL	TPH
BLENTON/THISTLE EVENT A	.25	.41	.26		.15			
BLENTON/THISTLE EVENT B	.57	.76			.68		.36	.86
BLENTON/THISTLE EVENT C		.34	.17	.26	.21	.34	.23	
BLENTON/THISTLE EVENT D			.23	.47	.55	.33	.25	.42
BLENTON/THISTLE EVENT E		.28	.26	.55	.50	.29	.36	.17

which are shown in Figures 53 to 56. The correlation values obtained for Events A and C for all the stations are lower than those obtained for Events B, D and E. These results, considered in the theoretical frame presented in the Theory section of this study, suggest a multiple source for Event B and a single explosion for Events A and C. No indication of the nature of Events B and E is provided by the correlation.

In an attempt to explain the variation of the correlation values obtained for these events at different stations, the values of the correlation at zero lag for each event have been plotted versus the azimuth of the corresponding stations. The correlation values for the correlation of Events A through E with BLENTON/THISTLE at each station are shown in Figure 57. On the basis of this figure, it is apparent that for the majority of the events considered the correlation is somewhat dependent upon the azimuth. In general, the higher values appear in the neighborhood of 200 degrees.

In Figure 58, the correlation values of each event at each station are plotted versus the difference in depth. The depth difference was defined as the difference between the depth of BLENTON/THISTLE and the depth of the event being considered. It can be seen by inspection of this figure that, in general, as the difference in depth between the sources of the events being correlated increases, the

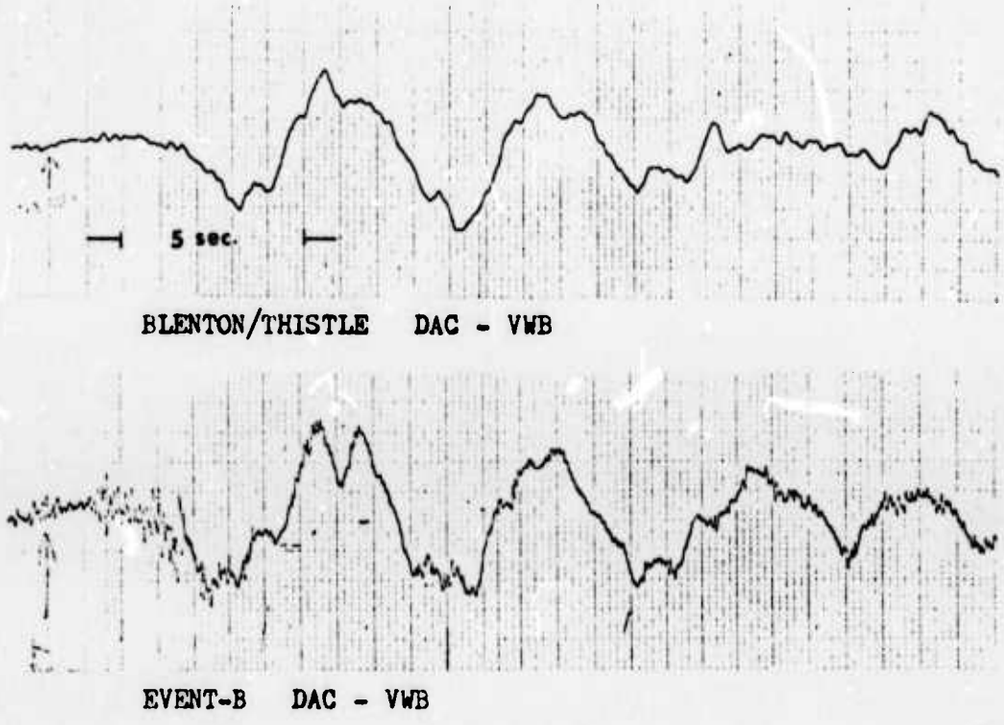

Figure 53. Analog records of BLENTON/THISTLE and B events recorded at DAC station.

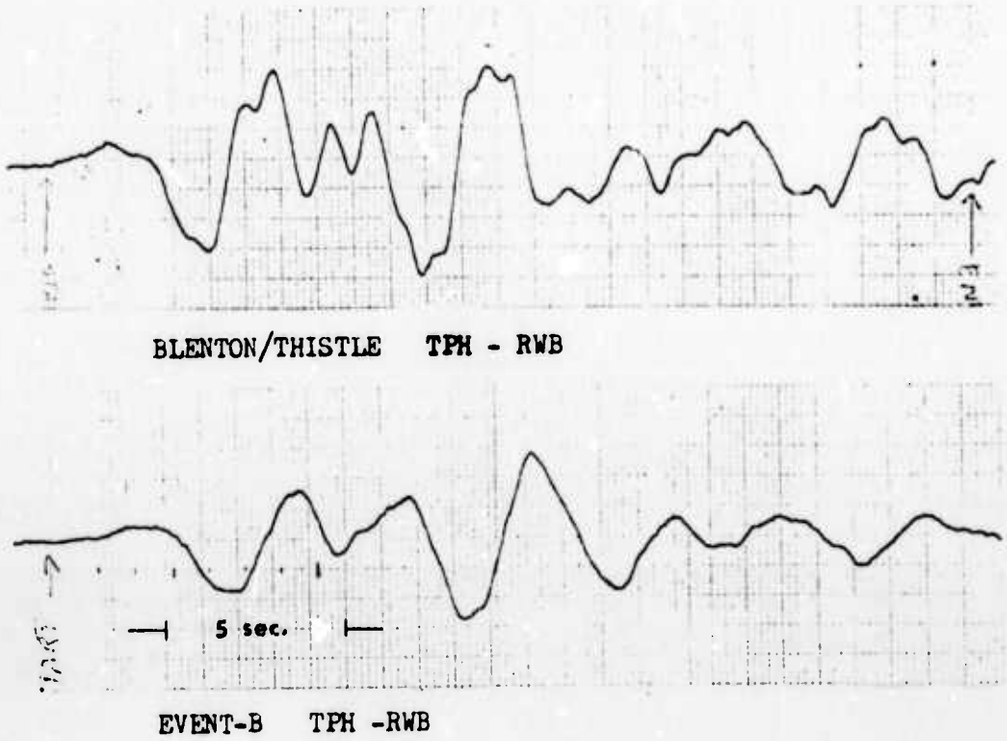

Figure 54. Analog records of BLENTON/THISTLE and B events recorded at TPH station.

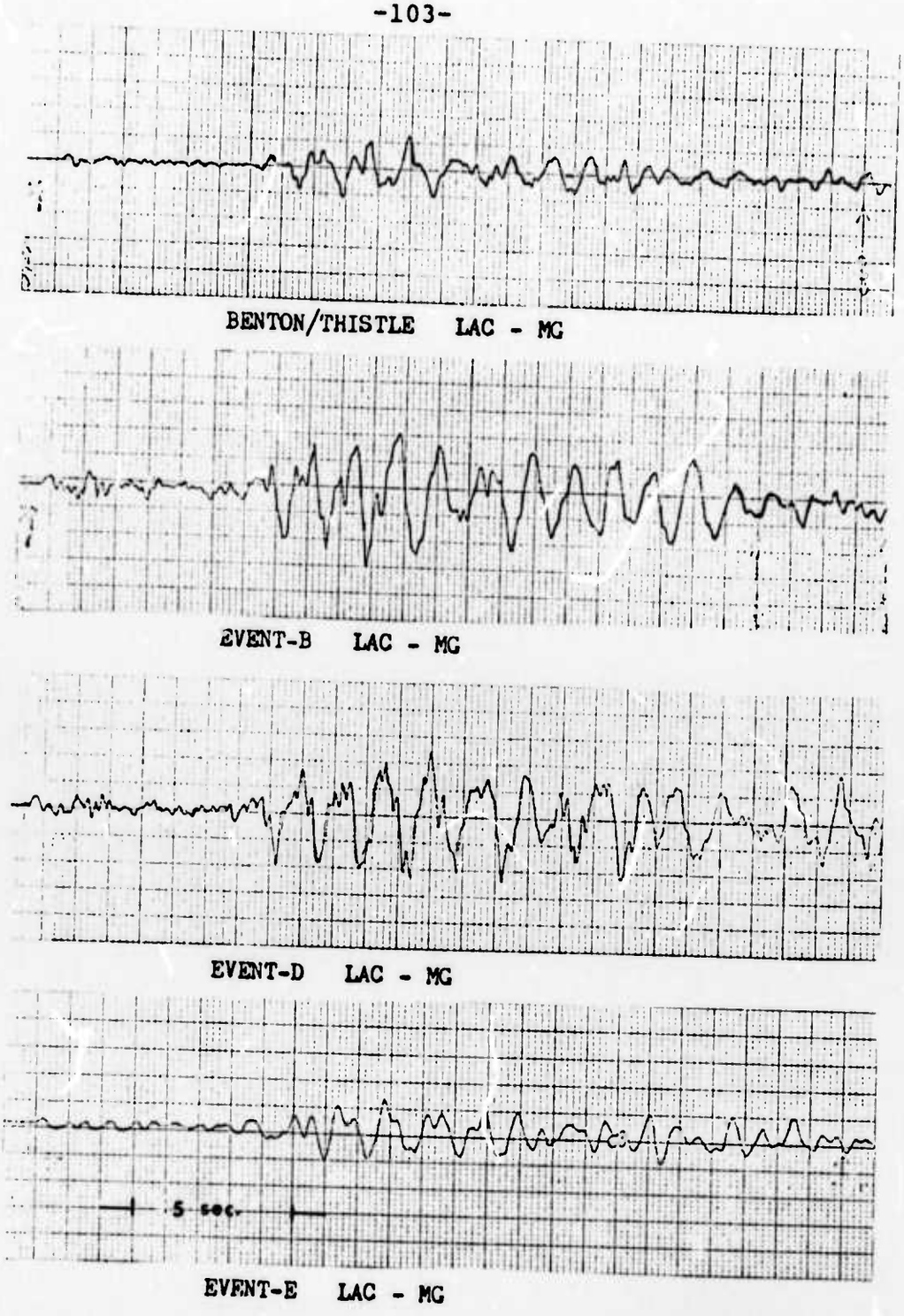

Figure 55. Analog records of BLENTON/THISTLE, B, D, and E events recorded at LAC station.

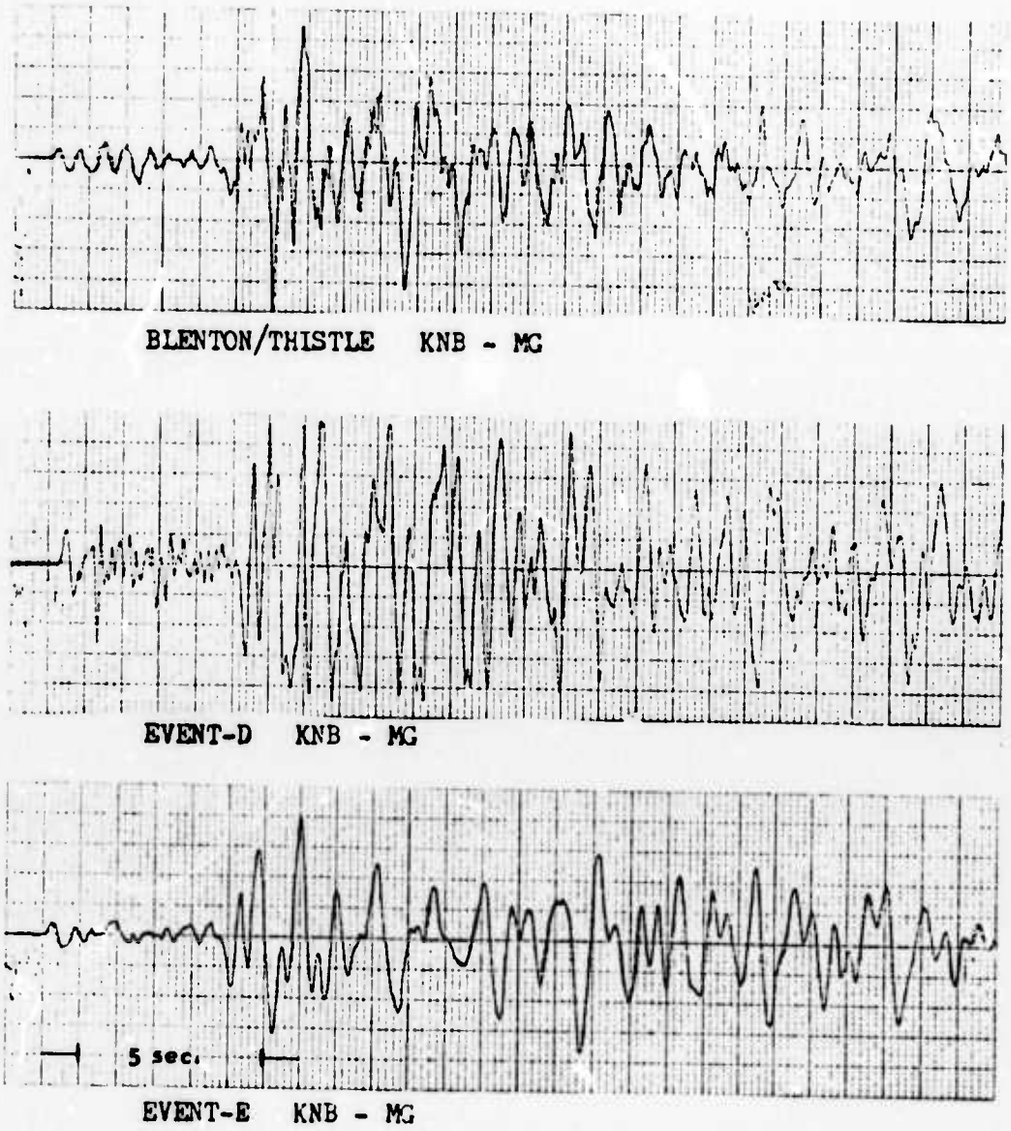

Figure 56. Analog records of BLENTON/THISTLE, D, and E events recorded at KNB station.

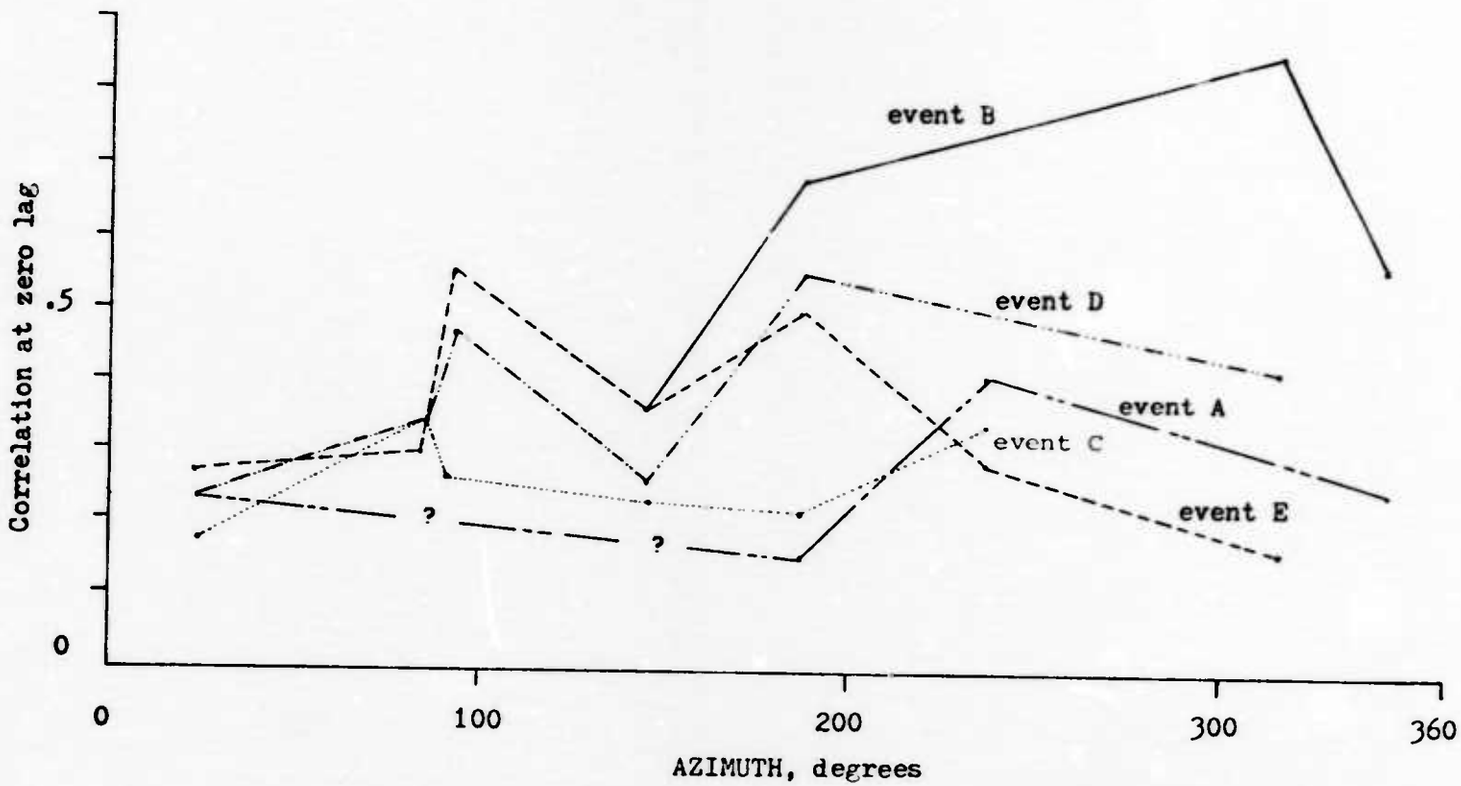

Figure 57. Correlation value at zero lag of A, B, C, D, and E events with BLENTON/THISTLE explosion versus the azimuth with respect to BLENTON/THISTLE of the corresponding stations.

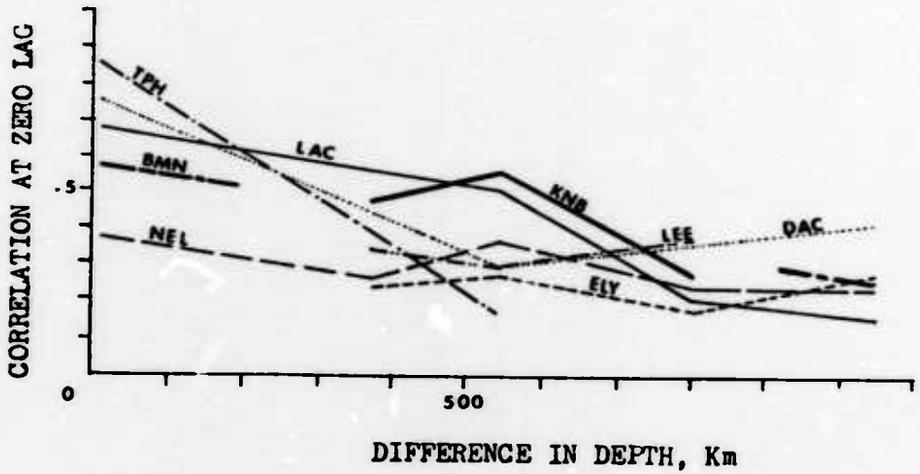

Figure 58. Correlation values at zero lag of A, B, C, D and E events with BLENTON/THISTLE explosion versus the differences in depth between each event and BLENTON/THISTLE.

correlation at zero lag decreases. This depth difference dependence appears to limit the utility of correlation methods for identification.

Suggestions for Further Investigation

Considering the positive results obtained with the limited number of events used in this study regarding the different behavior of the slope of the displacement spectra in the lower range of frequencies, in addition to the possibility of this test being performed by analogue methods, further research should be conducted to provide a more proper evaluation of the efficacity of this test and give it statistical support. Any future application of the slope test should be conducted with data obtained with a broad band-pass seismic system.

Further research should be done toward the investigation of particular arrangements of multiple explosions having an additive effect on the lower frequencies which might cause the failure of the slope test.

Based on the differences of the calculated source radii for the different events utilized in this study, further research in this direction is recommended. Although based on a limited number of data, the positive results of the correlations used in this study suggest that these techniques are a potential method of discrimination between natural and manmade seismic events and identification of multiple nuclear events. Additional investigation on a more complete set of data than that used in this research is suggested in order to fully evaluate the differentiating abilities of the method.

REFERENCES CITED

Aki, K., 1967, Scaling law of seismic spectrum: Jour. Geophys. Res., v. 72, p. 1217-1231.

Archambeau, C. B., 1964, Elastodynamic source theory: Ph.D. thesis, California Institute of Technology, Pasadena.

Berchkhemer, H. and Jacob, K. H., 1968, Investigation of the dynamical process in earthquake foci by analyzing the pulse shape of body waves: Final Report, Contract AF61(052)-801, Air Force, Cambridge Research Laboratories.

Brune, J. N., 1970, Tectonic stress and the spectra of seismic shear waves from earthquakes: Jour. Geophys. Res., v. 75, p. 8042-8055.

Brune, J. N., 1971, Correction to Brune (1970): Jour. Geophys. Res., v. 76, p. 5002.

Brune, J. N., Espinosa, A., and Oliver, J., 1963, Relative excitation of surface waves by earthquakes and underground explosions in the California-Nevada region: Jour. Geophys. Res., v. 68, p. 3501-3513.

Cooley, J. W. and Tukey, J. W., 1965, An algorithm for the machine calculation of complex Fourier series: Mathematics of Computation, v. 19, p. 297-309.

Ekren, E. B., 1968, Geologic setting of the Nevada Test Site and Nellis Air Force Range: Geol. Soc. America Memoir 110, p. 11-19.

Evernden, J. F., 1969, Identification of earthquakes and explosions by use of teleseismic data: Jour. Geophys. Res., v. 74, p. 3828-3856.

Evernden, J. F., Best, W. J., Pomeroy, P. W., McEvilly, T. V., Savino, J. M., and Sykes, L. R., 1971, Discrimination between small-magnitude earthquakes and explosions: Jour. Geophys. Res., v. 75, p. 4997-5009.

Fischer, F. G., Papanek, P. J., and Hamilton, R. M., 1972, The Massachusetts Mountain earthquake of 5 August 1971 and its aftershock, Nevada Test Site: U.S. Geol. Survey Rept., USGS-474-149, 20 p.

Hanks, T. C. and Wyss, M., 1972, The use of body-waves spectra in the determination of seismic-source parameters: Bull. Seismol. Soc. America, v. 62, no. 2, p. 561-589.

Haskell, N. A., 1964, Total energy and energy spectral density of elastic wave radiation from propagating faults: Bull. Seismol. Soc. America, v. 54, p. 1811-1841.

Haskell, N. A., 1966, Total energy and energy spectral density of elastic wave radiation from propagating faults, 2: A statistical source model: Bull. Seismol. Soc. America, v. 56, p. 125-140.

Healy, J. H., King, C., and O'Neill, M. E., 1971, Source parameters of Salmon and Sterling nuclear explosion from seismic measurements: Jour. Geophys. Res., v. 76, no. 14, p. 3344-3355.

Hinrichs, E. N., 1968, Geologic structure of Yucca Flats area: Geol. Soc. America Memoir 110, p. 239-246.

Kasahara, K., 1957, The nature of seismic origins as inferred from seismological and geodetic observations, 1: Bull. Earthquake Res. Inst., Tokyo Univ., v. 35, p. 473-532.

King, C., Bakum, W. H., and Murdock, J. N., 1972, Source parameters of nuclear explosions MILROW and LONGSHOT from teleseismic P-waves: Geophys. Jour. Roy. Astron. Soc., v. 31, p. 27-44.

King, C., Abo-Zena, A. M., and Murdock, J. N., 1974, Teleseismic source parameters of the LONGSHOT, MILROW, and CANNIKIN nuclear explosions: Jour. Geophys. Res., v. 79, no. 5, p. 712-718.

Liebermann, R. C., King, C. Y., Brune, J. N., and Pomeroy, P. W., 1966, Excitation of surface waves by the underground nuclear explosion LONGSHOT: Jour. Geophys. Res., v. 78, p. 4333-4339.

Liebermann, R. C. and Pomeroy, P. W., 1969, Relative excitation of surface waves by earthquakes and underground explosions: Jour. Geophys. Res., v. 74, p. 1557-1590.

Matti, J. C. and others, 1974, Summary of Silurian and Lower Devonian basin and basin-slope limestones, Copenhagen Canyon, Nevada: Geology, v. 2, no. 12.

Powel, T. and Fries, D., 1964, Handbook: World-Wide Standard Seismograph Network: Inst. Science and Technology, The University of Michigan.

Press, F., Dewart, G., and Gilman, R., 1963, A study of diagnostic techniques for identifying earthquakes: Jour. Geophys. Res., v. 68, p. 2909-2928.

Rohrer, R. and Springer, D., 1972, The Massachusetts Mountain earthquake at the Nevada Test Site, August 5, 1971, compared to an underground explosion at NTS: Lawrence Livermore Laboratory Memorandum, 9 p.

Savage, J. C., 1966, Radiation from a realistic model of faulting: Bull. Seismol. Soc. America, v. 56, p. 577-592.

Savage, J. C., 1972, Relation of corner frequency to fault dimensions: Jour. Geophys. Res., v. 77, no. 20, p. 3788-3795.

Sharpe, J. A., 1942, The production of elastic waves by explosive pressures, 1: Theory and empirical field observations: Geophysics, v. 7, p. 144-154.

Tarazona, Carlos, 1975, An investigation of selected methods for the discrimination of natural and explosive seismic sources: unpub. M.S. thesis, Dept. Geological Sciences, Univ. Wisconsin-Milwaukee, 132p. + appendix.

Tsai, Y. B. and Aki, K., 1971, Amplitude spectra of surface waves from small earthquakes and underground nuclear explosions: Jour. Geophys. Res., v. 76, p. 3940-3952.

Willis, D. E., 1963, Comparison of seismic waves generated by different types of sources: Bull. Seismol. Soc. America, v. 53, no. 5, p. 965-978.

Willis, D. E., DeNoyer, J. N., and Wilson, J. T., 1963, Differentiation of earthquakes and underground nuclear explosions on the basis of amplitude characteristics: Bull. Seismol. Soc. America, v. 53, no. 5, p. 979-988.

Willis, D. E., DeNoyer, J. N., and Wilson, J. T., 1963, Spectral differences in earthquakes and underground nuclear explosions: presented at I.U.G.G. Meetings in Berkeley, California, August 30, 1963.

Wyss, M. and others, 1971, Comparison of P-wave spectra of underground explosions and earthquakes: Jour. Geophys. Res., v. 76, no. 11, p. 2716-2729.

Yacoub, N. K., Scott, J. H., and McKeown, F. A., 1968, Computer technique for tracing seismic rays in two-dimensional geologic models: U.S. Geol. Survey Open File Report, August 1.

Yacoub, N. K., Scott, J. H. and McKeown, F. A., 1970, Computer ray tracing through complex geological model for ground motion studies: Geophysics, v. 35, no. 4, p. 586-602.

Zimdars, M.A., 1974, Cepstrum analysis applied to the problem of multiple event discrimination: unpub. M.S. thesis, Dept. of Geological Sciences, Univ. Wisconsin-Milwaukee, 124 p.

APPENDIX A

DISPLACEMENT SPECTRA OF MASSACHUSETTS MOUNTAIN EARTHQUAKE AND NUCLEAR EXPLOSIONS

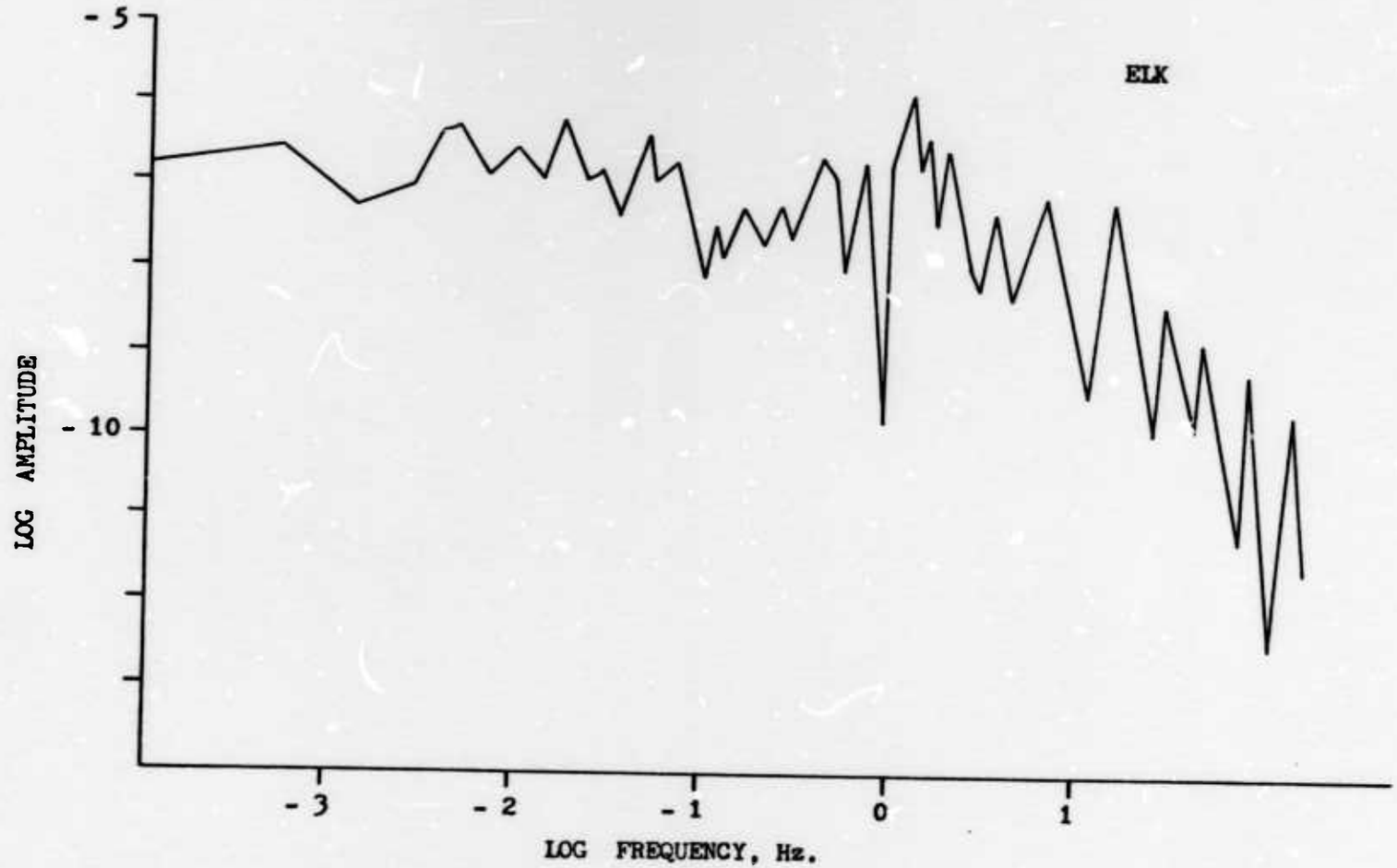

Figure A1. Displacement spectrum of the Massachusetts Mountain earthquake for ELK station ($\log_e$ 2.7, Hz = 0).

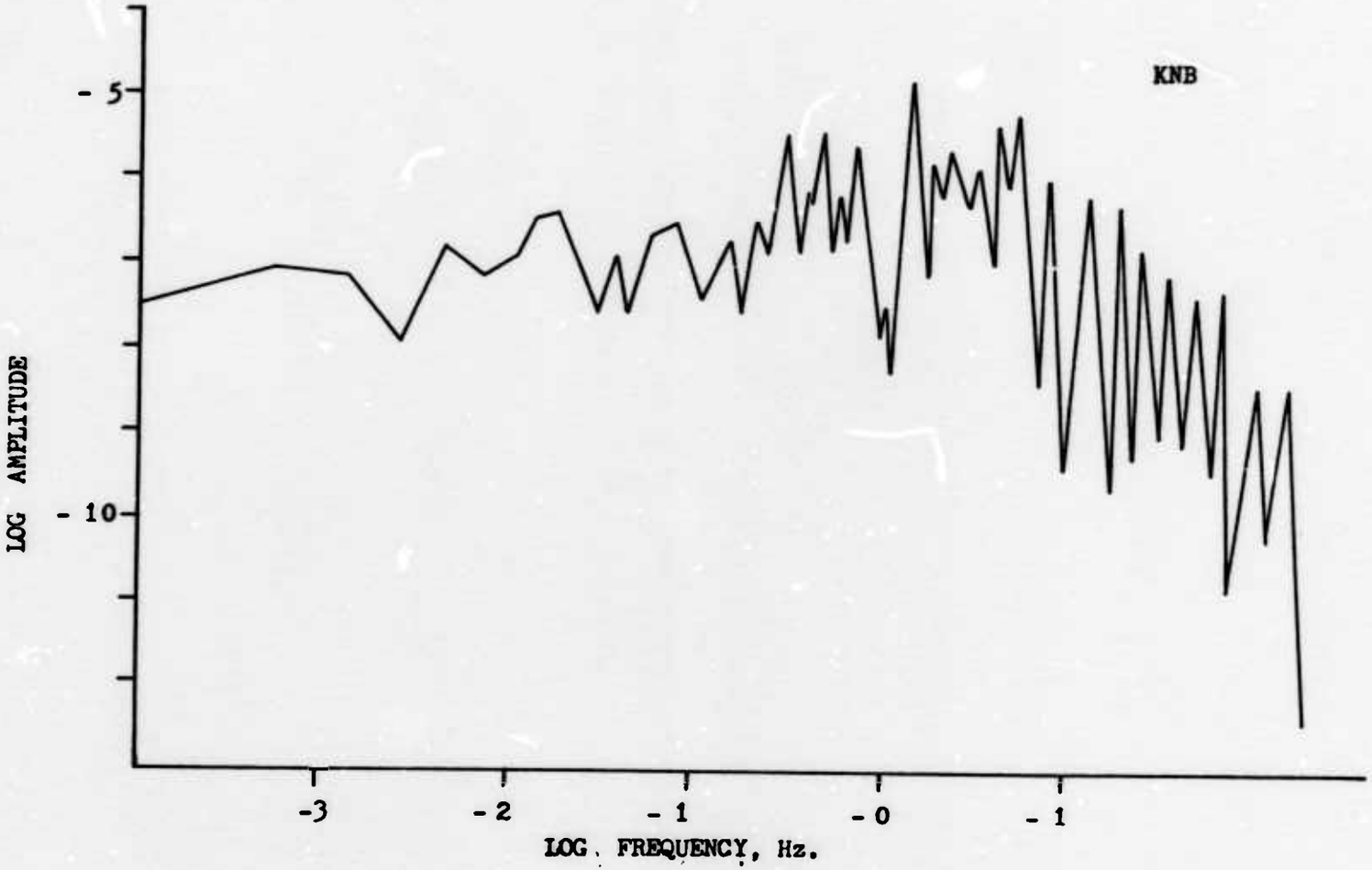

Figure A2. Displacement spectrum of the Massachusetts Mountain earthquake for KNB station ($\log_e$ 2.7, Hz = 0).

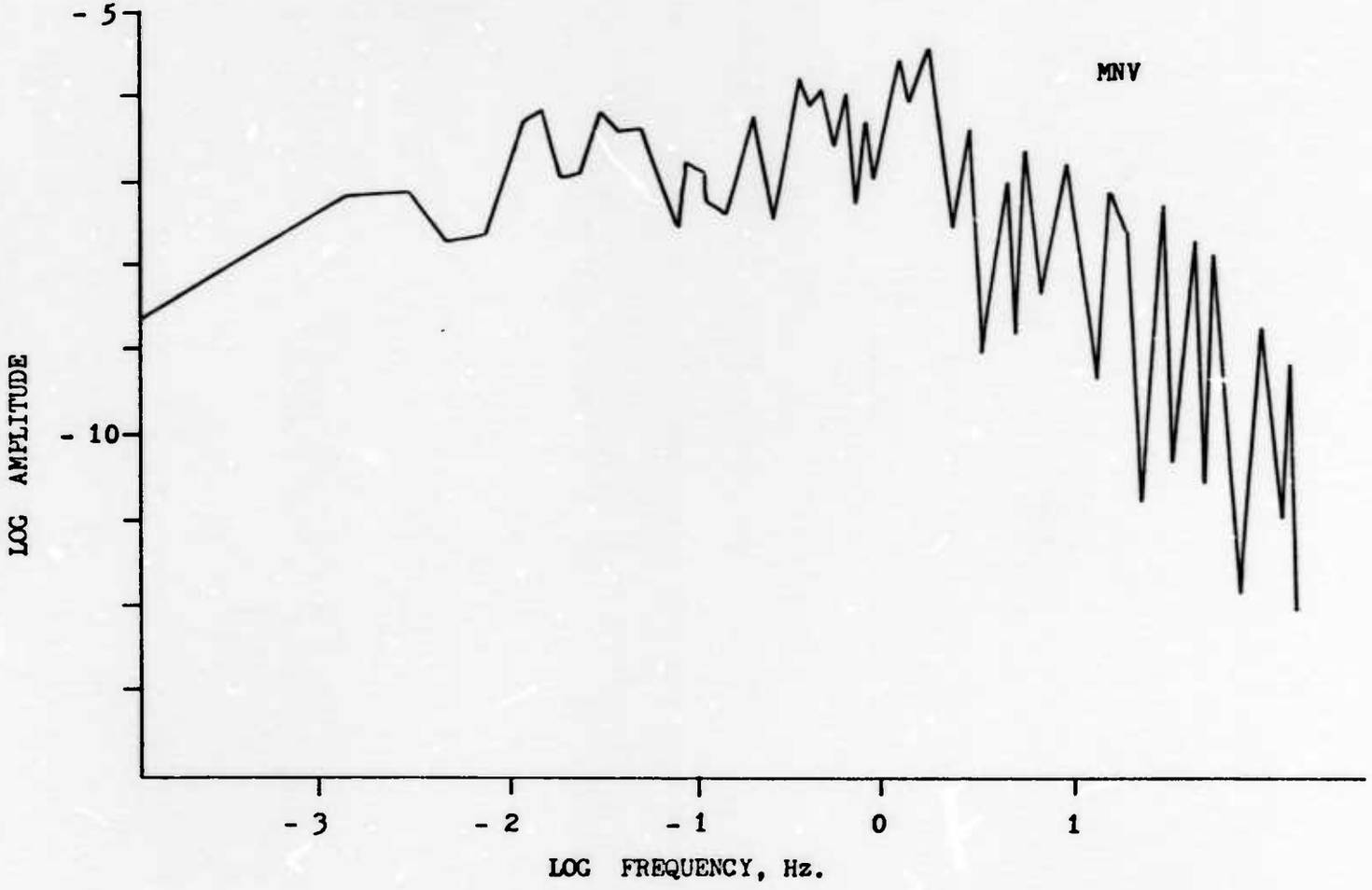

Figure A3. Displacement spectrum of the Massachusetts Mountain earthquake for MNV station ($\log_e$ 2.7, Hz = 0).

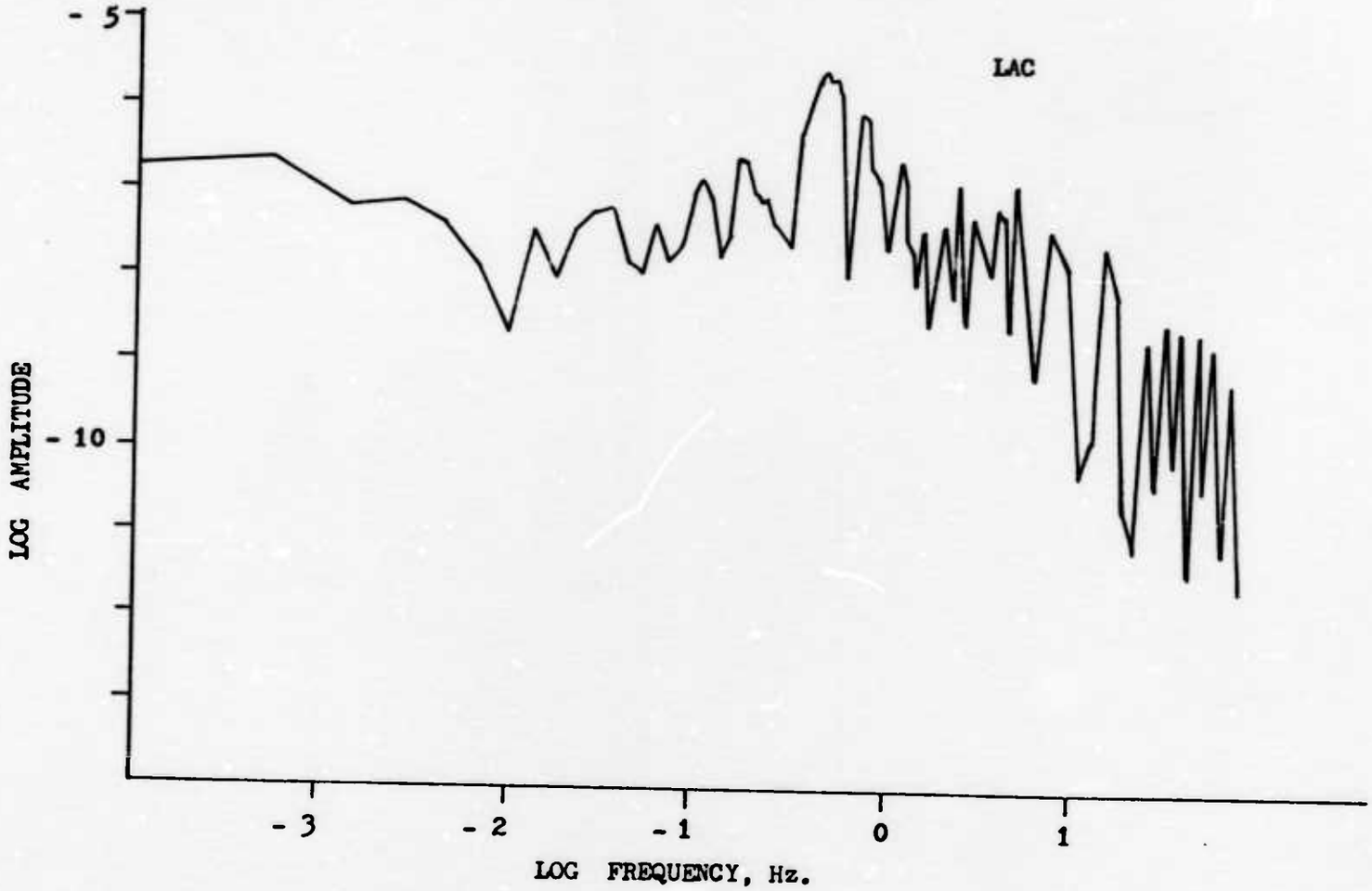

Figure A4. Displacement spectrum of BLENTON/THISTLE event for LAC station ($\log_e$ 2.7, Hz = 0).

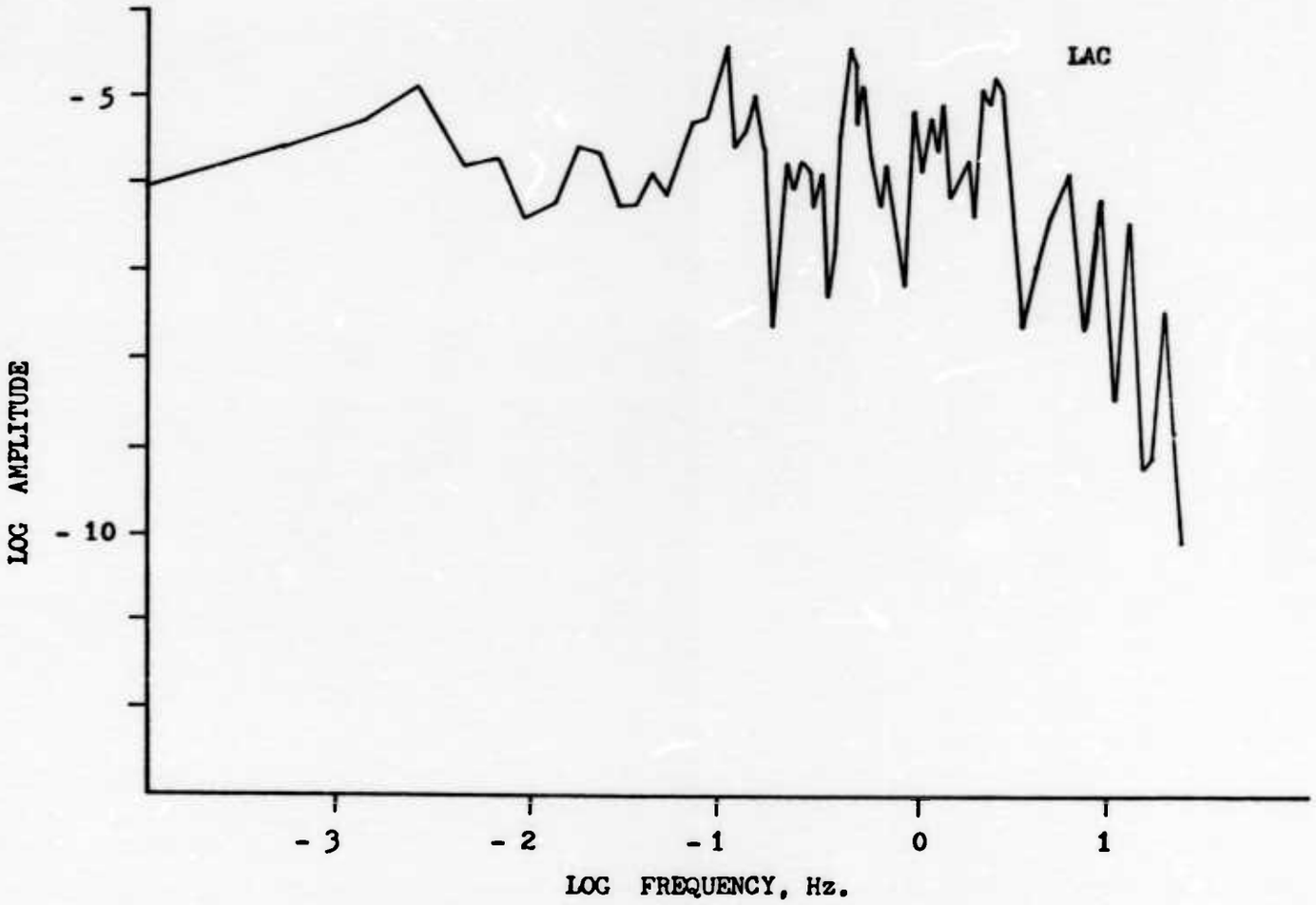

Figure A5. Displacement spectrum of A event for LAC station ($\log_e$ 2.7, Hz = 0).

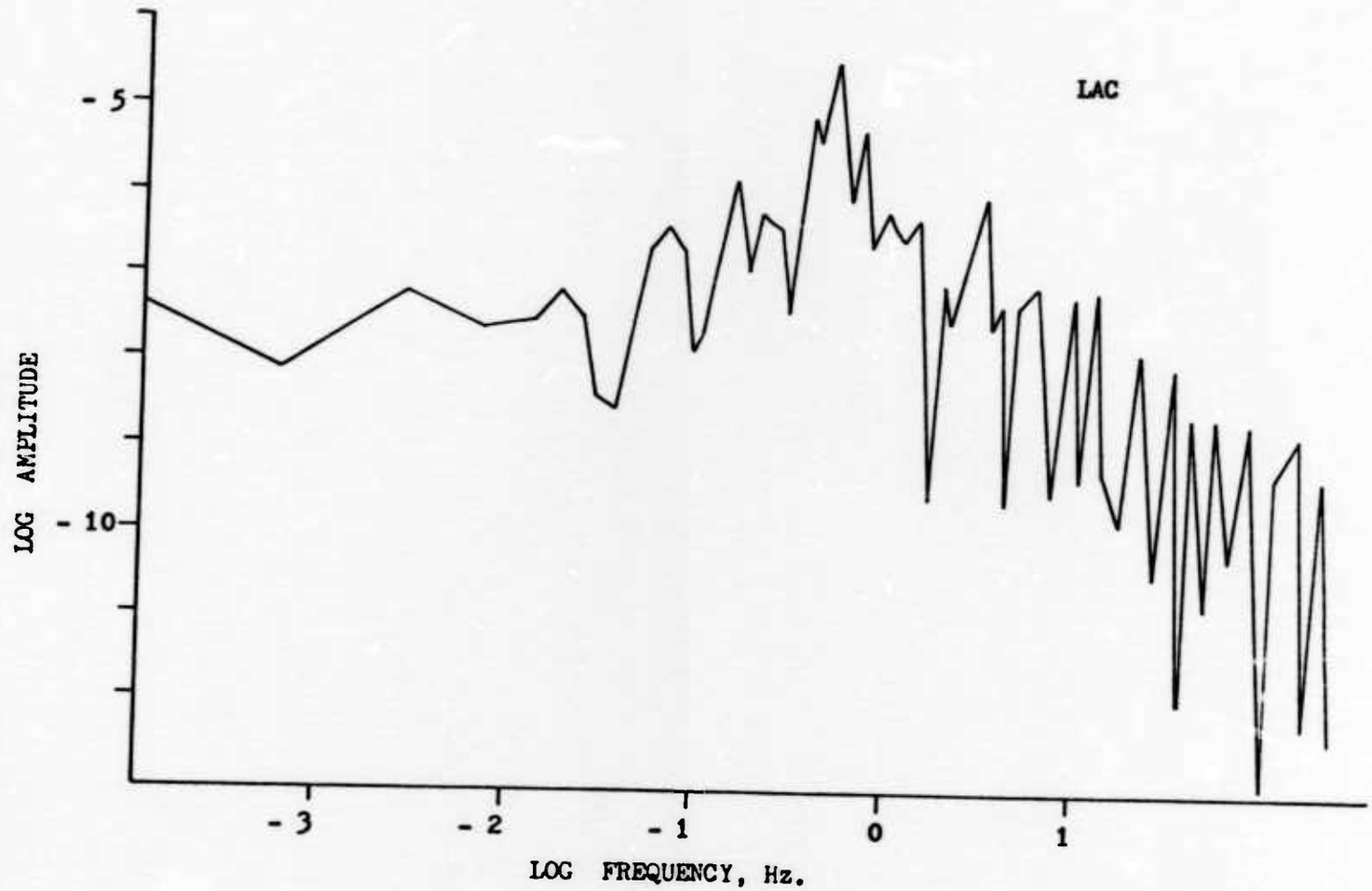

Figure A6. Displacement spectrum of B event for LAC station ($\log_e$ 2.7, Hz = 0).

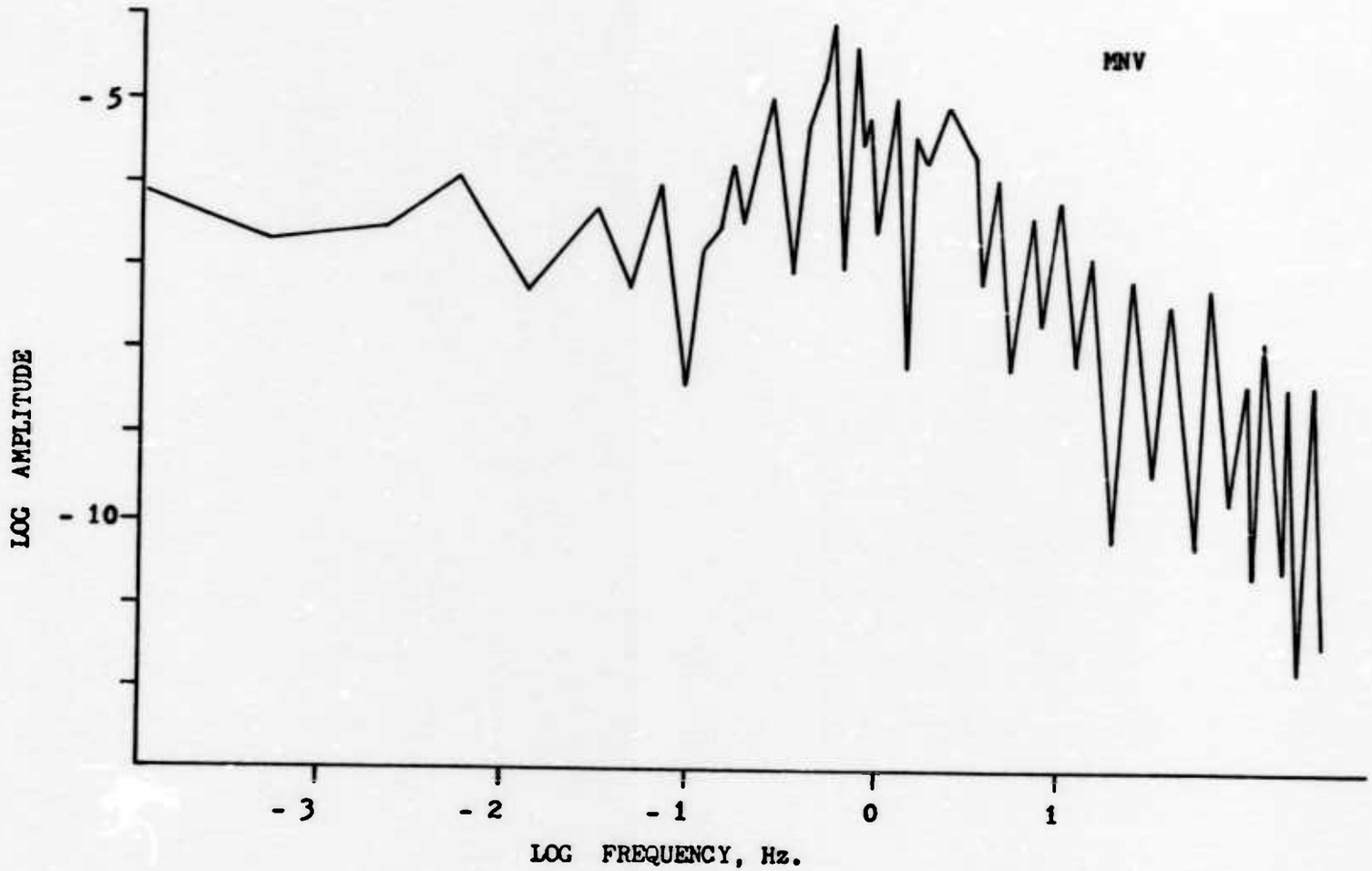

Figure A7. Displacement spectrum of B event for MNV station ($\log_e$ 2.7, Hz = 0).

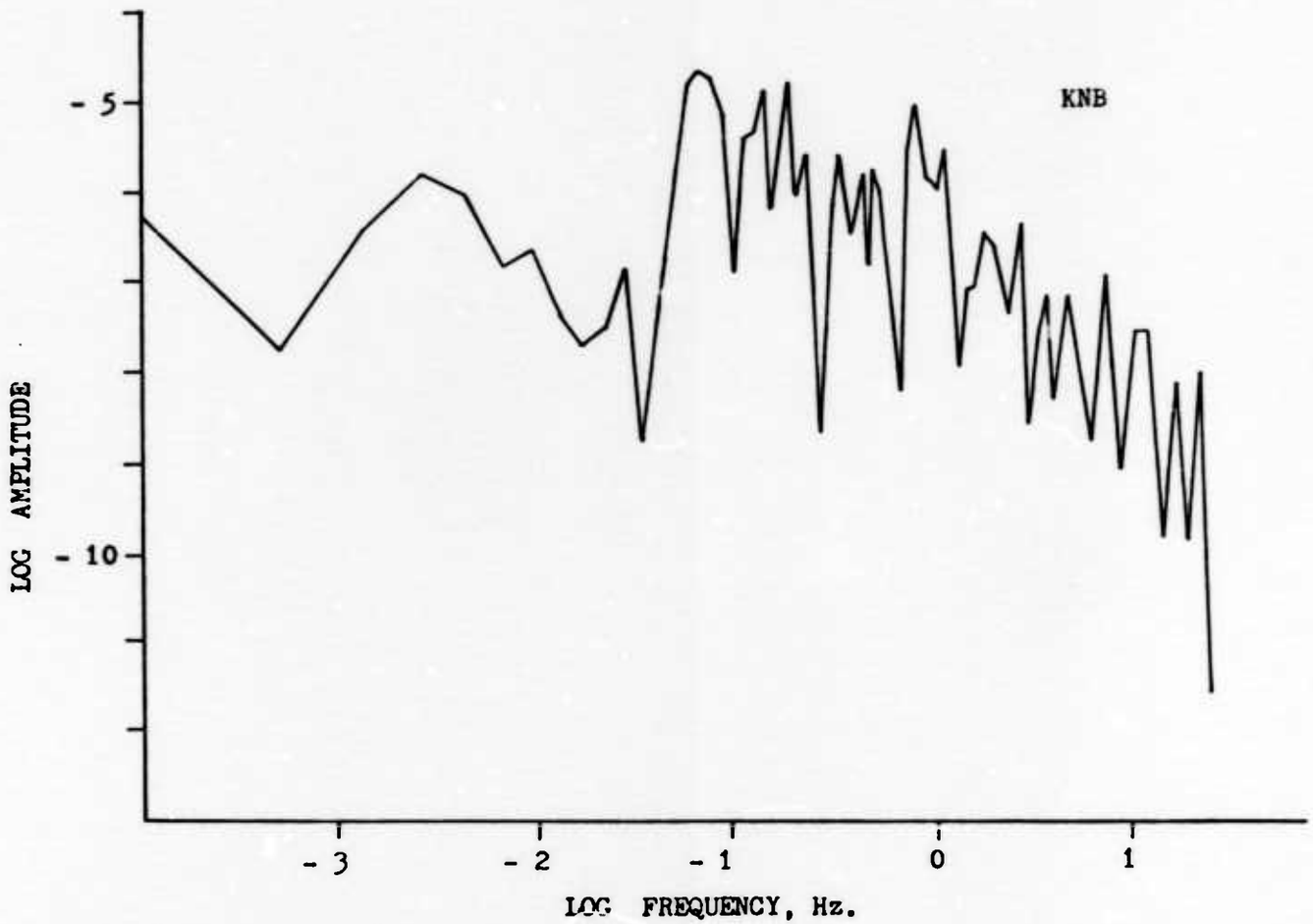

Figure A8. Displacement spectrum of C event for KNB station ($\log_e$ 2.7, Hz = 0).

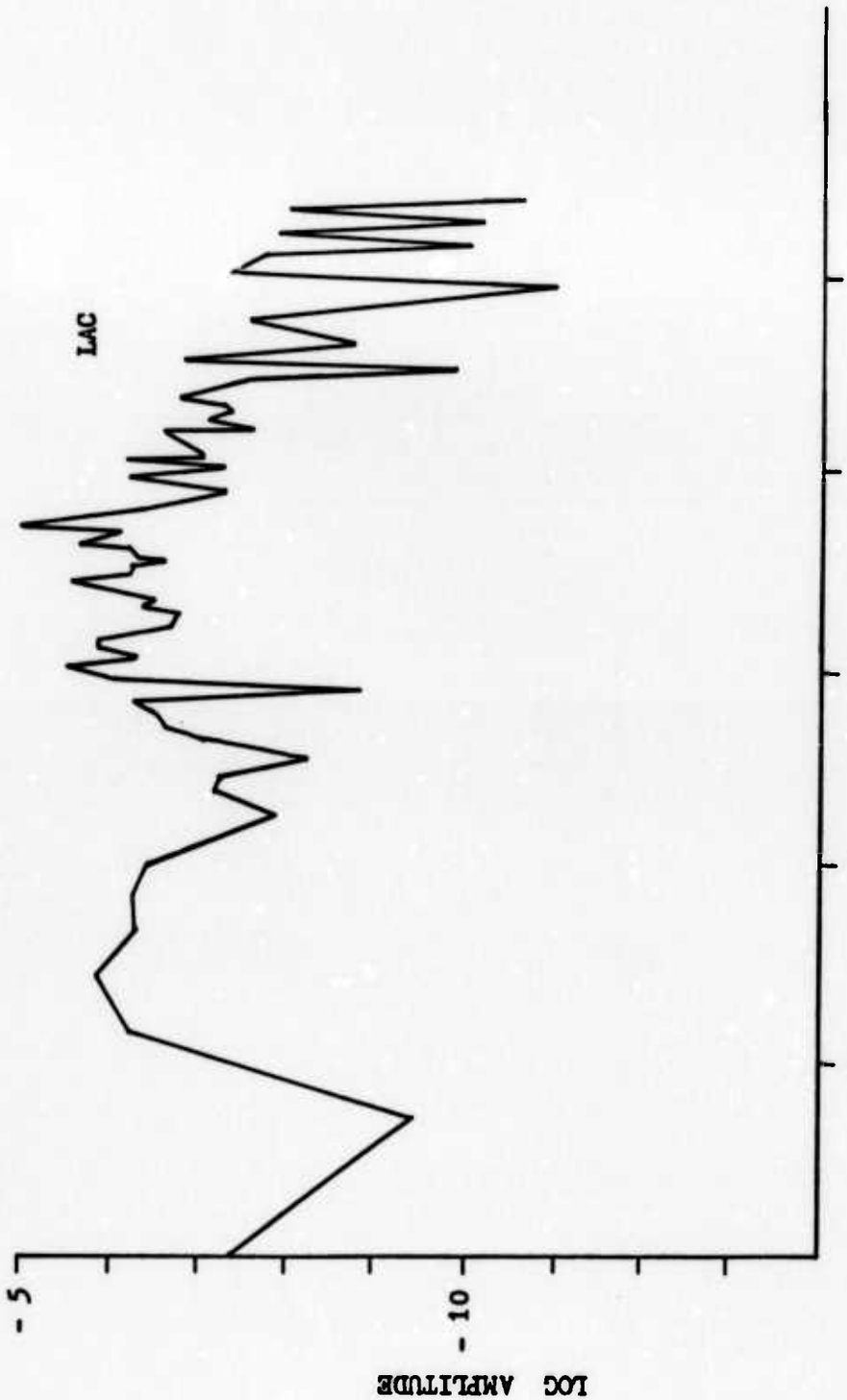

Figure A9. Displacement spectrum of C event for LAC station ($\log_e$ 2.7, Hz = 0).

Figure A10. Displacement spectrum of C event for MNV station ($\log_e$ 2.7, Hz = 0).

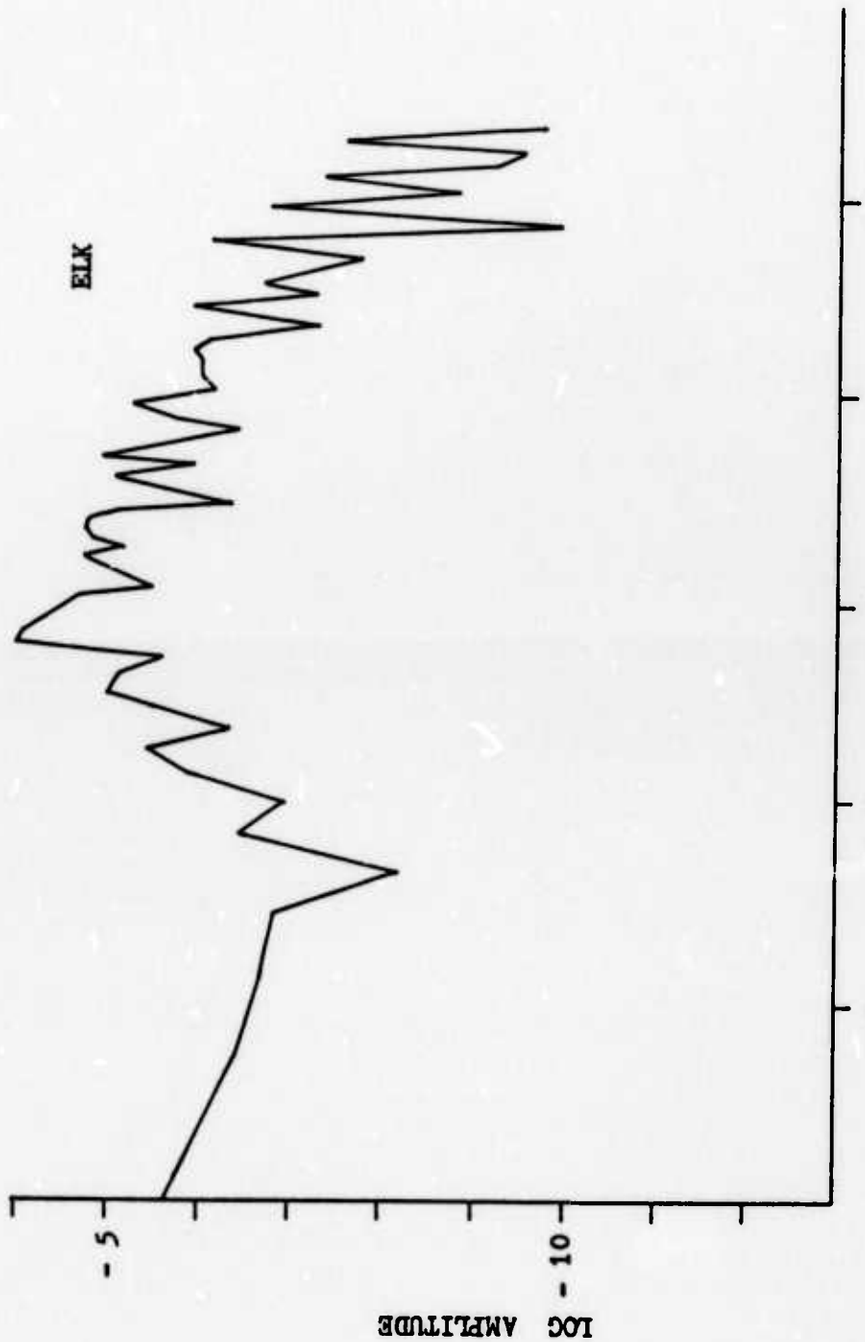

Figure A11. Displacement spectrum of D event for ELK station ($\log_e$ 2.7, Hz = 0).

Figure A12. Displacement spectrum of D event for KNB station ($\log_e$ 2.7, Hz = 0).

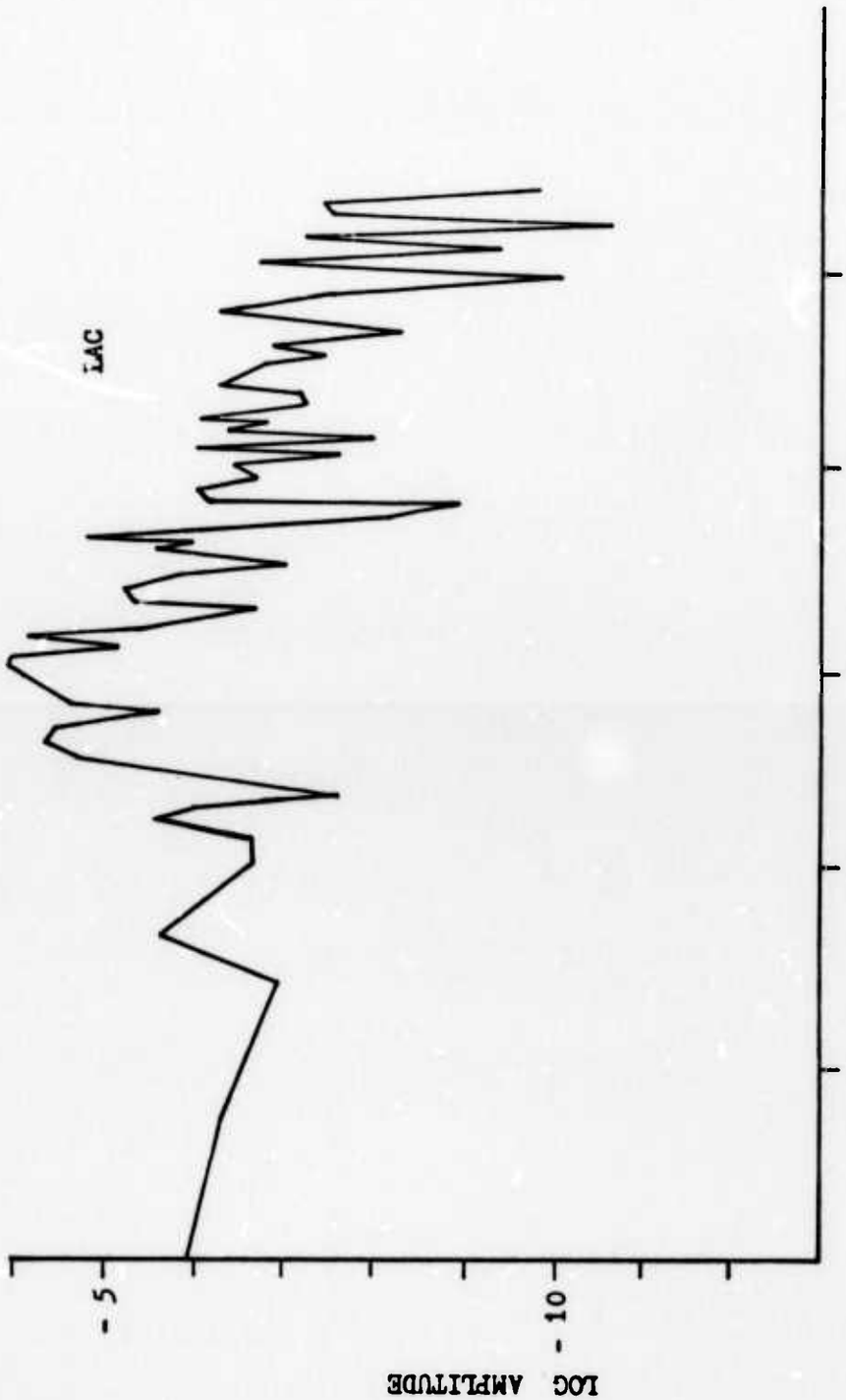

Figure A13. Displacement spectrum of D event for LAC station ($\log_e$ 2.7, Hz = 0).

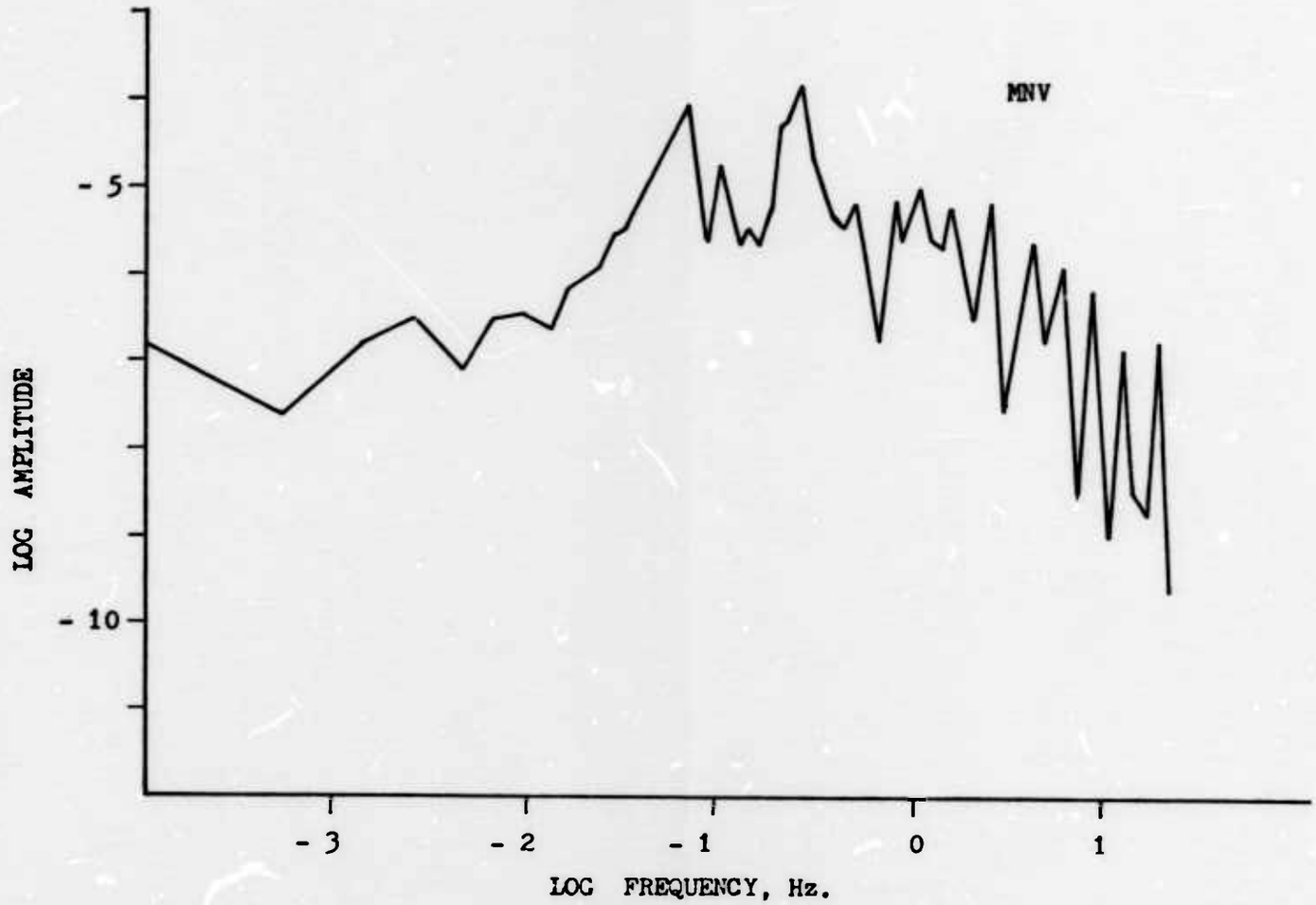

Figure A14. Displacement spectrum of D event for MNV station ($\log_e$ 2.7, Hz = 0).

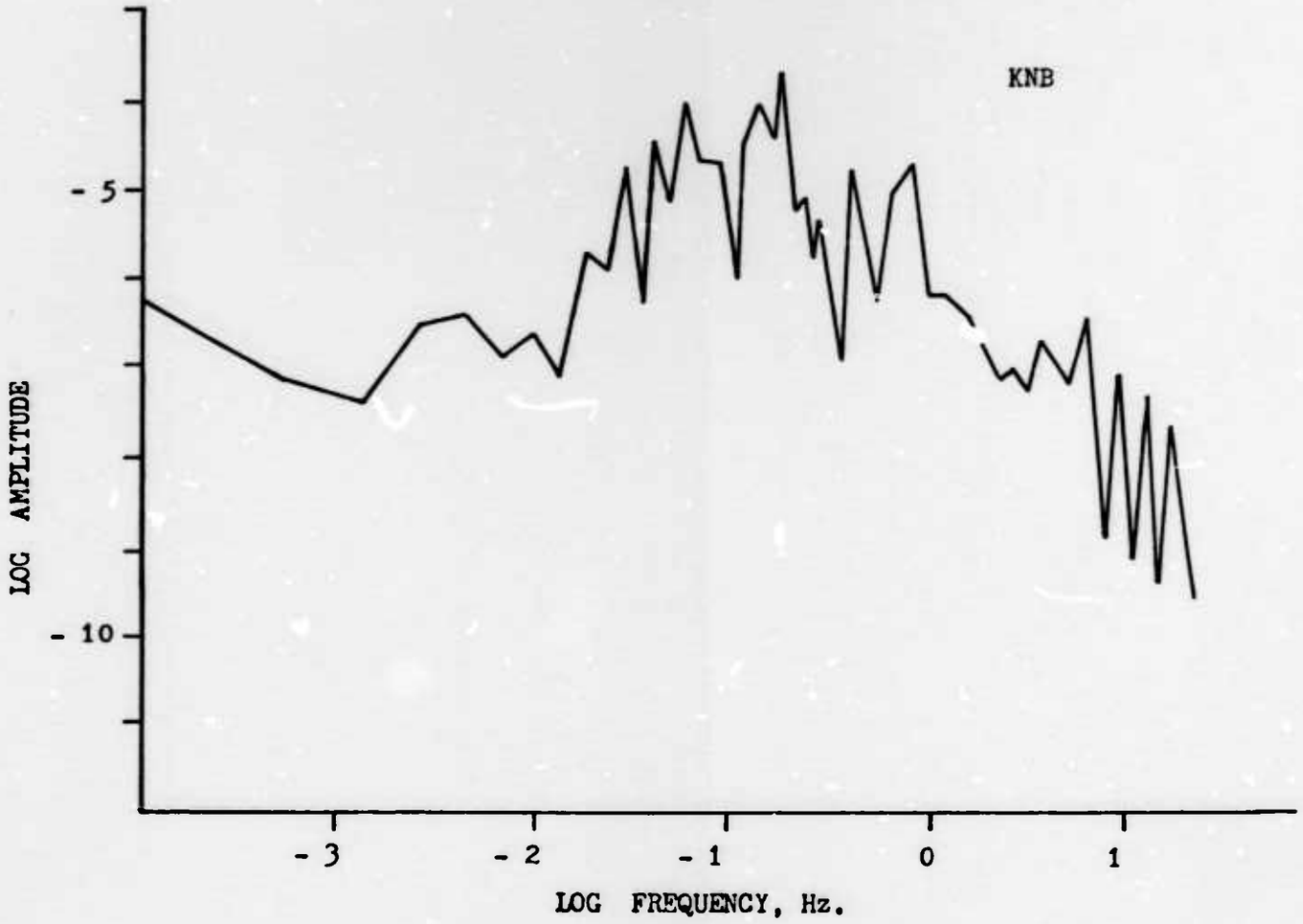

Figure A15. Displacement spectrum of E event for KNB station ($\log_e$ 2.7, Hz = 0).

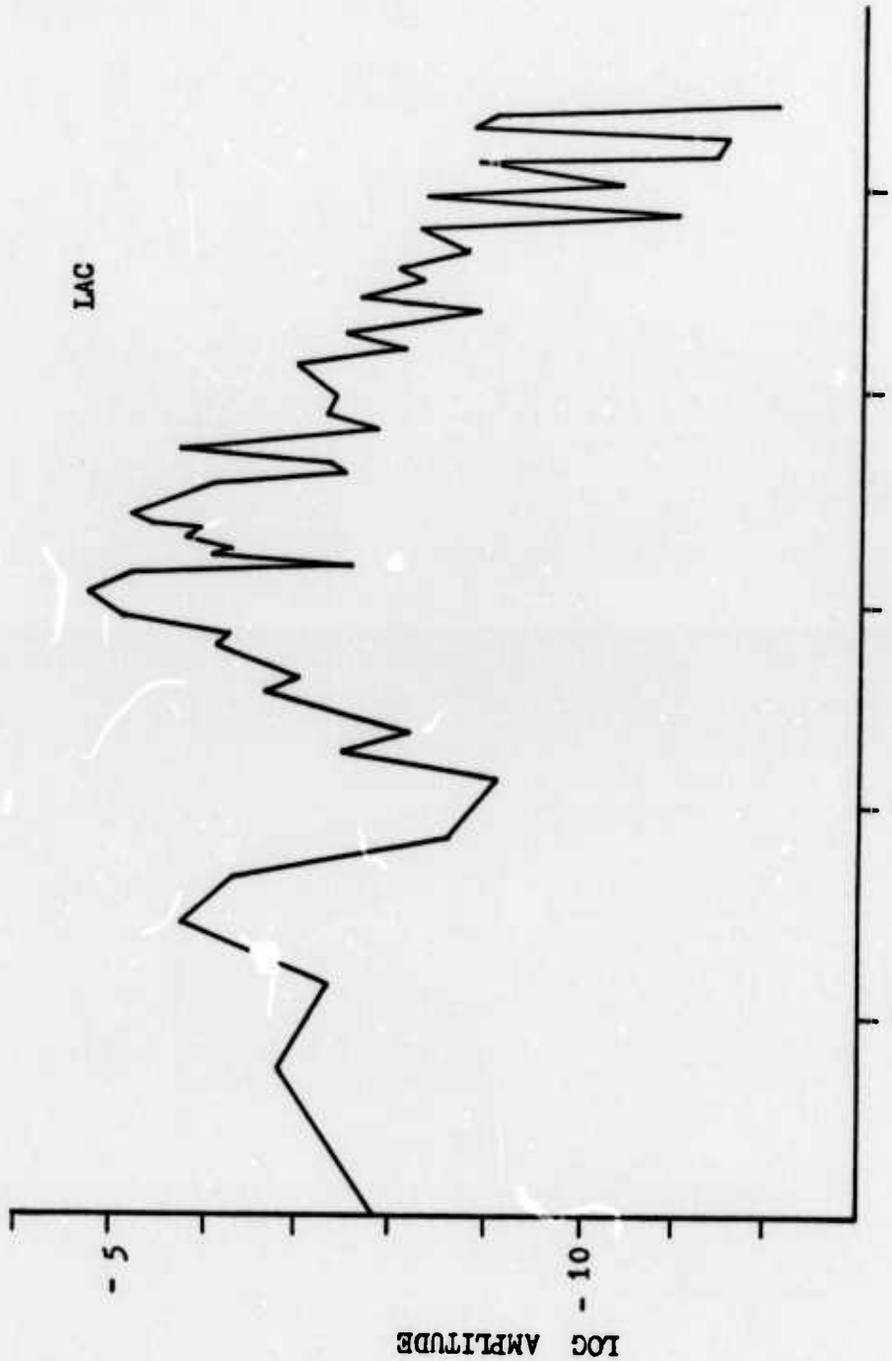

Figure A16. Displacement spectrum of E event for LAC station ($\log_e$ 2.7, Hz = 0).

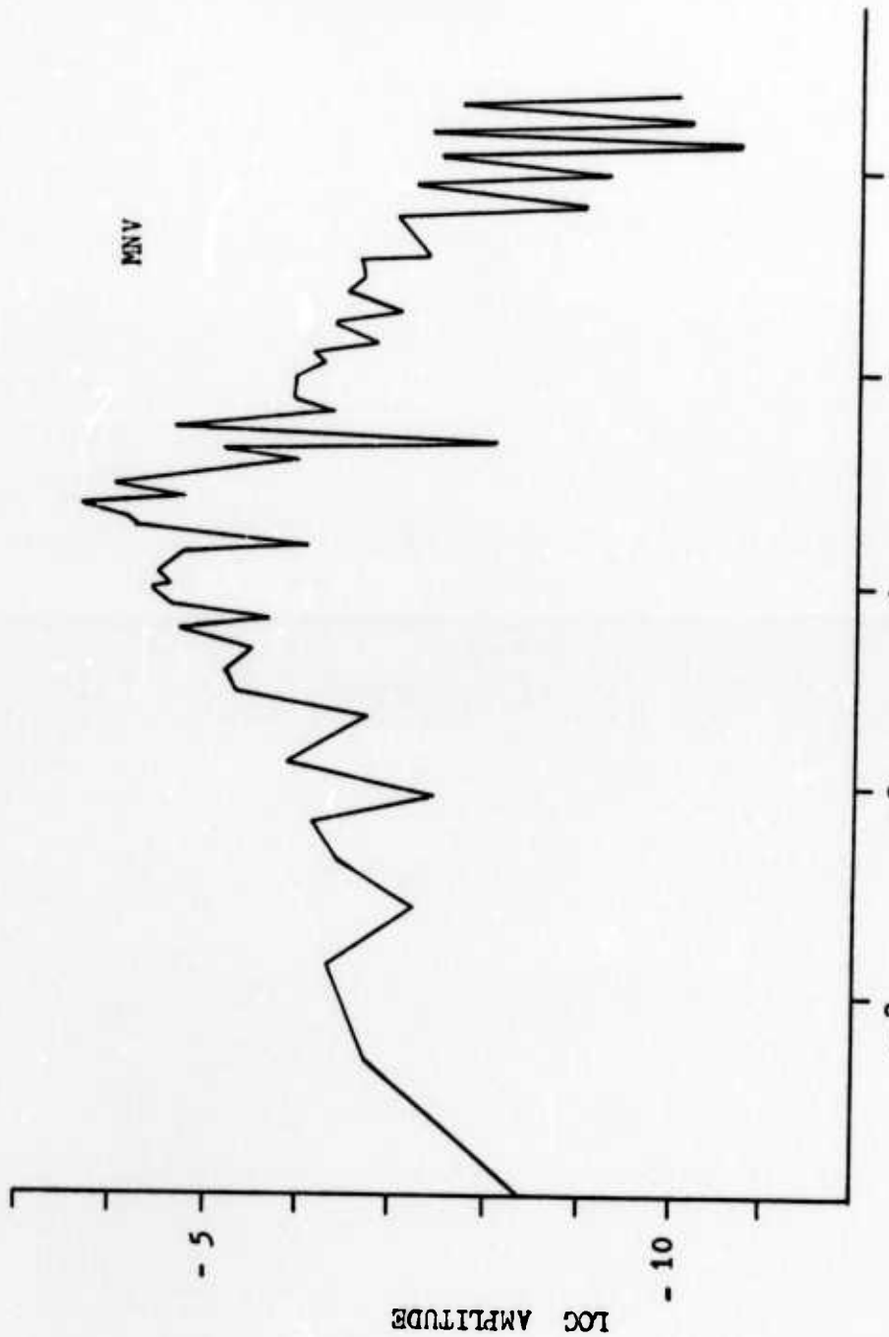

Figure A17. Displacement spectrum of E event for MNV station ($\log_e$ 2.7, Hz = 0).

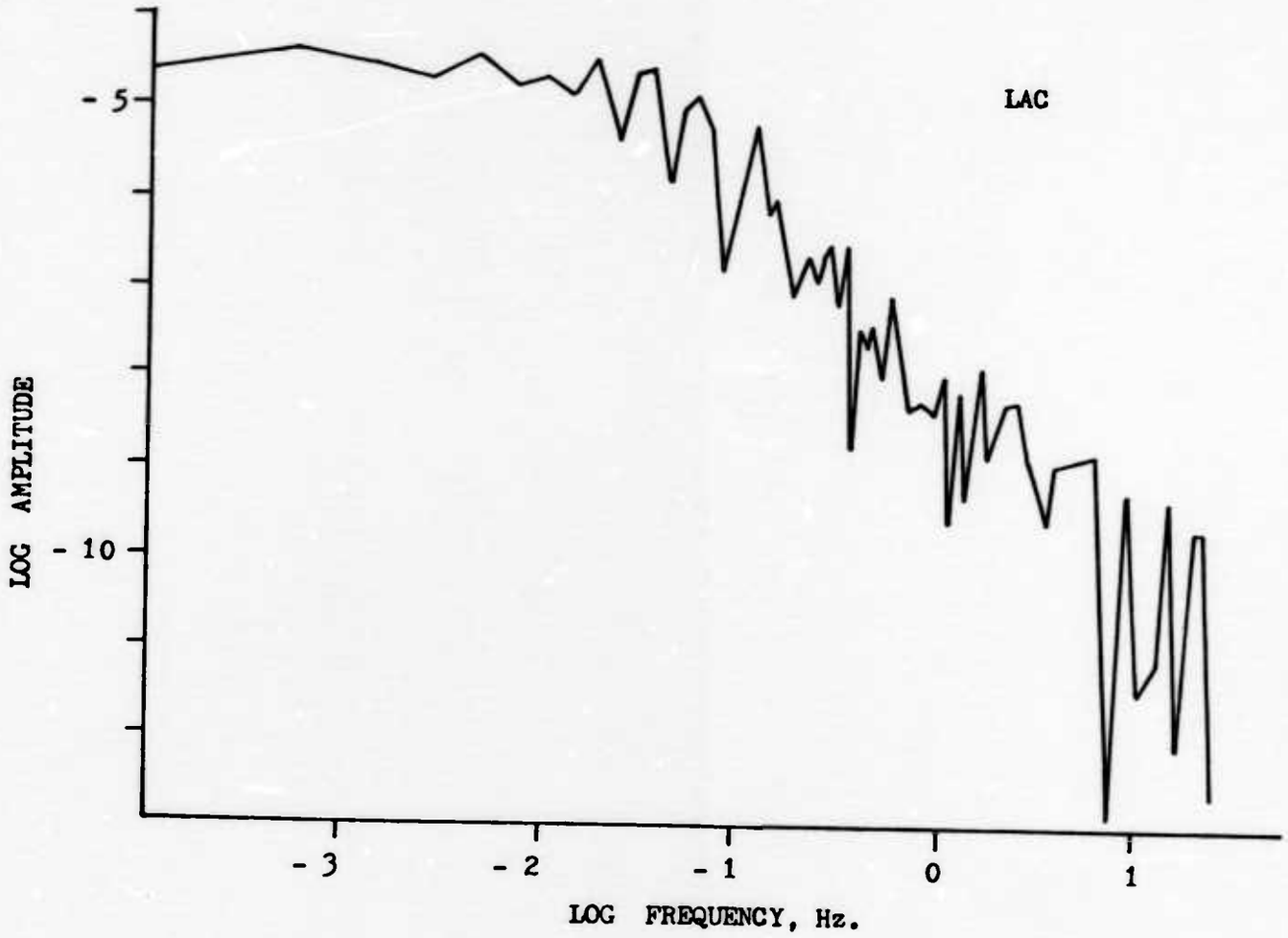

Figure A18. Displacement spectrum of F event for LAC station ($\log_e$ 2.7, Hz = 0).